# Extending Photoinduced Charge Separation

## Molecular-semiconductor assemblies for solar energy conversion

VALERIA SAAVEDRA BECERRIL

THESIS FOR THE DEGREE OF DOCTOR OF PHILOSOPHY

# Extending Photoinduced Charge Separation

Molecular-semiconductor assemblies for solar
energy conversion

VALERIA SAAVEDRA BECERRIL



Department of Chemistry and Chemical Engineering
CHALMERS UNIVERSITY OF TECHNOLOGY

Göteborg, Sweden 2017

Cover:
**Front:** Cartoon illustrating a molecular-semiconductor assembly where electron transfer from a photosensitizer to a catalyst is facilitated by the semiconductor material.

**Back:** Photograph by Johan Bodell

Extending Photoinduced Charge Separation:
Molecular-semiconductor assemblies for solar
energy conversion

VALERIA SAAVEDRA BECERRIL
Department of Chemistry and Chemical Engineering
Division of Chemistry and Biochemistry - Physical Chemistry
Chalmers University of Technology

## Abstract

The conversion of solar energy into chemical energy by harvesting visible-light with synthetic molecules presents several scientific and technological challenges. This thesis is dedicated to the investigation of approaches to long-lived charge separation, one of the crucial aspects for the photochemical generation of solar fuels. Charge separation was characterized in molecular and molecular-semiconductor hybrid assemblies by using optical spectroscopic techniques. The assemblies studied were designed with the purpose of either solar fuel generation or for mere mechanistic understanding and proof of principle studies on relevant aspects for solar-to-chemical energy conversion.

The photophysical characterization of a Ru-Mn supramolecular complex for photochemical water oxidation, and related Ru(II)-complexes, revealed the reasons behind the difficulty of obtaining a long-lived charge separation state. This prevented the photochemical water oxidation, exemplifying the limitations of supramolecular approaches to solar fuels. This work justifies the need to explore other alternatives for the creation of a stable material where all the basic functions of natural photosynthesis can be imitated in a simplified way.

A viable option is the construction of nanoarchitectures that incorporate light-harvesting units and catalysts on a semiconductor surface. As demonstrated in this thesis, the modification of the individual components of these assemblies, e.g. macroscopic structure of the dye-sensitized semiconductor and the electrolyte composition, can be used to extend not only the lifetime, but also the distance of charge separation. One of the most remarkable findings of this thesis, is that the lifetime of charge separation in dye-sensitized semiconductors can be extended by several orders of magnitude, by implementing a photoanode design consisting of a repetitive pattern of $SnO_2$ and $TiO_2$ μm-thick layers. The main feature of this design is the possibility of trapping electrons at dye-free areas on the film, where they reside for longer times before recombining with dye molecules. In addition, such materials can be used for visible-light generation of catalytically active sites on the surface through electron transfer from the photosensitizer. This process, being facilitated by the conduction band of the semiconductor, as demonstrated by time resolved spectroscopic studies on dye-semiconductor-catalyst assemblies.

The work summarized in this thesis is intended to encourage the development of dye-sensitized semiconductors to expand the possibilities of their application in solar fuel technology.

**Keywords**: Artificial photosynthesis, Back-electron transfer, Charge separation, Charge recombination, Conduction band mediated, Dye-sensitized, Ruthenium complexes, Solar energy conversion.

*"Livet behöver inte vara enkelt – bara det inte är tomt."*
*"Life need not be easy, provided only that it is not empty"*

-Lise Meitner

*To my family*

# List of Publications

This thesis is based on the following publications and manuscripts, referred to in the text as:

**Paper I**
E. Karlsson, B-L. Lee, R.-Z. Liao, T. Åkermark, M.D. Kärkäs, V. Saavedra Becerril, P.E.M. Siegbahn, X. Zou, M. Abrahamsson and B. Åkermark **Synthesis and Electron-Transfer Processes in a New Family of Ligands for Coupled $Ru-Mn_2$ Complexes**
*ChemPlusChem* **2014**, 79(7), 936-950

**Paper II**
V. Saavedra Becerril, D. Franchi and M. Abrahamsson **Ionic liquid-Induced Local Charge Compensation. Effects on Back Electron-Transfer Rates in Dye-Sensitized $TiO_2$ Thin Films**.
*J. Phys. Chem. C* **2016**, 120 (36), 20016-20023

**Paper III**
V. Saavedra Becerril, E. Sundin, M. Mapar and M. Abrahamsson **Extending charge separation lifetime and distance in patterned dye-sensitized $SnO_2-TiO_2$ μm-thin Films**
*Phys. Chem. Chem. Phys.* **2017**, DOI: 10.1039/c7cp04486k

**Paper IV**
V. Saavedra Becerril, E. Sundin and M. Abrahamsson **Conduction Band Mediated Electron Transfer in dye-$TiO_2$-acceptor thin films.**
*Manuscript in Preparation*

iv

# Contribution Report

**Paper I**. Performed the photophysical characterization of the complexes and contributed to the discussion and writing of the paper.

**Paper II**. Suggested the project. Performed all sample preparation together with D. Franchi. Performed all transient absorption measurements and data analysis. Wrote most of the paper.

**Paper III**. Suggested the project. Designed the sample fabrication method together with M. Mapar. Designed and performed the experiments together with E. Sundin. Performed most of the data analysis and wrote the paper.

**Paper IV**. Designed and performed the experiments and analyzed the data together with E. Sundin. Contributed to the writing of the manuscript.

# LIST OF ABBREVIATIONS

**Abbreviations**

| | |
|---|---|
| A | Electron acceptor |
| BET | Back-electron transfer |
| CB | Conduction band |
| CBM | Conduction band mediated |
| CBM-ET | Conduction band mediated electron transfer |
| CE | Counter electrode |
| CCD | Charge-coupled device |
| CSS | Charge separated states |
| CV | Cyclic voltammetry |
| DFT | Density functional theory |
| DSSC | Dye-Sensitized Solar Cell |
| DSPEC | Dye-Sensitized Photoelectrochemical Cell |
| D | Electron donor |
| ET | Electron transfer |
| HOMO | Highest occupied molecular orbital |
| IL | Ionic liquid |
| IRF | Instrument response function |
| KWW | Kohlrausch-Williams-Watts |
| LUMO | Lowest unoccupied molecular orbital |
| MLCT | Metal-to-ligand charge transfer |
| OEC | Oxygen evolving complex |
| OPO | Optical parameter oscillator |
| PET | Photoinduced electron transfer |
| PMT | Photomultiplier |
| RE | Reference electrode |
| TCSPC | Time correlated single photon counting |
| TDDFD | Time-dependent density functional theory |
| UV | Ultraviolet |
| VB | Valence band |
| WE | Working electrode |
| OEC | Oxygen Evolving Complex |
| PSII | Photosystem II |

**Molecules and Chemicals**

| | |
|---|---|
| $BMIMPF_6$ | 1-Butyl-3-methylimidazolium hexafluorophosphate |
| $CH_3CN$ | Acetonitrile |
| $CO_2$ | Carbon dioxide |
| $CO_2Et$ | Ethyl ester |
| CoPPIX | Protoporphyrin IX cobalt (III) chloride |
| dcb | Bis(2,2'-bipyridyl-4,4'-dicarboxylic acid) |
| DMSO | Dimethyl sulfoxide |

| | |
|---|---|
| FePPIX | Protoporphyrin IX iron (III) chloride |
| FTO | Fluorine-doped tin oxide |
| $H_2$ | Hydrogen gas |
| HMIMPF | 1-Hexyl-3-hexylimidazolium hexafluorophosphate |
| $LiClO_4$ | Lithium perchlorate |
| NADPH | Nicotinamide adeninde dinucleotide phosphate |
| $O_2$ | Molecular oxygen |
| $OMIMPF_6$ | 1-Octyl-3-hexylimidazolium hexafluorophosphate |
| P-Q | Porphyrin-quinone dyad |
| $Ru-Mn_2$ | Ruthenium-manganese dyad complex |
| $[Ru(bpy)_3]Cl_2$ | Tris(bipyridine)ruthenium(II) chloride |
| $TiO_2$ | Titanium dioxide |
| $SCN^-$ | Thiocyanate |
| $SnO_2$ | Tin dioxide |

# Contents

# Introduction

*"If our black and nervous civilization, based on coal, shall be followed by a quieter civilization based on the utilization of solar energy, that will not be harmful to progress and to human happiness."*

The above sentence is taken from "The photochemistry of the future",[1] a lecture given by the pioneer of photochemistry Giacomo Ciamician in 1912. Undeniably, a man ahead of his time as well as a true visionary, Camician was concerned about the future of a coal dependent society and was aware of the potential and urge of making use of solar radiation. One century later we can ask ourselves if someday his dream will come true. Modern society is facing the challenges of sustaining or increasing life standard without compromising the ecological stability. While a large scientific community is investing their efforts in finding efficient ways to use solar energy and other renewable sources, the world´s primary energy is still mainly supplied by oil, coal and natural gas.[2]

By the early 20th century, the scientific basis that would allow the emergence of solar energy technology had already been established. The work of Planck and Einstein, among others, laid the foundation of quantum physics, which could explain the nature of the photoelectric effect[3]. In the middle of the 20th century, the first p-n junction silicon solar cell was invented and later commercialized.[4] Since then, significant progress has been made, not only in the development of photovoltaic devices but also in understanding the principles of natural photosynthesis, and applying this knowledge to the creation of artificial systems aming to convert solar energy into chemical energy. Interestingly, this concept—known today as artificial photosynthesis—was suggested for the first time by Ciamician during the afore-mentioned lecture as in the following lines:*"For our purposes the fundamental problem from the technical point of view is how to fix the solar energy through suitable photochemical reactions. To do this it would be sufficient to be able to imitate the assimilating processes of plants"*.[1]

The first practical demonstration of such concept was carried out successfully by Fujishima and Honda in 1972. Using titanium dioxide and platinum as electrode materials, photoelectochemical water decomposition into hydrogen ($H_2$) and oxygen ($O_2$) was achieved by irradiation with wavelengths shorter than 415 nm.[5] Since then, a number of approaches for artificial photosynthesis has been proposed, with a specific focus on the application of visible light, with the aim of maximizing the use of solar radiation. However, in spite of the extensive knowledge regarding the mechanisms of the photochemical processes involved and the modern advances of nanotechnology, a solar powered device for solar-to-fuel conversion is not yet available. Among other reasons, this can be primarily attributed to the complexity of designing stable and efficient chemical systems that selectively yield the products of interest such as $H_2$ or methanol. Consequently, it is clear at this stage that there is a need to further extend the knowledge and conceive new methods enabling the development of artificial photosynthetic devices.

# 1.1   From light to chemical energy

There are three primary photosynthetic energy conversion processes that are essential for the production of solar fuels. These are (1) efficient light capture, (2) long-lived charge-separation and (3) accumulation of high energy multiple redox equivalents.[6] Replication of these processes in man-made systems has been regarded as biomimetic[6,7] or chemical[8,9] approaches to artificial photosynthesis. These man-made structures are either entirely synthetic molecular assemblies or hybrid assemblies composed of molecules, enzymes, conducting or semiconducting nanomaterials.

Figure 1.1 illustrates a simplified representation of the charge-separation processes in plants' photosynthesis. Light capture is initiated in photosystem II (PSII) when pigment antennas, consisting of chlorophyll molecules, absorb photons and transfer the excitation energy to a reaction center to yield a singlet excited state. Electrons from this state are moved away from their initial location through a series of rapid, energetically down-hill steps, passing by several intermediates before reaching photosystem I. Here, another photon is absorbed, followed by a new cascade of electron transfer (ET) events until the electron reaches the final acceptor to yield nicotinamide adenine dinucleotide phosphate (NADPH), a reducing agent which is later used in the light-independent reactions of photosynthesis for the reduction of $CO_2$.[10] This set of down-hill stepwise ET processes results in long-lived charge separation by preventing rapid electron recombination with the oxidized donor (backward or back-electron transfer). Observed recombination rates from the primary acceptor in PSII are in the order of $10^{-3}$s.[11]

Oxidized chlorophyll molecules are regenerated by electrons released during the four-electron oxidation of water into protons ($H^+$) and $O_2$. This reaction is catalyzed by the oxygen evolving complex (OEC), a $Mn_4O_5Ca$ complex surrounded by a protein environment that controls the reaction parameters and provides chemical stability.[12]

In artificial photosynthetic systems, light capture antennas and electron donor (D) units are typically replaced by synthetic photosensitizers that are designed to have large extinction coefficients in the visible region of the electromagnetic spectrum like clorophyll molecules. In general, synthetic photosensitizers can be grouped into four main categories: (1) transition metal coordination complexes[13,14] or organic molecules[15] (dyes); (2) semiconductor nanocrystals (quantum dots)[16] and (3) the more recently emerging organometal halide perovskites.[17] Charge separation is achieved by coupling the electron donor to a suitable electron acceptor (A). An ideal donor-acceptor (D-A) system for artificial photosynthesis should generate sufficiently long-lived charge separated states (CSS) to allow time for the redox reactions of solar fuel synthesis to occur. This is a contemporary problem in the development of materials for artificial photosynthesis.[18,19] Electron donor-acceptor assemblies have been a topic of increasing interest during the past decades and much of the research efforts have been dedicated to the study of purely molecular systems. Some of which have been successfully designed to form CSSs with lifetimes in the ms range[20,21] and to produce sufficient chemical potential to carry out redox reactions of interest such as oxidation of water or reduction of $CO_2$.[22] However, integration of all natural photosynthetic primary functions in a single supramolecular system is, if not impossible, tremendously challenging from the design and synthesis point of view. Incorporation of inorganic materials has been a viable alternative, making hybrid
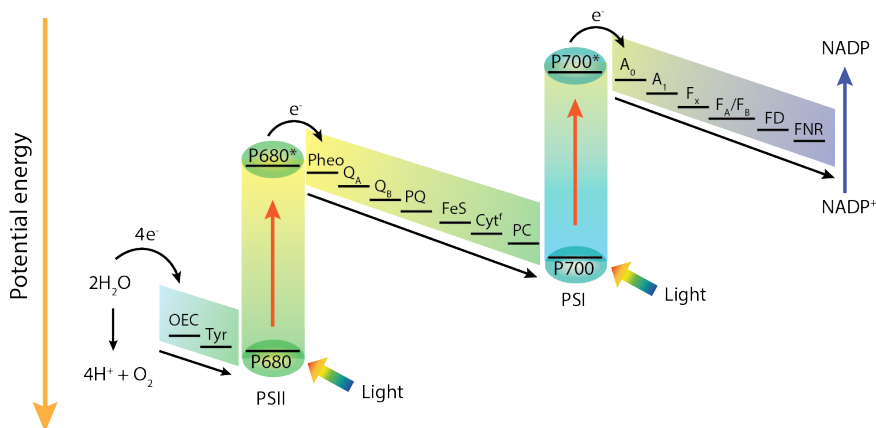
**Figure 1.1:** Simplified representation of the light harvesting and charge separation processes in plant's photosynthesis. P680: Primary electron donor of PSII; $P680*$:excited state of P680; Pheo: Phephytin, the primary electron acceptor in PSII. $Q_A$, $Q_B$, PQ, FeS, $Cyt^f$, PC: Intermidiate electron acceptors in PSII; P700: electron donor in PSI; $P700*$: excited state of P700; $A_0$: primary electron acceptor of PS1; $A_1$, $F_x$, $F_A F_B$, FD, FNR: Intermidiate electron acceptors in PSI; NADP: Nicotinamide adenine dinucleotide phosphate. Adapted from work by Tachibana *et al.*[10]

systems the most promising in terms of operation and stability. An example of this is the relatively new concept of dye-sensitized photoelectrosynthesis cell (DSPEC).[19] This approach combines the light-harvesting and catalytic properties of chromophore-catalyst assemblies with the high energy bandgap of semiconductor metal oxides. This strategy allows the separation of photogenerated redox equivalents which are used at different compartments to drive the reactions of solar fuel synthesis. I believe that this "solar reactors" could be an efficient way to harvest the energy of the sun and provide clean power in the future.

## 1.2 Scope of this thesis

The research work presented in this thesis targets significant aspects and current challenges associated with the development of materials suitable for artificial photosynthesis. The various electron donor-acceptor assemblies studied during this work were designed to mimic one or more of the essential functions of artificial photosynthesis. Spectroscopic methods were used to investigate their photophysical and photochemical properties with

several purposes. First, these studies were intended to gain mechanistic insight into the loss mechanisms competing with light harvesting and charge separation reactions. Some strategies to counteract these processes were suggested and put into practice. Additionally, these experimental methods were used to demonstrate relevant concepts for the progress of artificial photosynthesis research. An important point of this work is to emphasize the need for simplified systems from both the fabrication and function point of view, considering that the ultimate goal is the large-scale implementation of this technology. This thesis is comprised of the following research projects:

In the first project, **Paper I**, a series of $Ru-Mn_2$ complexes designed to perform photocatalytic water oxidation were studied. Photophysical characterization of the complexes revealed that intramolecular quenching of the excited state prevents the system from efficient charge separation and subsequent photoinduced water splitting.

Charge separation in dye-sensitized semiconductor assemblies was another subject of interest in this thesis. On this matter, work was dedicated to explore strategies to extend the lifetime of charge separation. In **Paper II**, it was shown that ionic liquid (IL) electrolytes could be used for this purpose. The role of the structure of IL cations and photosensitizers was investigated, and a mechanism based on electrostatic interactions at the dye-semiconductor interface was proposed. In **Paper III**, a patterned design of a dye-sensitized $SnO_2-TiO_2$ thin film was presented. It was shown that both the lifetime and distance of charge separation could be increased compared to traditional dye-sensitized semiconductor thin films. Moreover, the dye-sensitization method presented here, opened up the possibility of depositing photosensitizers and catalysts on selected areas of the same semiconductor surface. In doing so, undesired interactions between the different molecules are minimized while electron transfer between them is still possible. This type of semiconductor structure could be implemented in future photoelectrochemical devices such as DSPECs.

In the last project, **Paper IV**, a hybrid assembly was presented as a proof of concept of conduction band mediated (CBM) electron transfer. The assembly was fabricated by immobilizing a photosensitizer and a model electron acceptor at a nanoporous $TiO_2$ surface. The feasibility of transferring electrons from the dye to the acceptor through the conduction band (CB) of the semiconductor was shown. A first indication of this was the observed elongation of the CSS lifetime when the acceptor was present. Photoexcitation of the dye leads to the reduction of the acceptor as shown by transient absorption data.

The collection of results presented in this thesis point towards the same direction: the assembly of molecular units and semiconductor materials is a versatile and promising way to integrate the components and functions required in solar fuel synthesis. Although an ongoing research field that still requires significant advances, the possibilities of developing this technology are countless. This research work is a contribution to the scientific knowledge that is necessary for the accomplishment of photochemical solar fuel production.

# Mimicking the primary functions of photosynthesis

# 2.1 Light-harvesting and charge separation

## 2.1.1 Bioinspired molecular donor-acceptor models

In plants, the primary electron donor in photosystem II (PSII) is a tetramer of equally spaced chlorophyll *a* molecules known as P680 (nomenclature given by its absorption maximum at 680 nm).[23] In PSII, charge separation is initiated when an electron from the electronic excited state $P680^*$ is transferred to the primary acceptor pheophytin[24]. Before the discovery of pheophytin, a plastoquinone molecule known as $Q_A$ was mistaken as the primary acceptor in PSII. Based on this knowledge, covalently linked porphyrin-quinone dyads (P-Q) are among the first and most studied donor-acceptor (D-A) photosynthetic models.[25,26]

A very important feature of P680 is the very high oxidation potential of the $P680^{\bullet+}$ radical cation, which has been determined to be 1.17 V vs standard hydrogen electrode (SHE).[27] This redox potential is high enough to extract four electrons from two water molecules at physiological pH. An artificial photosynthesis D-A system therefore must have enough oxidizing power to achieve this. Moreover, the generated charge-separated state must be sufficiently long-lived in order for the relatively slow reactions of solar fuel formation to occur.

A large number of P-Q dyads which meet the energetic criteria have been successfully designed. However, CSS lifetimes are typically no longer than hundreds of picoseconds, as a result of the rapid charge recombination reaction.[28] The answer to this problem lies within the PSII where the electron-hole pair is separated by a considerable distance in a series of short-range consecutive ET steps. Thus, addition of acceptor and donor units to create covalently linked large molecules of the type D-D-D-A-A for example, has resulted in extended lifetimes of charge-separation on the order of miliseconds.[29,30]. Obtaining a D-A molecular model where backward electron transfer is thermodynamically unfavored is possible through structural design. A remarkable example is the work by Suenobu and co-workers where fullerene is used as the acceptor.[18] Fullerene and porphyrins have also been used in or donor-bridge-acceptor or antenna-donor-acceptor assemblies to achieve long lived and long-range charge separation.[31,32]

Besides porphyrins, ruthenium tris-bipyridyl ($[Ru(bpy)_3]^{2+}$)-type complexes have been extensively studied as model photosensitizers for their interesting photophysical properties. They exhibit very high extinction coefficients in the visible region and long excited state lifetimes given by their excited triplet state $^3$MLCT (see Chapter IV). Intermolecular electron transfer from this excited state to an external electron acceptor results in a redox state with sufficient electrochemical potential to carry out water oxidation.[19] Based on this, many covalently linked $[Ru(bpy)_3]^{2+}$-type photosensitizer-catalysts assemblies have been developed as models for artificial photosynthesis.

As it can be understood from the above, obtaining long-lived charge separation in molecular D-A models is no longer a problem. The thought of mimicking the electron transfer chain in PSII and the formation of a highly oxiziding species has been materialized. However, realization of a complete molecular system capable of photocatalytic water oxidation remains a challenge.[22,30] So what are the impediments that delay this accomplishment? The answer to this is found in the chemistry of water oxidation and

fuel forming reactions. While these are multielectron processes, the predominantly single photon absorption in D-A systems leads to single electron-hole pairs. Accumulation of multiple charges after sequential absorption of several photons is therefore a function that must be integrated in order to complete solar fuel forming reactions. Unfortunately, besides electron-hole recombination, there are several additional complications associated with consecutive photon absorption and accumulative electron transfer. In a second photon absorption and ET step, quenching of the excited photosensitizer (P*) by the oxidized donor ($D^+$) or reduced acceptor ($A^-$) is possible by reverse ET,[33] energy transfer or paramagnetic quenching.[34] Moreover, the existence of intermediate states where multiple charges are located at the donor and acceptor sides, results in decreased CSS lifetimes due to additional pathways for electron-hole recombination.[35] Finally, the potentials of succesive redox reactions need to lie within a narrow range since the various ET steps are driven by the power of the same photosensitizer. These complications and requirements hinder the design of a supramolecular system for accumulative electron transfer. A potential solution to this problem has involved the incorporation of metal oxide semiconducting materials to build molecular-semiconductor hybrid assemblies where several electrons can be accumulated in the conduction band of the metal-oxide.[34,36] The details of this approach will be discussed in the following section.

## 2.1.2 Molecular-semiconductor hybrid assemblies

Since the work of Fujishima and Honda[5], significant efforts to increase the efficiency of metal oxide photocatalyts have been made. Examples of this include incorporation of inorganic co-catalysts,[37] modification of electronic structure *via* elemental doping,[38,39] construction of composite heterojunction materials[40], engineering of the nanostructure morphology[41,42] and plasmonic metal sensitization[43,44]. One of the main disadvantages of these approaches is the material´s low absorption in the visible-region. An attractive alternative to target this problem is the inclusion of photosensitizers, also known as dye-sensitization.

The study of photocurrent generation through dye sensitization of semiconductors started with the work of Gerisher and co-workers in the 1960´s.[45] Their experiments lead to the discovery that excited dye molecules are able to inject electrons into the conduction band or to accept electrons from the valence band (hole injection) of the semiconductor. The relative position of the semiconductor energy bands and the molecule energy levels dictates the direction of the charge transfer.[46]

The application of this concept for the fabrication of an efficient photovoltaic device was demonstrated by Grätzel and O´Regan in 1991. Their dye-sensitized solar cell (DSSC) consisted of a film of nanoscaled $TiO_2$ particles deposited on a conducting glass substrate and sensitized with a ruthenium complex. Another conducting glass substrate was used as the counterelectrode and a iodide/triiodide redox electrolyte was used to mediate the charge transfer between the electrodes.[47] Figure 2.1 illustrates a typical DSSC. The efficiencies of DSSCs have been optimized by structural design of photosensitizers, redox mediators or hole transport materials, photoanode and cathode materials. Solar-to-electric power conversion efficiencies as high as 14.3% have been reported for DSSCs based on organic dyes and a liquid electrolytes.[48]
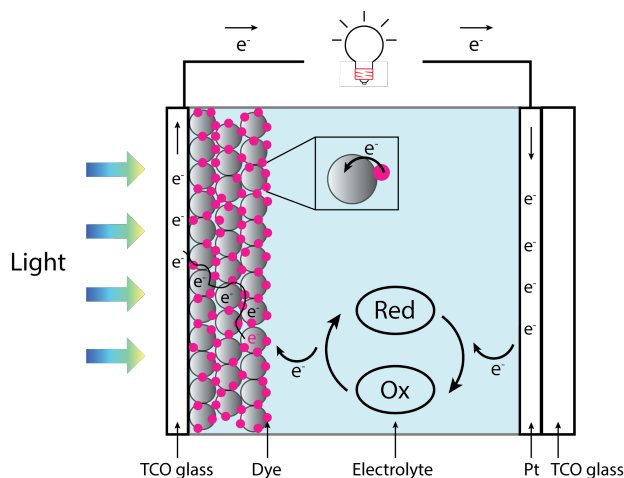
**Figure 2.1:** Illustration of a typical DSSC. Upon dye photoexcitation electrons are injected into the semiconductor nanoparticles. Electrons diffuse into the conducting glass substrate (TCO glass) and reach the counter electrode where Pt catalyses electron transfer to the redox electrolyte. The dye is regenerated by ET from the electrolyte.

As it was mentioned above, fuel formation reactions such as water oxidation and reduction of $CO_2$ require the transfer of multiple electrons, and therefore, a material where multiple charges can be accumulated needs to be incorporated in the artificial photosynthesis assembly. Dye-sensitized semiconductors are great candidates for this for several reasons. First, electron injection times at dye-sensitized semiconductors can be as fast as hundreds or tens of femtoseconds and with quantum yields near unity[49–51]. This means that loss processes such as radiative and non-radiative excited state decay and other quenching pathways are minimized.[52] Second, because each semiconductor nanoparticle can accommodate many dye molecules, several electrons can be injected into the same nanoparticle and the charges can be accumulated for a long time before recombining with the photosensitizer.[53,54] Accumulative charge transfer[36,55,56] and visible-light driven water splitting[57] in molecular-semiconductor assemblies has already been demonstrated. However, many advances are still needed before efficient device fabrication is accomplished.

Besides oxidative reactions such as water splitting, reductive reactions such the reduction of $CO_2$ or the generation of $H_2$ from protons, are possible with dye-sensitized semiconductors materials. P-type semiconductors such as NiO can be used to perform reductive photocatalysis.[58] This can be understood by thinking of a DSSC working in the reverse direction. For example, an excited photosensitizer attached to NiO can transfer electrons to a catalyst for $CO_2$ reduction. The photosensitizer would be regenerated by transferring of electrons from the NiO material.

Reductive photocatalysis can also be achieved by conduction band mediated electron transfer (CBM-ET).[59–61] That is, the transfer of electrons accumulated in the CB of semiconductors to catalysts that are active in their reduced states. To achieve visible-light

induced CBM photocatalysis is a challenging problem from the point of view that many different ET processes can take place simultaneously. Thus, it requires the design of functional nanoplatforms integrating photosensitizers and catalysts, where ET to the catalyst is favored. In this thesis, dye-sensitized semiconductor assemblies where CBM-ET is facilitated are presented in **Papers III** and **IV** (Chapter VI).

Dye-sensitized photoelectrosynthesis cells (DSPEC) are devices where both, oxidative and reductive solar fuel reactions take place by incorporating the properties of semiconductors and molecular chromophore-catalysts assemblies[19], Figure 2.2. In these devices, water splitting and fuel formation are separated into two half-reactions taking place at different compartments. By doing so, the need of matching the rates of both reactions can be eliminated. Moreover, problems such as (i) the mixing of oxygen and fuel products and (ii) the generation of undesired byproducts, can be avoided.[35]
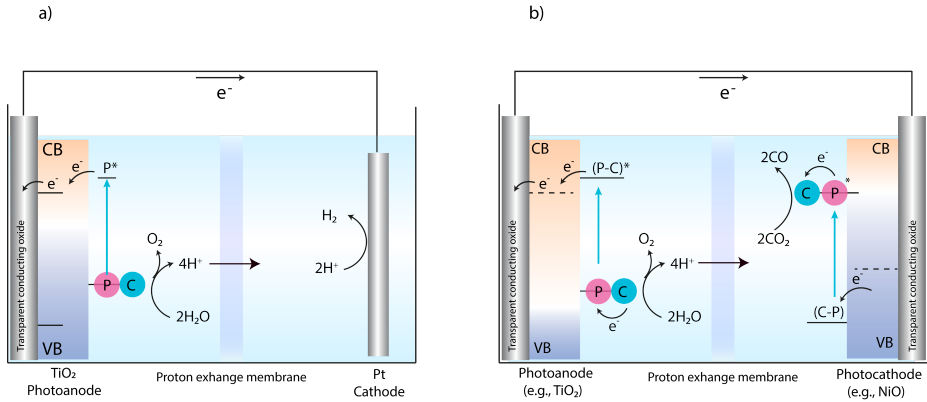


**Figure 2.2:** (a) Dye-sensitized photoelectrosynthesis cell for water splitting into hydrogen and oxygen. (b) Dye-sensitized photoelectrosynthesis cell for water oxidation and CO2 reduction. Adapted from reference 19.

## 2.2 Water oxidation function

Water oxidation—often referred to as water splitting—, Equation 2.1, requires the transfer of four electrons and four protons. Theoretically, the thermodynamic potential of this reaction is $E^0 = -1.23V$.[62] However, an overpotential is required to drive the photogenerated charge carriers to catalytic sites and to promote reduction and oxidation reactions.[63]

$$2H_2O\,(l) \rightarrow 2H_2\,(g) + O_2\,(g) \tag{2.1}$$

Photochemical water splitting requires the subsequent transfer of four electrons and consequently the absorption of four photons. In green plants, water oxidation is catalyzed

at the active site of the photosystem II (OEC) by a $Mn_4CaO_5$ cluster, which cycles through redox intermediates known as $S_i$ states $(i = 0 - 4)$.[64]. This involves a series of proton-coupled electron transfer steps in which one proton leaves the reaction center with each electron that is extracted. This mechanism results in a significantly reduced overpotential for the subsequent electron transfer steps.[62] The exact mechanism of O-O bond formation remains unknown, but most likely involves a high-valent manganese centre (IV or V) with a terminal oxyl radical and/or oxo species. Density functional theory (DFT)[1] calculations and characterization of model synthetic metal-complexes for water oxidation have supported the suggestion that a $Mn^{IV}$-oxyl radical in the center of the OEC is required for O-O bond formation.[65,66]

Based on the structure of the OEC and the knowledge regarding the mechanism of photosynthetic water oxidation, several synthetic bioinspired water oxidation catalysts consisting of mono-nuclear or di-nuclear metal complexes based on manganese, ruthenium, iridium, cobalt and iron have been developed.[67–73]. Photochemical water oxidation resulting in $O_2$ evolution has been achieved in homogeneous systems using bioinspired complexes and external sacrificial electron acceptors.[69,74]. However, linking a photosensitizer and catalyst in a supramolecular assembly can result in several detrimental excited state deactivation pathways which prevent efficient charge separation, such as in the example presented in **Paper I**. A better approach to photochemical water oxidation is therefore photoelectrochemical cells[57,75–79]. By anchoring chromophores and catalysts or chromophore-catalysts assemblies to semiconductors subsequent photon absorption and accumulation of charges and the use of sacrificial agents can be avoided. These photoelectrochemical cells are regenerative, which implies that products are constantly released as long as reactants and light are supplied and charge carriers are transported between the electrodes. Although the effectiviness of these approach has been demonstrated, obtaining long term stability and high overall solar energy conversion efficiencies remain a central challenge.[75]

## 2.3  Reductive chemistry

During the light independent reactions of photosynthesis in plants, reduction of $CO_2$ yields intermediates for the synthesis of sucrose and starch.[80] In contrast, reduction of (i) protons to generate hydrogen gas and (ii) reduction of $CO_2$ to produce fuels such as methane or methanol are the reduction reactions of interest in artificial photosynthesis. Therefore, the design principles of catalyst for $H^+$ or $CO_2$ reduction find inspiration in processes and molecules that are not related to photosynthesis. Accordingly, there are many different types of catalysts for the reduction of $H^+$ and $CO_2$, however, describing each of them is beyond the scope of this thesis. Therefore, I will only mention some relevant examples to the discussion topics in this work. The reader is referred to the cited references for more details.

Metal oxide semiconductors containing metallic co-catalyts such as platinum or gold have been the most widely studied materials to promote light-induced $H_2$ evolution.

---

[1]A quantum-mechanical method used to calculate the electronic structure of atoms, molecules and solids

To be able to drive this reaction with visible-light, sensitization of the semiconductor has become a common approach as in the water oxidation case. There are many examples of visible-light induced $H_2$ evolution in sensitized metal oxides using ruthenium photosensitizers[81–84], organic dyes[85,86] or quantum dots[87,88].

The reduction of $CO_2$ reduction is particularly challenging. The high stability of this molecule requires a large amount of energy to dissociate the C=O bond. Besides, reduction of $CO_2$ can yield a large variety of products such as carbon monoxide, formaldehyde and formic acid, among others.[89]. Moreover, hydrogen formation is a competitive reaction that occurs in the presence of water. Thus, developing a selective catalyst for the reduction of $CO_2$ into products of interest is a complicated task. The most studied heterogeneous catalysts for $CO_2$ photoreduction are based on metal oxide semiconductors and semiconductor-metal cocatalyst assemblies. These are often more stable compared to homogeneous molecular catalysts. However, heterogeneous catalyst are often poor in selectivity and cannot outcompete proton reduction.[90] Most of the molecular $CO_2$ reduction catalyst are metal complexes containing nickel, cobalt, rhenium or iron metal centers.[91] There are several reports on the photocatalytic reduction of $CO_2$ to CO using visible light and a homogeneous catalyst.[92–94]. However, photocatalytic conversion of $CO_2$ to methanol or methane requires the use of sacrificial agents or[95–97] potentially toxic materials[98,99]. Otherwise, homogeneous catalysts have not been able to maintain a constant photocatalytical activity over long periods of time.[100]

A particular group of molecular catalysts for $CO_2$ reduction are iron and cobalt metalloporphyrins and related metallomacrocycles.[91] In **Paper IV**, a cobalt porphyrin was used as a model electron acceptor in dye-sensitized semiconductors for the demonstration of CBM-ET in dye-sensitized semiconductor assemblies.

# Theory and experimental methods

## 3.1 Spectroscopy. Light-matter interactions

*Spectroscopy relies on a set of tools designed for the measurement and interpretation of the electromagnetic radiation resulting from light-matter interactions. The aim of this section is to describe the relevant theoretical considerations and spectroscopic methods for the study of the photophysical processes of solar energy conversion.*

### 3.1.1 Theory of electronic transitions

In order to understand the mechanisms behind the processes of solar energy conversion it is necessary to consider the principles of light-matter interactions. One of these fundamental principles is the wave-particle duality of elemental particles. The energy of photons—the elementary particles of electromagnetic radiation— depends on the frequency of the electromagnetic wave according to

$$E = h\nu = \frac{hc}{\lambda} \qquad (3.1)$$

where $h$ is Planck´s constant and $\nu$ is the frequency of the electromagnetic wave, which is equal to the speed of light divided by the wavelength, $\lambda$.

The mathematical description of the wave-like behavior of electrons in an atom is given by the atomic orbitals (wave functions $\Psi$). These represent the probability of finding an electron at a certain position relative to the nuclei.[101] The distribution of the electrons in molecules is represented by molecular orbitals (MOs), which are constructed by linear combination of the atomic wave functions. For electronic transitions, the assumption that the nuclei has fixed spatial coordinates is valid. This results in decoupling of the motion of electrons from that of nuclei (*Born-Oppenheimer approximation*). Under this approximation the wave function of a molecule can be simplified by separating its electronic and nuclear components, Equation 3.2.

$$\Psi_{total} = \Psi_{electronic}\Psi_{nuclear} \qquad (3.2)$$

The energies of the different electronic states corresponding to the wave functions can be obtained by solving the Schrödinger wave equation, Equation 3.3. In this equation, H is the Hamiltonian operator,[1] $\Psi$ is a wave function in a stationary (time-independent) state and E is the energy of the state. The values of energy are quantized (restricted to a discrete set of values).

$$\text{H}\Psi = \text{E}\Psi \qquad (3.3)$$

The photophysical processes involved in solar energy conversion are related to photoexcitation of electrons. That is, the promotion of electrons from lower to higher energy states—molecular orbitals—due to their interaction with light. For a photon to be absorbed by a molecule and produce an electronic transition, the first requirement is that the frequency of the electromagnetic radiation must match the energy gap between the

---

[1]A sum of operators corresponding to the kinetic and potential energies of the system

energy levels involved in the transition. For electronic transitions, this energy difference corresponds to ultraviolet (UV) and visible electromagnetic radiation.

Photoexcitation produces a displacement of electrons within the molecule thus inducing a dipole moment.[102] Mathematically, this can be described by considering the interaction of the electric field component of light with the charged particles of molecules. For an electronic transition between an initial state $m$, and a final state $n$, there is an associated electric dipole moment operator $\mu$, Equation 3.4. In this equation, $q_i$ and $r_i$ are the charge and position vector of each particle (electron or nucleus).

$$\mu = \sum_i q_i r_i \tag{3.4}$$

For an electronic transition to be allowed, the transition moment integral, Equation 3.5 must not equal zero.[103] The magnitude of the transition is given by the scalar product of the electric field vector of the radiation and the dipole moment vector of the molecule.[102] According to spectroscopic selection rules which contain symmetry, spatial (overlap) and electron spin (angular momentum) requirements, a transition with $R^{nm} = 0$ is said to be forbidden. For example, transitions between states of different total spin are strictly forbidden as the angular momentum is not conserved. However, these transitions may be permitted by interaction of the electron spin with the orbital motions of other electrons (spin-orbit interaction).[104] The square of the magnitude of $R^{nm}$ is the transition probability and it is related to the rate of change of population of the state $n$.

$$R^{nm} = \int \Psi_n^* \mu \Psi_m d\tau \tag{3.5}$$

To illustrate the different electronic states of a molecule and possible transitions between them a Jablonski diagram can be used, Figure 3.1.

After excitation to higher electronic and vibrational states, rapid excess energy dissipation (vibrational relaxation) to the lowest vibrational level of the electronic excited state occurs. DUe to the speed of this process, deactivation of the excited state by emission of a photon always originates from the lowest vibrational level (Kasha´s rule).[105] Emission between singlet states (fluorescence) or between states of different multiplicity (phosphorescence) is possible. Typical rate constants of phosphorescence are much smaller than those of fluorescence because of the forbidden nature of this process, which translates into slower kinetics.[105] Nonradiative transitions between states of the same or different multiplicity are known as internal conversion (IC) and intersystem crossing (ISC), respectively. Both processes are isoenergetic, that is, the energy of the system is maintained during the transition to the other state. These electronic transitions do not all have the same probability to occur and therefore, the intensities of the measurable properties related to the transitions, e.g. absorption and emission, are variable.

Following the *Born-Oppenheimer´s* approximation, the energy of a molecule in each electronic state can be described as a function of only the nuclear coordinates. These functions can be graphically represented by potential energy surfaces that contain vibrational energy levels. Upon an electronic transition, there is a simultaneous change in vibrational energy (vibronic transition). Compared to nuclear motion, vibronic transitions
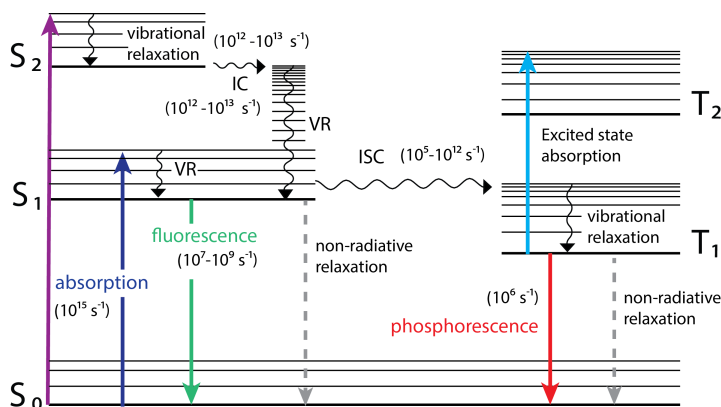
**Figure 3.1:** Jablonski diagram representing the electronic states of a molecule and the possible transitions between them. The thin horizontal lines represent vibrational levels within the electronic level. $S_i$ represent singlet states (all electrons paired, total $spin = 0$) and $T_i$ represent triplet states (two unpaired electrons, total $spin = 1$). The numbers represent typical rate constant values for each type of transition.

to higher states occur very rapidly. Thus, transitions between the potential energy surfaces are more likely to occur vertically and their intensity is proportional to the overlap between the vibrational wavefunctions of the two states, Figure 3.2. This is known as the *Franck-Condon principle*.

In large polyatomic molecules, electronic transitions involves manifolds of vibronic levels which are closely spaced; so the probability $P_n$ of a transition contains contributions from all individual levels and becomes an integral over the energy range of the transition. The approximate solution to this integral is given by Equation 3.6. The derivative of this expression with respect to time is known as the *Fermi´s golden rule* and represents the rate at which the transition occurs, Equation 3.7.[102] In these equations $\rho_n$ is the density of states (the number of available vibronic states) and $H_{nm} = \langle \Psi_n | \hat{H}\prime | \psi_m \rangle$ where $\hat{H}\prime$ represents any perturbation responsible for driving the transition from the initial to the final state.

$$P_n = \frac{2\pi}{\hbar} H_{nm}^2 \rho_n t \tag{3.6}$$

$$\frac{d}{dt} P_n = \frac{2\pi}{\hbar} H_{nm}^2 \rho_n \tag{3.7}$$

The quantum yield $\Phi$ of a transition is a measure relating to its probability, reflecting the efficiency of the process, Equation 3.8.[104]

$$\Phi = \frac{\text{No. of events}}{\text{No. of photons absorbed}} \tag{3.8}$$

For an emissive deactivation pathway there is an associated natural lifetime, $\tau_r^0$, which is defined as the reciprocal of the radiative rate constant $k_r^0$, Equation 3.9. This
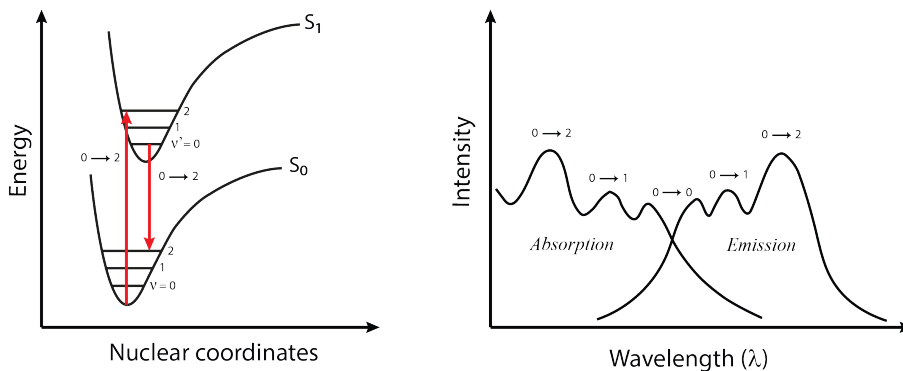
**Figure 3.2:** Left: schematic representation of the Franck-Condon principle. The curves represent potential energy surfaces of the ground state and and first excited singlet states of a molecule. The vertical lines inside the curves represent vibrational energy levels within the electronic levels. Right: representation of absorption and emission spectra resulting from electronic transitions between the potential surfaces displayed to the left. Adapted from Lakowicz (2006).[105]

kinetic property corresponds to the isolated radiative process in which the excited state decays spontaneously as a function of time. This process follows first-order kinetics so it depends on the first power of the concentration of electronically excited molecules $[\text{M}^*]$, Equation 3.10.[102]

$$\tau_r^0 = \frac{1}{k_r^0} \tag{3.9}$$

$$-\frac{d}{dt}[\text{M}^*] = k_r^0[\text{M}^*] \tag{3.10}$$

In the same manner, there is a rate constant $k_{nr}$ associated with any nonradiative deactivation process. The observed lifetime $\tau$ of an excited state is that resulting from the contributions of all deactivation pathways and can be expressed as

$$\tau = \frac{1}{\sum_i k_i} = \frac{1}{k_r^0 + \sum k_{nr}} \tag{3.11}$$

The quantum yield of any deactivation process $i$, $\Phi_i$, can be expressed in relation to the rate constants $k_j$ of all other deactivation pathways as follows

$$\Phi_i = \frac{k_i}{\sum_j k_j} = k_i \times \tau \tag{3.12}$$

The process by which the quantum yield of emission decreases is known as quenching and it occurs by different mechanisms. Collisions with surrounding molecules, dynamic quenching, or the formation of non-fluorescent species in the ground state, static quenching, are two examples. Also, the energy of the excited molecule may be transferred to an acceptor in its ground state by dipole-dipole interactions in a process known as resonance

energy transfer, resulting in a lower quantum yield. This process is highly dependent on the distance between the two species, and the extent of overlap between the emission spectrum of the donor and the absorption spectrum of the acceptor. Electron transfer from the excited state of a donor to an acceptor is another process that also results in the quenching of emission. This process is especially relevant for solar energy conversion because it results in a charge separated state. The details of this process are discussed in section 3.2.

### 3.1.2 Spectroscopic techniques

The intensity of absorption and emission of molecules are usually represented as a function of the wavelength $\lambda$ in so-called spectra. The shape of the spectra depends on the chemical structure, the solvent in which the molecule is dissolved as well as the distribution of vibrational and rotational states.[105] Absorption and emission spectra of molecules are broad as a result of this distribution. In most cases, the emission spectrum of a molecule is the mirror image of the $S_0$ to $S_1$ absorption band and, since the transition involves the same vibrational levels, the spectra are symmetric. However, the energy of the emission is typically lower than that of absorption (Stokes shift) as a consequence of Kasha´s rule. Furthermore, emission spectra are typically independent of the wavelength of excitation. Absorption and emission spectra cross at the 0-0 (zero zero) transition, which corresponds to electronic transitions to and from the lowest vibrational states in each electronic state.

Measurement of absorption and emission spectra of molecules and materials is fundamental for the characterization of their photophysical and photochemical properties. Illustrations of typical instrumental setups to perform these measurements are depicted in Figure 3.3 and Figure 3.4.
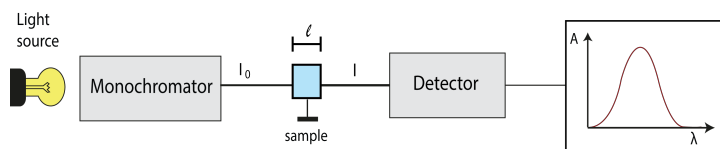


**Figure 3.3:** Schematic representation of a single beam spectrophotometer setup

According to the Lambert-Beer law, the absorbance A of a sample at a particular wavelegth $\lambda$, has a linear dependence with the product of the molar absorption coefficient $\varepsilon(\lambda)$, the path length of the travelling light beam $l$, and the concentration $C$ of the molecules in the solution, Equation 3.13. Here, $I_0$ and $I$ are the light intensities of the beam before and after passing through the sample respectively. The molar absorption coefficient $\varepsilon$ is proportional to the probability of transition between two electronic states, and thus is used as a quantitative measure of the light harvesting capability of a molecule.

$$\mathrm{A}(\lambda) = -log\frac{I_0}{I} = \varepsilon(\lambda)lC \tag{3.13}$$

The Lambert-Beer law is valid for low concentration solutions. At high concentrations, alteration of the refractive index or formation of aggregation complexes result in deviations from this law.
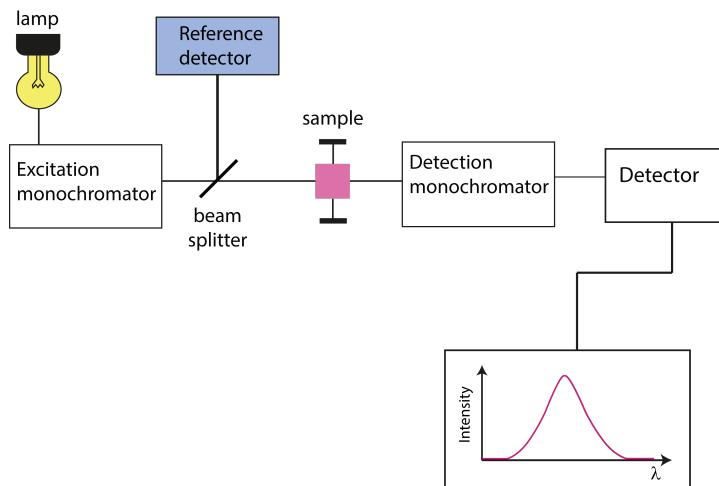
**Figure 3.4:** Schematic representation of a right-angle spectrofluorometer setup

From Equation 3.8, it can be derived that determination of the emission quantum yield, $\Phi_r$, requires measurement of the radiation intensity and the number of emitting molecules. These quantities are directly related to the intensities of absorption, $A$, and emission, $I$. Accordingly, the quantum yield of emission can be expressed as in Equation 3.14. However, this is only valid under steady-state conditions[2] and if the intensities are recorded under identical conditions of irradiance and detection.[102] Due to these difficulties, the quantum yield of emission is usually determined with the use of a reference with a known $\Phi_r$ and then the emission quantum yield of the sample is given by Equation 3.15, where $R$ and $S$ are used to indicate properties of the reference and the sample respectively.

$$\Phi_r = \frac{I}{A} \tag{3.14}$$

$$\Phi_r^S = \Phi_r^R \frac{A_R}{A_S} \frac{I_S}{I_R} \left(\frac{\eta_S}{\eta_R}\right)^2 \tag{3.15}$$

On the other hand, direct quantification of photons comes with several complications and therefore an indirect method is commonly used. This aproach involves the use of a chemical actinometer, an emitter with a known quantum yield and a concentration that can be easily determined.

Measurement of emission lifetimes is possible by using time-resolved spectroscopic techniques. Time correlated single photon counting (TCSPC) is one of the most commonly used methods for this purpose, Figure 3.5.

During this measurement the sample is excited with a pulsed monochromatic light source with a defined repetition frequency. A time to amplitude converter (TAC) generates a voltage ramp initiated at the time of the excitation pulse ($t_1$). The ramp builds up

---

[2]Continuous light irradiation supply and build up of steady concentration of excited molecules

linearly with time until the arrival of an emitted photon to the detector at $t_2$. The voltage is amplified and converted to a numerical value by an analog-to-digital converter (ADC). The values are collected until a desired number of events is reached and a histogram of number of counts versus time is built. To obtain the real emission decay of the sample, the instrument response function (IRF), a response of the instrument to a sample with zero lifetime is deconvoluted from the intensity decay. The IRF gives the overall timing precision of the system and depends on the detector characteristics and the timing electronics.[105]
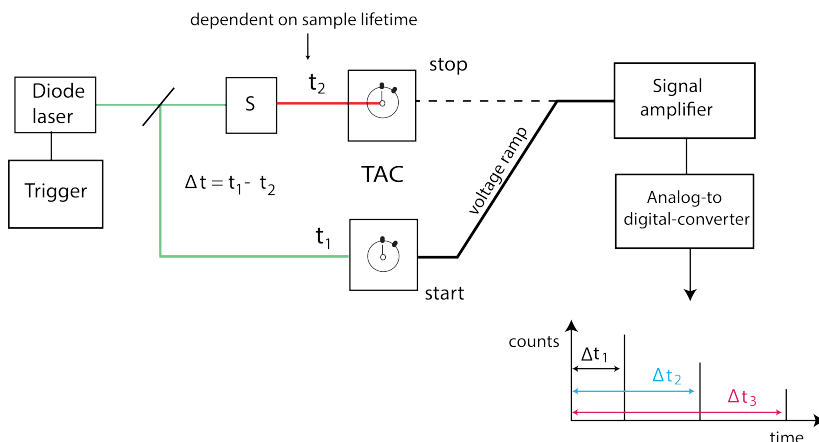


**Figure 3.5:** Schemematic of the instrumental components and principles of a TCSPC measurement.

## 3.2 Photoinduced charge separation

### 3.2.1 Theory of photoinduced electron transfer

Photoinduced electron transfer (PET) is the process by which a photoinitiated charge separated state is generated. During this process, an electron transfer between a donor and an acceptor where either one of them is in the excited state occurs. Intramolecular PET between a donor in the excited state and an acceptor in the ground state can be represented as in Equation 3.16. Here, D*|A is the excited donor-acceptor complex (or charge transfer complex), a state formed by electrostatic interaction, and D$^+$|A is the charge separated state. The direction of the electron transfer is determined by the redox potentials of the ground and excited states.[105]

$$ D \mid A \xrightarrow{h\nu} D^* \mid A \xrightarrow{k_{ET}} D^+ \mid A^- \qquad (3.16) $$
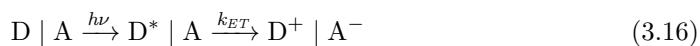
The change in standard Gibbs energy for such a reaction occurring in a solvent with a dielectric constant equal to $\epsilon$ can be described by Equation 3.17.[106] Here, the first and second terms are the oxidation and reduction potentials of the donor and the acceptor

respectively, and $\Delta G_{00}$ is the energy of the 0-0 electronic transition of the donor. The last term is the electrostatic force in the ionic pair formed after the electron transfer, where $d$ is the distance between the charges.

$$\Delta G = E(\text{D/D}^+) - E(\text{A/A}^-) - \Delta G_{00} - \frac{e^2}{\epsilon d} \tag{3.17}$$

A classical physical description of photoinduced electron transfer is provided by *Marcus theory*. According to this theory, the potential energy surfaces of the donor-acceptor complex (DA) and charge separated state can be represented as parabolic functions.[106] At the crossing point of the parabolas there is a transition state through which the donor-acceptor complex moves to the charge separated state if enough activation energy $\Delta G^{\ddagger}$ is supplied.[107] Equilibrium relaxation to the charge separation state requires reorganization of the system for the new charge distribution. The energy dissipated through this relaxation is known as the reorganization energy, $\lambda$,[3] and it is proportional to the separation between the minima corresponding to the initial and final states, $q_R$ and $q_P$, and to a force constant, $f$ as in Equation 3.18.[108]

$$\lambda = \frac{1}{2}f\big(q_R - q_P^2\big) \tag{3.18}$$

The reorganization energy term contains contributions from nuclear configuration distortions (inner $\lambda$) and from polarization reorientation of the surrounding solvent molecules (outer $\lambda$).

By recalling the Arrhenius relationship between rate constant and activation free energy, the rate constant of the electron transfer, $k_{ET}$ can be written as in Equation 3.19. Here, $\Delta G^0$ is the overall free energy of the reaction, $\lambda$ is the reorganization energy, $k_B$ is the Boltzmann constant and $A$ is a prefactor depending on the probability of crossing the barrier top.[108]

$$k_{ET} = A\exp\left[-\frac{(-\Delta G^0 + \lambda)^2}{4\lambda k_B T}\right] \tag{3.19}$$

According to this equation, three possible cases in the *Marcus* model are possible,[109] Figure 3.6:

- The normal region where the rate of ET increases with the driving force: $\Delta G_0 < \lambda$

- The special case where there is no activation barrier for the reaction: $\Delta G_0 = \lambda$

- The inverted region where the rate of ET decreases with driving force: $\Delta G_0 > \lambda$

Photoinduced long-range electron transfer (such as that needed in molecular models for artificial photosynthesis) is known to occur *via* two main different mechanisms: (1) multistep hopping with intermediate states where the electron-hole pair is temporarily localized and (2) direct tunneling from donor to acceptor.[32,108,110] In the tunneling mechanism, the crossing of an energy barrier is not required, and quantum effects need to be introduced (semi-classical description). The rate of ET is distant dependent and is

---

[3]Notice that $\lambda$ is also used as a symbol for wavelength in other contexts
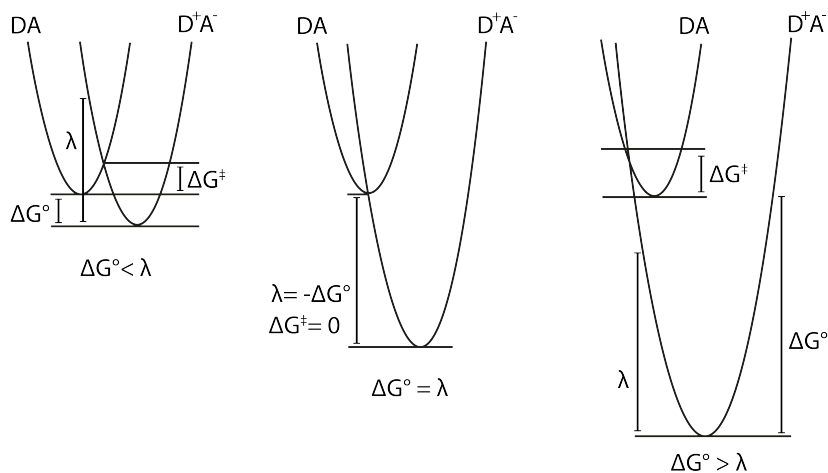
**Figure 3.6:** Simplified representation of three cases for Marcus theory of electron transfer. The normal region (left), the activationless case (center) and the inverted region (right). Adapted with permission from Metzger R.[109]

given by the density of acceptor states and the electronic matrix element that combines the donor and acceptor states, electronic coupling.[108] Such is the case of PET from a photosensitizer bound to a metal oxide which will be discuss in the next Section (section 3.2.2).

As mentioned in Chapter 2, several examples of artificial models with photoinduced long-range charge separation have been reported in the literature. However, rapid charge (electron-hole) recombination prevents the system from maintaining the charge separated state for enough time to allow for fuel forming reactions. Thus charge recombination is regarded as one of the main loss processes in solar energy conversion. However, charge separation can become inefficient due to the occurrence of other electronic transitions that prevent the charge from being transferred to the final acceptor. For example, the photogenerated energy might be lost due to the charge being localized at other parts of the molecule—electron transfer—, or by intramolecular energy transfer. Thereafter, emissive or non-emissive relaxation to the ground state can occur without reaching the final desired separated state. Such is the case of the model $Ru-Mn_2$ model complexes that will be discussed in Chapter 4.

### 3.2.2 Photoinduced electron transfer at dye sensitized semiconductors

So far, electronic transitions in molecular systems have been described in terms of energy levels and molecular orbitals. However, when it comes to solid state materials, band structure is a better approach for the description of their electronic and optical properties. In large arrangements of periodic lattices of atoms such as crystals, the atomic orbitals of each atom overlaps with those of its neighbors broadening the orbitals into band

energy levels which are sets of energy levels so closely spaced that they can be considered a continuum.[111] The energy difference between the top of the highest occupied band (valence band, VB) and the bottom of the lowest unoccupied band (conduction band, CB) is the *bandgap* of a material. When electrons exist in the conduction band, they can move freely in the material and act as charge carriers. Solid materials can be classified according to the size of the bandgap, Figure 3.7
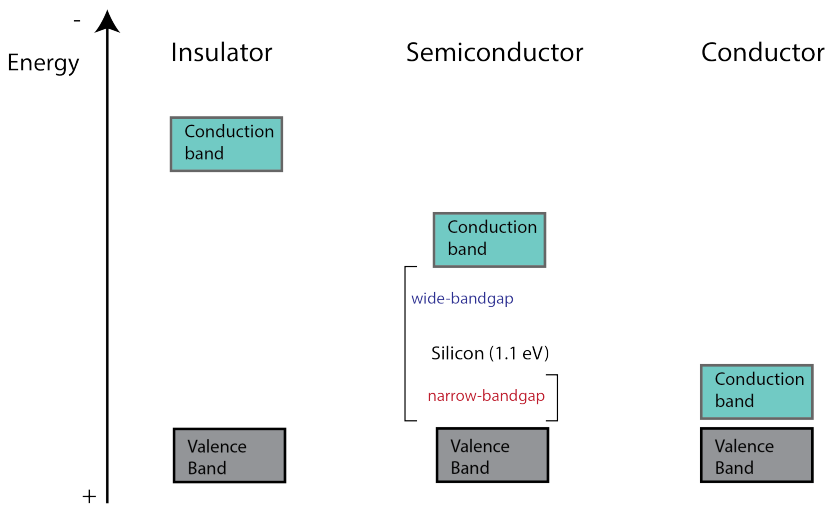


**Figure 3.7:** Relative size of the bandgap of solid materials

Compared to the bandgap of silicon, the relatively wide bandgap of metal oxide semiconductors requires dye-sensitization for their use in visible-light harvesting applications. $TiO_2$ is so far the most commonly used semiconductor in dye-sensitized photoelectrochemical cells and photocatalysis applications. The fabrication of this non-toxic material is of low cost and it possesses good stability, high photocatalytic activity and strong oxidizing power.[112] $TiO_2$ is considered to be an n-type semiconductor although formally, an n-type semiconductor is one which has been doped with impurities that contribute with energy levels close to the conduction band. In doing so, the population of free electrons is increased resulting in increased conductivity. This is, however, not the case for $TiO_2$. The existence of oxygen vacancies in its structure gives rise to states in the band gap by localization of electrons at $Ti^{3+}$ centers, resulting in a similar effect.[113,114] Moreover, the principles of dye-sensitized semiconductor devices imply that the population of the conduction band by electron injection from the dye results in electrons being the majority charge carriers, which also falls within the definition of an n-type semiconductor.

Sensitization of metal oxide semiconductors arises from chemical interactions between the semiconductor atoms and specific anchoring groups in the dyes such as carboxylic and cyanoacrylic acid. The conduction band of the semiconductor can be populated by photoinduced electron transfer—electron injection— from the photoexcited dye if there is a driving force for this process to occur, a mechanism that was first verified by Gerisher, Tributsch and co-authors,[115] see Figure 3.8. For efficient charge separation

in dye-sensitized semiconductors the rate of electron injection must be fast enough to compete with intramolecular relaxation. The fastest PET in dye-sensitized $TiO_2$ occurs in the subpicosecond timescale, however, injection rates as slow as hundreds of picoseconds have been measured.[51]
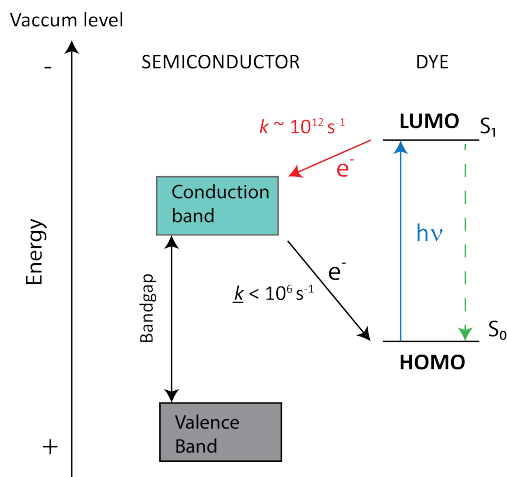


**Figure 3.8:** Schematic representation of the relative energy levels of dye and semiconductor and the direction of forward and back- electron transfer processes.

A description of this electron transfer process can be done by recalling Marcus theory and representing the acceptor as a manifold of parabolas being a continuum of available states, Figure 3.9. Each point of the reactant surface energy curve is then a transition state and consequently, the rate of ET would be exclusively determined by the electronic coupling.[116]
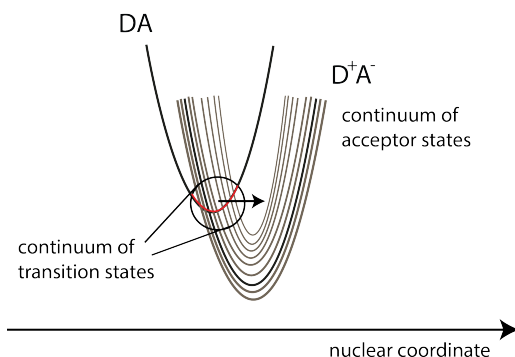


**Figure 3.9:** Marcus theory representation of PET in dye-sensitized semiconductors.

The efficiency of charge separation in dye-sensitized semiconductors is to a large extent dependent on the rate of electron injection, which in practice not only depends on the electronic coupling but also on several factors such as the structure of the dye,[117,118] the environment (solvent choice and pH) and the relative energies of the excited dye level and the unoccupied semiconductor acceptor states.[51]

Once the electron has been injected into the conduction band, a CSS will exist until the electron recombines with the cation radical of the photosensitizer. This process is referred to as charge recombination or back-electron transfer (BET), see Figure 3.8. In contrast to the forward electron transfer, BET is thermally activated and it does not involve a continuum of energy levels of the acceptor. Therefore, despite the large driving force, it is a significantly slower process which is believed to lie in the Marcus inverted region.[119–121].

### 3.2.3 Experimental methods for the characterization of PET

**Time-resolved absorption spectroscopy**

The characterization of PET mechanisms and intermediate transient states is possible by measurement of the absorbance of a sample as a function of time after excitation with a pulse of light— a spectroscopic technique known as flash photolysis or transient absorption spectroscopy.[122] Data is usually represented as the difference between the initial absorption of the sample ($A_{GS}(\lambda)$) and its absorption after photo-excitation ($A_{ES}(\lambda)$) as in Equation 3.20. Negative differential absorption ($\Delta A$) signals appear due to ground state depopulation while positive signals correspond to absorption in the excited state. Monitoring ($\Delta A$) signals as a function of time– transient absorption curves– is useful for the calculation of the lifetime of a CSS and the rate constants of charge recombination. To illustrate this, photoinjection from a dye adsorbed onto a semiconductor results in a positive ($\Delta A$) at the wavelengths of absorption of the dye radical cation. The decay of this signal as a function of time corresponds to the kinetics of the radical cation-electron recombination.

For the experimental work presented in this thesis, a flash photolysis experimental setup as illustrated in Figure 3.10 was used. Pulsed excitation light with 10 Hz repetition rate was generated using a Nd:YAG laser and an optical parameter oscillator (OPO). Probe light was generated with a Quartz Tungsten Halogen (QTH) lamp. Transient absorption spectra were measured using either a charge-coupled device (CCD), or constructed from single-wavelength transient absorption decays. Transient absorption decays were measured using either a photomultiplier (PMT) or a photodiode-based detection system.

$$\Delta A(\lambda) = (A_{ES}(\lambda) - A_{GS}(\lambda)) \tag{3.20}$$

**Redox potentials**

Experimental determination of the donor and acceptor redox potentials can be done by electrochemical techniques. The redox potential $E^0$ of a half reaction can be measured by cyclic voltammetry (CV), an experiment usually performed in a three electrode cell
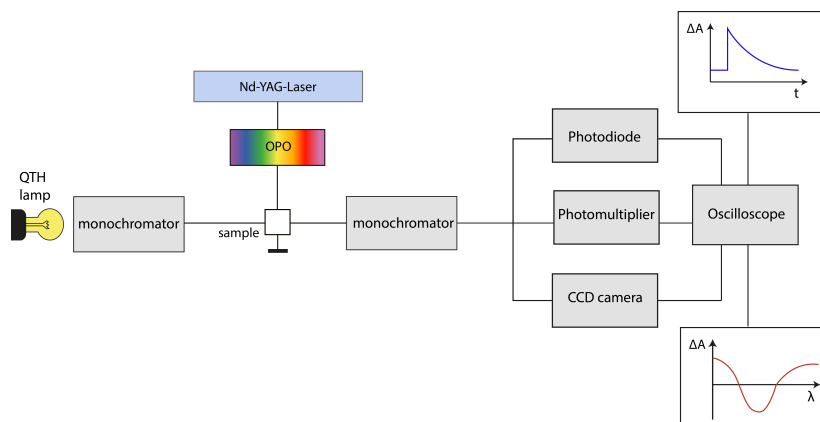
**Figure 3.10:** Schematic representation of a flash photolysis experimental setup.

configuration. During a CV measurement, the potential of a working electrode (WE) is linearly varied with time, starting from a potential where no reaction occurs at the electrode and moving to potentials where either reduction or oxidation occurs. As the potential is varied, electrical current, $i$, flows between the WE and a counter or auxiliary electrode (CE) as the chemical species in the solution are oxidized or reduced. The current reaches a maximum at the peak current, $i_p$, and then decreases. Thereafter, the direction of the linear sweep is reversed at time = $t_R$. The variation in the WE's potential is measured against a reference electrode (RE), which the potential is constant.[123] A plot of $i$ versus E is constructed and the formal potential, $E^{0\prime}$ is calculated as follows: $E^{0\prime} = \frac{1}{2}(E_{pc} - E_{pa})$, see Figure 3.11.
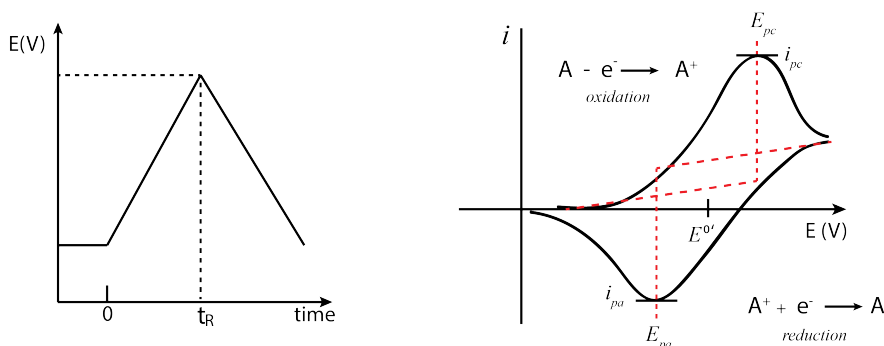


**Figure 3.11:** Left: Variation of the potential as a function of time in cyclic voltammetry. Right: A typical CV response for a reversible oxidation-reduction reaction.

The redox potential of the excited state of a donor, D*, can be calculated by finding the intercept of the normalized absorption and emission spectra of the molecule.[124] This value corresponds to the $E_{0-0}$ gap, the difference in energy between the lowest unoccupied

molecular orbital (LUMO) and the highest occupied molecular orbital (LUMO)— the energy difference between the ground and excited electronic states for the vibrational 0-0 transition. The redox potential of the excited state can then be computed as in Equation 3.21.

$$E^{0\prime}_{D^*/D^{+*}} = E^{0\prime}_{D^+/D} + E^{0-0} \tag{3.21}$$

**Spectroelectrochemistry**

Combination of spectroscopic and electrochemical techniques is commonly employed in the characterization of photochemical and electrochemical reactions. Measurement of the spectroscopic properties of a chemical species while it is reduced or oxidized can be used to investigate reaction kinetics, Figure 3.12. It can also provide information that is later correlated to transient absorption data in order to identify reaction intermediates and determine rate constants of photoinduced reactions. Practical examples of this can be found in the following Chapters.
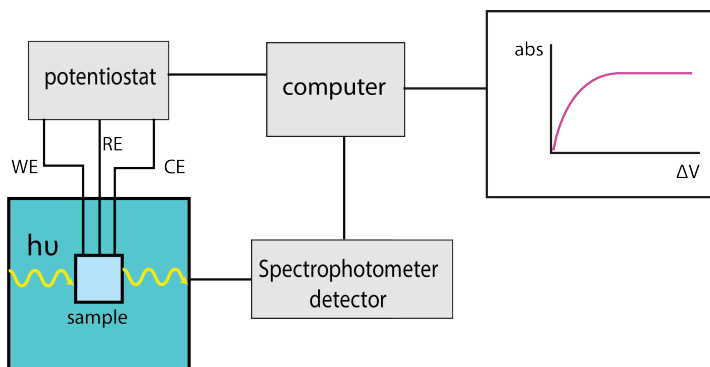


**Figure 3.12:** Schematic representation of an experimental setup for spectroelectrochemical measurements.

# A model Ru−Mn$_2$-complex for water splitting

*In this chapter, the photophysical properties of a Ru–Mn$_2$ complex for photochemical water oxidation are described, illustrating the challenges of supramolecular approaches to solar fuels.*

## 4.1 Photophysics of Ru(II)polypyridyl complexes

Due to their unique photophysical properties, ruthenium(II)polypyridyl complexes have been widely used as photosensitizers in the study of photochemical solar energy conversion. In particular, their high molar absorption coefficients in the visible region and their long excited state lifetimes makes them interesting for application in artificial photosynthesis. Moreover, the possibility of tuning their excited states properties by structural modification[13] makes them versatile photosensitizers that can be designed to target a desired application.

According to ligand field theory, coordination of the Ru(II) cation with electron donating ligands results in splitting of its degenerated d-orbitals into lower and higher energy orbitals. The resulting energies of the orbitals depend on the extent of electronic repulsion between electrons from the ligands and *d*-orbital electrons. Ru(II)polypyridyl complexes displaying long-lived excited states have an octahedral-like coordination geometry that results in a *d*-orbital splitting as that represented in Figure 4.1.
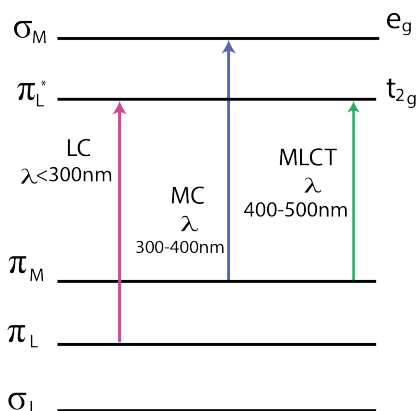


**Figure 4.1:** Schematic representation of the different absorption transitions in Ru(II)-polypyridil complexes.

The observed long lifetime of Ru(II)polypyridyl complexes corresponds to their triplet metal-to-ligand charge transfer ($^3$MLCT) state, which is generated after fast intersystem crossing from the lowest singlet metal-to-ligand charge transfer ($^1$MLCT) state.[125] The $^3$MLCT state decays to the ground state by either emission or non-radiative transitions. In the presence of molecular oxygen, the excited state of Ru(II)polypyridyl complexes is quenched by energy transfer to the triplet ground state of O$_2$ resulting in reduced emission quantum yield and shorter lifetime.[126] Therefore, removal of O$_2$ is essential when measuring the excited state properties of the complexes.

The design of many Ru(II)polypyridil complexes is based on the structure of the well known parent complex Ru(II)-tris-bipyridine ([Ru(bpy)$_3$]$^{2+}$. Its absorption spectrum and structure are shown in Figure 4.2. In deoxygenated acetonitrile (CH$_3$CN) solutions, its emission quantum yield is approximately 0.06[127] and its excited state lifetime is ca 1 μs.[127] Besides the charge transfer transition giving rise to the characteristic MLCT absorption band, there are additional bands corresponding to ligand-centered (LC) and metal-centered (MC) transitions.
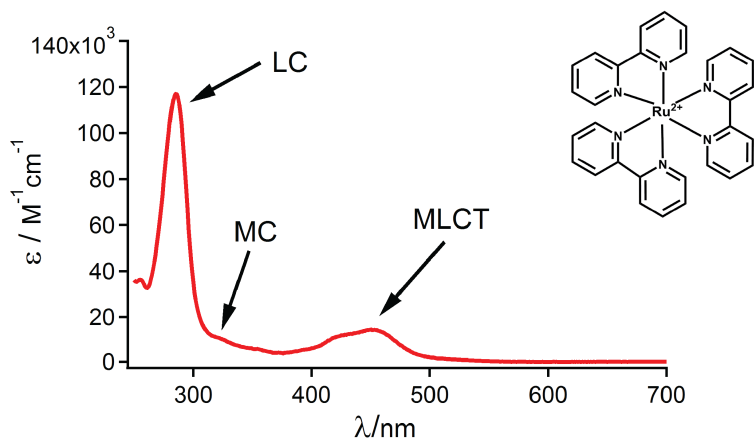


**Figure 4.2:** Absorption spectrum of [Ru(bpy)$_3$]Cl$_2$ in CH$_3$CN. The inset shows the structure of the complex.

Any modification on the bpy-ligands with electron withdrawing or donating groups will result in a change on the distribution of molecular orbitals and therefore on the electronic transitions and photophysical properties of the complex. Such is the case of the photosensitizers studied in Paper I, which structure was modified with a linker unit for the purpose of binding with the water oxidation catalyst.

## 4.2 Dinuclear manganese water oxidation complex

The bioinspired OEC dinuclear manganese complex (Mn$_2$-complex) used in **Paper I** was previously reported by Karlsson and co-workers and was the first of its type to catalyze water oxidation in the presence of [Ru(bpy)$_3$]$^{3+}$ as a single electron oxidant.[69] More importantly, this complex catalyzes photochemical water oxidation with a [Ru(bpy)$_3$]$^{2+}$ type photosensitizer when using sodium persulfate as an external electron acceptor as illustrated in Figure 4.3.

The structure of the (Mn$_2$-complex) is shown in Figure 4.4. The success on the design of this complex is the replacement of the benzylic amines present in many previously reported Mn-complexes with the negatively charged carboxylate groups, which reduced the redox potentials of the metal center in order to facilitate catalytic activity with
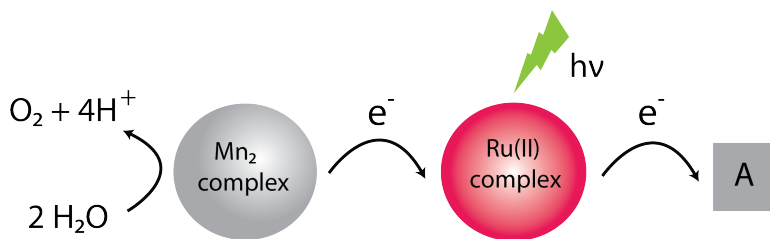
**Figure 4.3:** Schematic representation of photocatalytical conversion of water to oxygen by a Mn2-complex in the presence of a single electron oxidant $[Ru(bpy)_3]^{2+}$.

$[Ru(bpy)_3]^{2+}$-type photosensitizers.[69] The catalytic activity of the complex and the light-driven oxygen evolution are optimal at pH = 7.2.
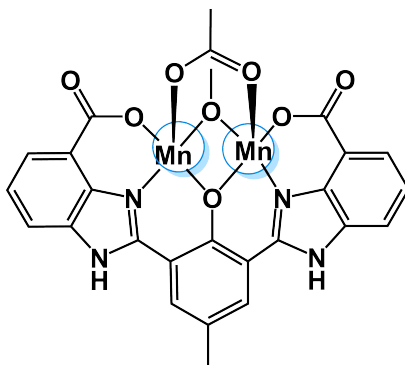


**Figure 4.4:** Structure of the dinuclear manganese complex mimicking the OEC.

The development of a supramolecular assembly where both light harvesting and water oxidation takes place is desirable. By bringing the photosensitizer and the catalyst closer together, it is thought that electron transfer could be facilitated and controlled in a more optimal way. However, this comes with several complications as discussed in more detailed the following Section (section 4.3).

## 4.3 Linking photosensitizer and catalyst

In **Paper I**, the dinuclear $Mn_2$-complex was linked to $[Ru(bpy)_3]^{2+}$-type photosensitizers to build a supramolecular assembly for photocatalytic water oxidation. To be able to couple the two units, one of the bipyridine ligands was substituted by a phenantroline ligand containing an imidazolium-phenol unit, named precursors $P_{a-c}$. Their structures are shown in Figure 4.5. From these precursors, three Ru(II) ligand-complexes were prepared named Ru(II)-complexes **a-c**. In complex **b**, electron withdrawing ethyl ester groups ($CO_2Et$) were introduced in the pyridine ligands with the purpose of delocalizing the excited state away form the $Mn_2$ center. An additional structural modification was made in complex **c** by introducing a phenyl substituent onto the central imidazole to decrease the planarity by increasing the steric strain. Complex **c** was used to prepare the $Ru-Mn_2$ dyad upon reaction with manganese(II) acetate. The dyad was insoluble in organic solvents, therefore, the photophysical characterization was performed in water-acetonitrile mixtures. Chemical water oxidation with the dyad was possible by using $[Ru(bpy)_3]^{3+}$ as an oxidant. However, the photochemical water oxidation in the presence of an external electron acceptor failed despite the high metal-based oxidation potential of the dyad (1.6 V *vs.* NHE). Studies of the photophysical properties of the dyad and the Ru-complexes was necessary to understand the reason behind this.
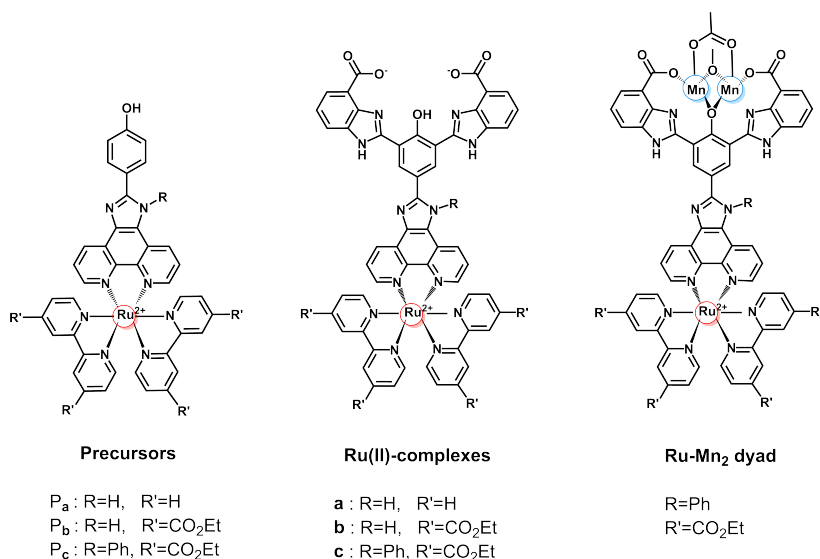


Precursors

$P_a$ : R=H,   R'=H
$P_b$ : R=H,   R'=CO$_2$Et
$P_c$ : R=Ph, R'=CO$_2$Et

Ru(II)-complexes

**a** : R=H,   R'=H
**b** : R=H,   R'=CO$_2$Et
**c** : R=Ph, R'=CO$_2$Et

Ru-Mn$_2$ dyad

R=Ph
R'=CO$_2$Et

**Figure 4.5:** Structures of the Ru(II)-ligand complexes, their corresponding precursors $P_{a-c}$ and the $Ru-Mn_2$ dyad.

## 4.4 Photophysical characterization

The absorption spectra of the Ru(II) ligand complexes, the precursor P$_a$ and the Ru−Mn$_2$ dyad are shown in Figure 4.6. They all display a pH sensitive MLCT band centered at $\lambda \approx 450nm$. The band is broad and has a hump at $\lambda = 480$nm in neutral pH. This could be interpreted as a mixed excited state that contains the MLCT state. Time-dependent density functional theory (TDDFT) calculations of the optimized precursor in water predicted that the lowest HOMO-LUMO transition should occur at $\lambda = 451$nm and corresponds to a charge transfer from the phenol to $\pi^*$ orbitals on the bpy ligands. It is postulated that the broad band contains both this and the MLCT transition. At high pH, the hump becomes more evident and the molar extinction coefficient increases, especially at lower wavelengths. For the precursor, an additional absorption feature is observed between 500–550 nm. This could be explained by a red-shifted HOMO-LUMO excitation in the deprotonated precursor as predicted by the TDDFT calculations.

At low pH a single peak appears, most probably representing the unperturbed MLCT state. This can be confirmed from the long emission lifetime of 858 ns measured for the precursor, comparable to the lifetime of $[\text{Ru(bpy)}_3]^{2+}$ in deoxygenated acetonitrile.
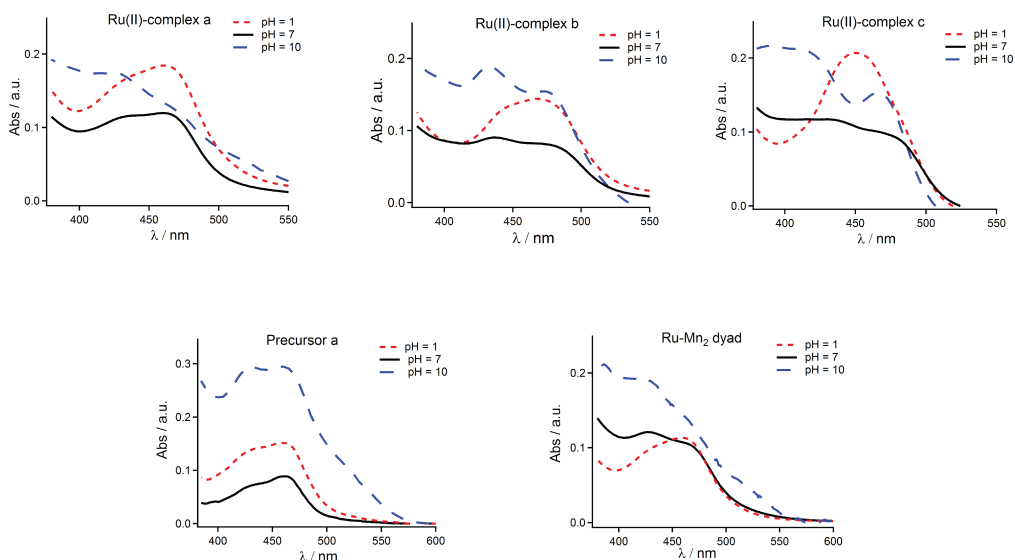


**Figure 4.6:** Absorption spectra of the Ru(II) ligand complexes, the precursor $P_a$ and the Ru−Mn$_2$ dyad displaying the MLCT band.

Emission of the Ru(II) ligand complexes and the Ru−Mn$_2$ dyad was strongly quenched as the pH was increased as exemplified in Figure 4.7. This was further confirmed by measuring the emission lifetimes, Figure 4.8. Emission quantum yields and lifetimes of the

precursor **a**, the ligand complexes and the dyad are reported in Table 4.1. The emission quantum yields, $\Phi$, were calculated according to Equation 4.1.

$$\Phi = (\eta/\eta_{ref})(\mathrm{A}_{ref}/\mathrm{A})(\mathrm{I}/\mathrm{I}_{ref})\Phi_{ref} \qquad (4.1)$$

where A and $\mathrm{A}_{ref}$ are the absorbance values of the samples at the excitation wavelength; I and $\mathrm{I}_{ref}$ are the emission intensities of the samples, given by the signed area of the emission spectra; $\Phi_{ref}$ is the quantum yield of the reference and $\eta$ is the refractive index. The reference sample consisted of $[\mathrm{Ru(bpy)_3}]^{2+}$ in a 1:1 mixture of acetonitrile/water and its quantum yield was calculated in relation to the quantum yield of $[\mathrm{Ru(bpy)_3}]^{2+}$ in acetonitrile with a value of 0.06.[127]

The excited-states lifetimes were obtained by fitting the individual decay curves to exponential decay models with a numerical reconvolution algorithm to account for the IRF. The emission decays of the Ru(II)-complexes at high pH were well described with a single-exponential model. At neutral and high pH, at least two exponential components were needed to describe the data. This was also the case for the decay curves of the dyad.
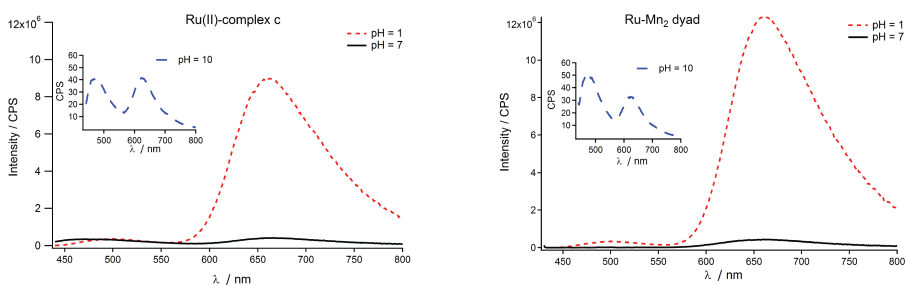


**Figure 4.7:** Steady state emission spectra of the Ru(II)-complex c (left) and the $\mathrm{Ru-Mn_2}$ dyad obtained with excitation at $\lambda = 425$ nm.

The short lifetimes of the Ru(II)-complexes **a-b** were unexpected but they could be explained by a large conjugation of the system and an essentially planar structure, which facilitates electronic transitions involving the orbitals localized at both the phenanthroline-benzimidazole ligand framework and those around the metal. However, the short lifetime of the Ru(II)-complex c was even more surprising, because the phenyl substituent on the central imidazole, which was introduced to destroy the planarity, did not seem to have any effect. Nonetheless, judging from the emission maxima, which are essentially the same for Ru(II)-complexes b-c and the $\mathrm{Ru-Mn_2}$ dyad but different for Ru(II)-complex a (Figure 4.9), introduction of the $(\mathrm{CO_2Et})_2$bpy ligands was successful in delocalizing the excited states over different parts of the molecule. Unfortunately, this was not enough to reduce the unwanted quenching of the $^3$MLCT state.

TDDFT calculations for the triplet excites state of the Ru(II)-complex **a**, predicted a manifold of states with similar energies involving either internal ligand charge transfer ($^3$ILCT), a metal centered transition ($^3$MC) or the $^3$MLCT transition. The $^3$ILCT and $^3$MC states are expected to be very shorted lived,[127] and if existing in equilibrium with the $^3$MLCT state would contribute to the short lifetimes observed in all the complexes.
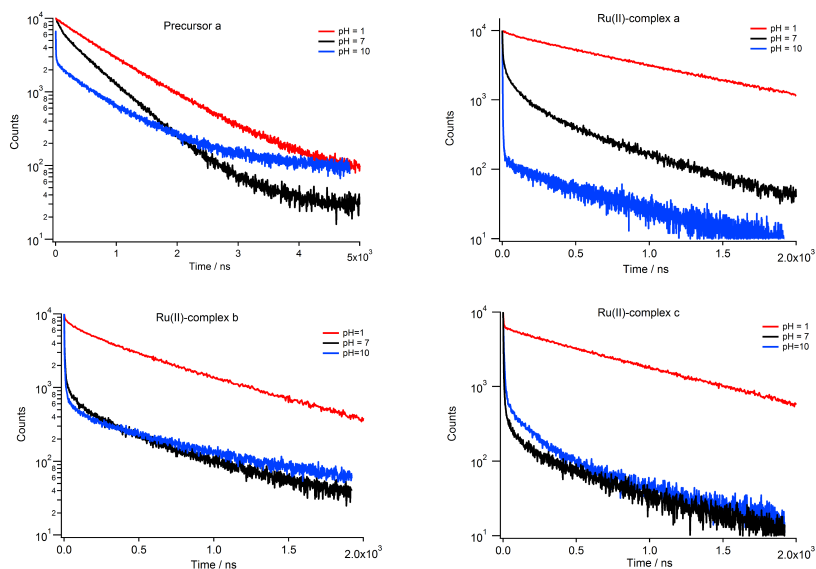
**Figure 4.8:** Emission decays measured at $\lambda = (610 \pm 10)$ nm by single photon counting with pulsed excitation at $\lambda = 405$ nm.

The multiexponential behavior of the emission decays observed in all the Ru(II)-complexes, the dyad and the precursor at neutral and high pH (Table 4.1), supports the existence of a manifold of excited states of similar energy.
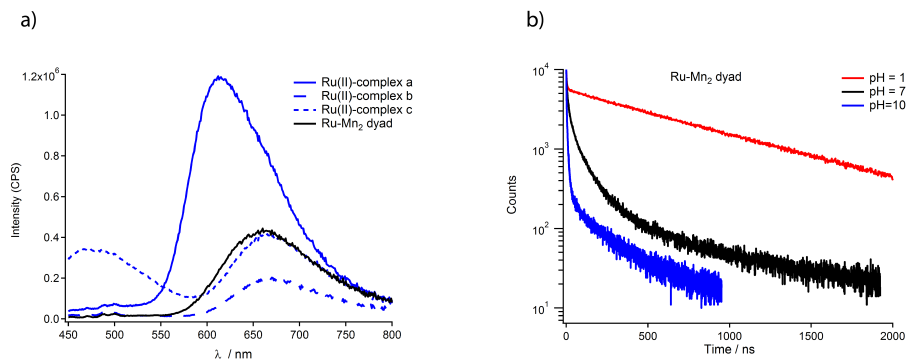


**Figure 4.9:** a) Steady state emission spectra of Ru(II)-complexes and the Ru–Mn₂ dyad in a deoxygenated 1:1 mixture of $CH_3CN/H_2O$ at neutral pH, obtained with excitation at $\lambda = 425$ nm. b) Emission decays of the Ru–Mn₂ dyad measured at $\lambda = (610 \pm 10)$ nm by single photon counting with pulsed excitation at $\lambda = 405$ nm.

**Table 4.1:** Emission properties of the precursor $P_a$, the Ru(II)-complexes and the Ru$-$Mn$_2$ dyad in a mixture of 1:1 acetonitrile water, at different pH values. Amplitudes, A, are reported as relative amplitudes and lifetimes with amplitudes lower than 4% have been ommitted.[a] Reprinted from **Paper I** with permission from the publisher. Copyright (2014) WILEY-VCH Verlag GmbH and Co.

| Sample | $A_1$ (%) | $\tau_1$ (ns) | $A_2$ (%) | $\tau_2$ (ns) | $A_3$ (%) | $\tau_3$ (ns) | $\lambda_{max}$ (nm) | $\phi$ (%) |
|---|---|---|---|---|---|---|---|---|
| $P_a$ (low) | - | - | - | - | 100 | 858 | 627 | - |
| $P_a$ (neutral) | - | - | 83 | 92 | 17 | 584 | 610 | - |
| $P_a$ (high) | - | - | 30 | 163 | 70 | 818 | 621 | - |
| LC-a (low) | - | - | 16 | 339 | 84 | 1032 | 630 | 2.12 |
| LC-a (neutral) | 68 | 15 | 22 | 135 | 10 | 635 | 613 | 0.16 |
| LC-a (high) | 98 | 1.4 | - | - | - | - | - | - |
| LC-b (low) | - | - | 46 | 303 | 54 | 823 | 662 | 2.35 |
| LC-b (neutral) | 94 | 3 | 4 | 58 | - | - | 667 | 0.08 |
| LC-b (high) | 98 | 1.8 | - | - | - | - | - | - |
| LC-c (low) | - | - | 31 | 541 | 69 | 965 | 658 | 3.74 |
| LC-c (neutral) | 98 | 2.2 | - | - | - | - | 661 | 0.16 |
| LC-c (high) | 96 | 3.6 | - | - | - | - | 624 | - |
| Dyad (low) | - | - | 12 | 354 | 88 | 830 | 659 | 4.17 |
| Dyad (neutral) | 80 | 7.9 | 18 | 60.6 | - | - | 660 | 0.19 |
| Dyad (high) | 65 | 1.5 | 33 | 8.3 | - | - | 621 | - |
| $[Ru(bpy)_3]^{2+}$ | - | - | - | - | 100 | 890 | 611 | 5.90 |

a. Low pH correspondes to pH$\sim$1 in aqueous solution, neutral to pH$\sim$7, and high to pH$\sim$10. The pH was adjusted by using HCl (12M) or NaOH (5M). Data for $[Ru(bpy)_3]^{2+}$ was obtained in $CH_3CN$.

Interestingly, Ru(II)-complex **c** displayed two emission peaks at neutral and high pH, Figure 4.7. Excitation spectra of Ru(II)-complex **c** suggested two emissive species originating from two different ground states, Figure 4.10. The peak centered around 450 nm was removed upon addition of manganese acetate, an indication of formation of the corresponding Ru–Mn$_2$ dyad, which did not display that peak in neutral conditions. This dual emission characteristic further supports the complicated pH dependent distribution of excited states in the Ru(II)-complexes, owing to the many different possible structures depending on the degree of protonation and the intramolecular type of interactions between the phenol and imidazole units.
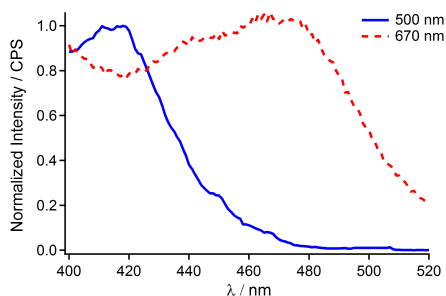


**Figure 4.10:** Excitation spectra of Ru(II)-complex **c** measured in deoxygenated mixture of 1:1 CH$_3$CN/H$_2$O at two different emission maximum.

The excited state lifetime of the Ru–Mn$_2$ dyad is similar to that of the Ru(II)-complexes and follows the same pH dependency trend, see Figure 4.9 and Table 4.1. Thus, it can be established that the strong excited state quenching observed in the dyad arises from similar mechanisms as in the complexes and not only from interaction with the manganese center.

From these results, it could be concluded that the main reason for the unsuccessful photosensitized water oxidation was due to the efficient quenching of the $^3$MLCT state which prevents the desired consecutive four-electron transfer from manganese to ruthenium. The quenching mechanism is most likely intramolecular, originating from the electronic structure of the Ru(II)-complexes and not by the introduction of the manganese atoms.

These results illustrates the challenges and disadvantages of supramolecular approaches for solar fuels. The difficulty of designing a single molecular entity where light harvesting, long-lived electron transfer and fuel forming reactions takes place points to a need for finding hybrid architectures where individual components for each function can be integrated. In the following chapters some assemblies of these type are presented.

CHAPTER 5

# Extending charge separation in dye-sensitized semiconductors

*The experimental work presented in this chapter has been aimed to increase the understanding of the mechanisms of BET and to contribute with strategies for extending charge separation in dye-semiconductor assemblies.*

## 5.1   Dye-sensitized nanoporous TiO$_2$ and SnO$_2$

TiO$_2$ and SnO$_2$ are wide-bandgap semiconductors with bandgap values around 3.2 (anatase) and 3.8 eV (rutile), respectively.[128]

For dye-sensitized photovoltaic or photocatalytic applications, the metal oxide semiconductor is typically a nanocrystalline, mesoporous structure of spherical nanoparticles that are a few tens of nanometers in diameter. This nanostructure provides a high surface area for the deposition of photosensitizers, which maximizes light harvesting. To fabricate the porous structure the nanoparticles are dispersed in colloidal pastes, which can be spread onto solid substrates. When heating the samples to temperatures up to 450–500 °C, the organic contents of the paste are decomposed and evaporated and only the semiconductor particles remain on the surface.[129]

Typically, the metal oxides are deposited on transparent conducting substrates. These are made of fluorine doped SnO$_2$ (FTO) coated glass. Fluorine impurities substitute oxygen atoms which results in increased electrical conductivity while preserving high optical transparency.[130]

As previously mentioned, ruthenium polypyridyl complexes are the most common transition metal photosensitizers. However, organic metal free dyes are potential, lower cost alternatives for photovoltaic and photocatalytic applications. Organic dyes with a donor-$\pi$-bridge-acceptor structure offer efficient forward electron transfer and slow down back-electron transfer by keeping the donor at a distance from the semiconductor nanoparticle and using the acceptor unit as anchoring group.[131] One of the best performing dyes of this type is the triphenylamine donor type D35 photosensitizer.[132–134]

All of the photosensitizers studied here contain carboxylic acid anchoring groups which are responsible for binding with TiO$_2$. The anchoring mechanism can be explained as a coordination bond between the carboxylate (COO-) and the Ti(IV) ions.[135]

## 5.2   Back-electron transfer vs charge transport

The lifetime of the charge separated state at dye/semiconductor interfaces depends on the kinetics of BET, which usually occurs on a microsecond to millisecond time scale.[54] The dynamics of BET have been extensively investigated with a variety of different photosensitizers. Although single-exponential recombination kinetics have been reported,[119,136] the data is usually not well described with a single exponential decay law as it is rather complex.[137] This behaviour has been explained by considering that after photoinjection, electrons can be trapped in a set of levels distributed below the conduction band, referred to as trap states.[121,138–140] The trapping/detrapping dynamics, as well as the density of electrons in the conduction band and trap states are determining factors in the kinetics of BET.[139,141] The kinetics are superlinearly dependent upon the electron density, which in turn is related to the electrochemical potential of the electrons

in the semiconductor (Fermi level). This has been demonstrated by intensity dependent measurements.[142,143]

The presence of ions or additives such as $Li^+$ ions and tert-butylpyridine (tBP) can influence the electronic structure of $TiO_2$ resulting in increased electron injection efficiency.[51,144–146] It is well accepted that a positive shift of the conduction band edge energy, due to adsorption of the $Li^+$ cations at the $TiO_2$/electrolyte interface, is responsible for this effect.[147,148]. The improved injection efficiency can be understood in terms of increased driving force or a better electronic coupling between the dye excited state and the $TiO_2$ acceptor states.[148] A downward shift in the conduction band edge will also have an effect on the BET by accelerating the recombination kinetics, given that BET is in the inverted Marcus region. However, this is not always the case for all photosensitizers as can be concluded from the observations presented in **Paper II**.

In DSSC, the photoinjected electrons are transported and collected at the conducting contact before recombining to the radical dye cations, which are regenerated in a much faster timescale by the redox electrolyte.[149] Thus, BET is not the main limiting factor of photocurrent generation in an efficient DSSC. However, in solar-to-chemical energy conversion, BET becomes a detrimental process given the relatively slower kinetics of solar fuel forming reactions such as water oxidation.[150] Thus, the efficiency of charge separation at dye-sensitized semiconductors without regenerating electrolytes depends on the interplay between the opposite forces of electron transport and electron recombination.

Electron transport depends on the electron mobility, which in turn is related to the electron diffusion coefficient. In nanostructured semiconductors, this parameter depends on the Fermi level and the charge carrier concentration,[151] and it is several orders of magnitude lower that than of single crystal metal oxides.[152] Although this observation has been explained by a trapping/detrapping dominated transport process[142,153,154], it has also been proposed that the transport could be a potential gradient dominated process.[155] Although macroscopically, diffusion can be described as an effect of a concentration gradient, in dye-sensitized semiconductors the presence of an electrolyte introduces electrostatic components to the diffusion coefficient, and consequently, a dependance on composition of electrolyte and concentration of ions.[156] Therefore, the density of injected electrons and the nature of the electrolyte becomes very important parameters when studying molecular-semiconductor assemblies. This is relevant for the discussion of the results presented in **Paper III**.

Since both charge transport and charge recombination are influenced by the same variables, extending charge separation is not a straight forward task but rather a complicated process in which many factors need to be considered. These factors are anything that could affect the electrochemical potential of the electrons in the semiconductor, the electron mobility, the concentration of charge carriers, the presence of energy level-determining species and the dynamics of trapping/detrapping of electrons.

## 5.3 Kinetic models of back-electron transfer

Kinetic modelling of charge recombination dynamics is needed for the mechanistic understanding of the electron transfer processes taking place in dye-sensitized semiconductors.

In order to kinetic parameters of the back-electron transfer reaction from experimental data, a suitable mathematical model for the description of the multiexponential nature of this reaction is required. In several reports, the kinetics of BET have been modelled with exponential functions containing up to four components.[121,140,143,157] However, over the past years it has become more popular to describe the kinetics of BET by a stretched exponential function,[158–163] which represents a distribution of rate constants as in Equation 5.1.[164]

$$f(t) = A \exp\left[ -\left(\frac{t}{\tau_0}\right)^\beta \right]$$  (5.1)

where $\tau_0$ is the most representative lifetime and $\beta$ is inversely related to the width of the underlying Levy distribution, $0 < \beta < 1$. A small $\beta$ value represents a wider distribution of the values of rate constants and a decay function with $\beta = 1$ represents an exponential decay function.

The mean lifetime for the kinetics of BET can be calculated by the first moment of the KWW function as in equation (5.2) where $\Gamma$ is the Gamma function.[165] The inverse of this lifetime is the effective rate constant $k_{obs}$.

$$\langle \tau_{WW} \rangle = \left(\frac{\tau_0}{\beta}\right) \Gamma\left(\frac{1}{\beta}\right)$$  (5.2)

Due to its application on the description of the discharge of a capacitor and the dielectric spectra of polymers, the stretched exponential model has adopted the name of Kohlrausch-Williams-Watts (KWW) function.[166,167] For electronic relaxation, a stretched exponential decay is generally attributed to a source of heterogeneity or disorder in the system related to dispersive transport.[168] Considering this, a physical meaning of the $\beta$ parameter can be understood as a property related to the heterogeneity of the analyzed process. When describing charge recombination in dye-sensitized semiconductors, $\beta$ would be related to the distribution of trap-states and other properties of the system that would affect the heterogeneity of the BET dynamics. Therefore, when comparing rate constants obtained from different samples, the $\beta$ values needs to be considered for proper interpretation of the data.

For description of the BET kinetics measured in the experimental work presented here, we have used both biexponential decay functions and the KWW model. The choice of the kinetic model was empirical and based on comparison of the residual and chi-squared values of the fit.

## 5.4 Local electrostatic effects at the interface

To facilitate the understanding of the next section some concepts related to electrostatic interactions at the semiconductor/dye/electrolyte interface must be considered.

In 2010, two research groups reported, almost simultaneously, on the effect of the local electric field created after electron injection from the excited dyes, on the absorption spectra of photosensitizers adsorbed on $TiO_2$.[169,170] Better known as the Stark effect, it consists of a shift of the ground state absorption spectrum of the dye molecules cause

by the electric fiels. The amplitude of the shift decreases over time by compensation or "screening" of the electric field by interfacial ionic reorganization.[170,171] The strength of this electric field as well as the kinetics of charge screening depend on the nature and concentration of the cations in the surrounding electrolyte.[172,173]

Considering the large strength of this local electric field, in the order of megavolts per centimeter,[171,172,174] it has been anticipated that it should have an effect on the electron transfer processes across the semiconductor/dye/electrolyte interface, e.g. charge recombination and dye regeneration.[170] However, it was not until the past couple of years that some investigations were dedicated to quantitatively measure this.[175]

In **Paper II**, these concepts were put in practice in efforts to understand how the size of organic cations in the surrounding electrolyte could affect the charge recombination kinetics in dye-sensitized $TiO_2$.

## 5.5 Extending charge separation

Several strategies to extend the lifetime of the CSS in dye-sensitized semiconductors have been proposed. These approaches have been based in structural modifications of the dye[161,176–180], surface modification of the semiconductor nanoparticles[157,181] or the use of core-shell metal oxide electrode structures[150,179,182]. The polarity of electrolyte solvents has also been shown to have an effect on the interfacial electron transfer processes in dye-sensitized metal oxides and therefore affects the efficiency of devices.[183,184] As already mentioned above, the presence of some chemical species in the electrolyte can influence the kinetics of back-electron transfer.

With these in mind, a strategy to extend the lifetime of the CCS in dye-sensitized nanoporous $TiO_2$ based on the use of ionic liquids was investigated in **Paper II**. A photoanode design based on $SnO_2 - TiO_2$ patterned thin films was investigated in **Paper III** aiming to extend not only the lifetime but also the distance of charge separation. A summary of the experimental findings resulting from these investigations is presented in the following sections.

### 5.5.1 Effect of ionic liquids

Ionic liquid (IL) electrolytes have been extensively studied as alternative electrolytes to organic solvent based electrolytes in DSSCs. ILs have interesting properties such as neglible volatility, high conductivity, high thermo-and electrochemical stability, and are good solvents for many inorganic and organic compounds.[185,186] For these reasons, they can bring versatility and stability to devices, however the slow mass transport usually results in lower photon-to-current conversion efficiencies.

Characterization of DSSCs based on IL electrolytes has revealed that in contrast to organic solvent-based devices, electron recombination is accelerated and regeneration of the photosensitizer is slowed down.[185,187,188] However, there has not been a study solely dedicated to investigate the effects of ILs on the back-electron transfer rates in dye-sensitized metal oxides. This problem was addressed as a part of the experimental work of this thesis (**Paper II**). The purpose of this study was to investigate if ILs could be used to extend the lifetime of the CSS in dye-sensitized nanoporous $TiO_2$. This idea emerged

from the hypothesis that the local electric field generated at the $TiO_2$/dye/electrolyte interface could be compensated by the IL cations reorganizing at the interface. This would probably change the orientation of the dye at the surface by steric hindrance and interfere with charge recombination.

This investigation started with the use of the organic photosensitizer D35. Imidazolium-based ILs of the type 1-alkyl-3-methylimidazolium were chosen for this study because they have been previously used in IL-based DSSCs.[189–192] The structures of the dyes and IL cations used in this work are displayed in Figure 5.1. The counterion of the ILs was hexafluorophosphate ($PF_6$), an "innocent" anion which does not have any reactivity with the dye like other anions such as thiocyanate $SCN^-$) and iodide $I^-$. Hereafter, the ILs are referred to as BMIMPF$_6$, HMIMPF$_6$ and OMIMPF$_6$, for alkyl chain contains six and eight carbons, respectively.



D35                     [Ru(dcb)$_3$]Cl$_2$                     N3

BMIMPF$_6$                     HMIMPF$_6$                     OMIMPF$_6$
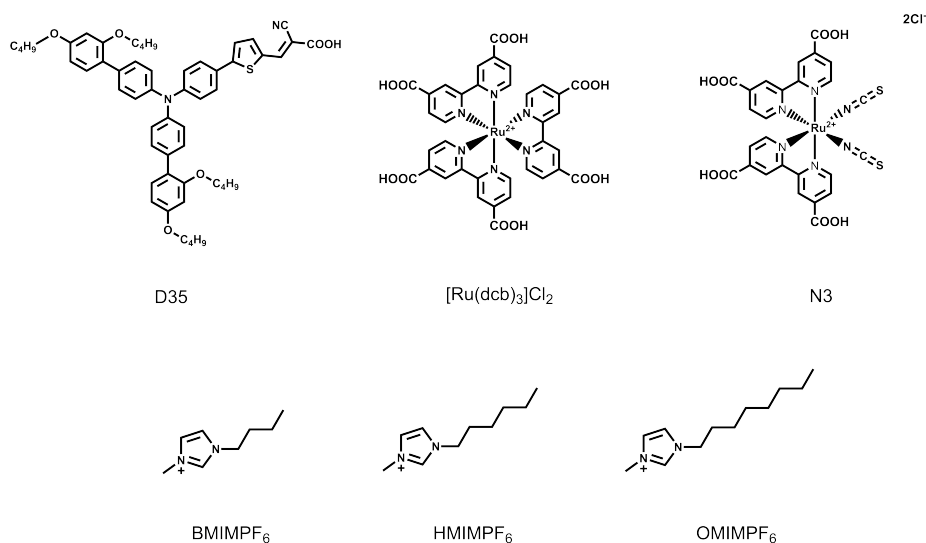
**Figure 5.1:** Structures of the photosensitizers and IL-cations used in **Paper II**

The kinetics of BET were measured using µs-ms transient absorption spectroscopy. The first results, clearly pointed out that there was a difference in the kinetics when introducing ILs compared to $CH_3CN$-based electrolytes. BET was slowed down in pure ILs but also in a mixture of $CH_3CN$/BMIMPF$_6$, see Figure 5.2. The effect was larger when using pure ILs and, therefore, only pure ILs were employed in the following experiments.

The study was extended by introducing ILs with longer alkyl chains. The results demonstrated that kinetics of BET were dependent on the length of the chain. These results were conclusive for D35, but for mechanistic understanding two more dyes were studied: N3 and $[Ru(dcb)_3]^{2+}$. Transient absorption measurements showed that the ILs affected the lifetime of the CSS in a similar way to that of D35 and $[Ru(dcb)_3]^{2+}$. However, the back-electron transfer kinetics were unaffected in the N3 case, see Figure 5.3. The kinetics of BET in D35 and N3 samples were well described by the KWW model,
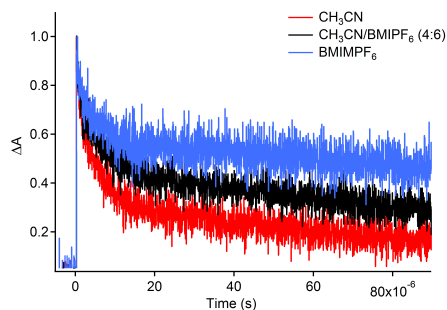
**Figure 5.2:** Single-wavelegth transient absorption kinetics recorded at 600 nm after pulsed 500 nm excitation of D35/TiO$_2$ thin films with various solvents.

however, [Ru(dcb)$_3$]$^{2+}$ samples were better described with a biexponential model. For this discussion, it is relevant to present the observed rate constants of BET for D35 and [Ru(dcb)$_3$]$^{2+}$ obtained from the corresponding model that was most appropriate in each case, see Table 5.1. A complete description of the kinetic parameters for all samples is available in **Paper II**.
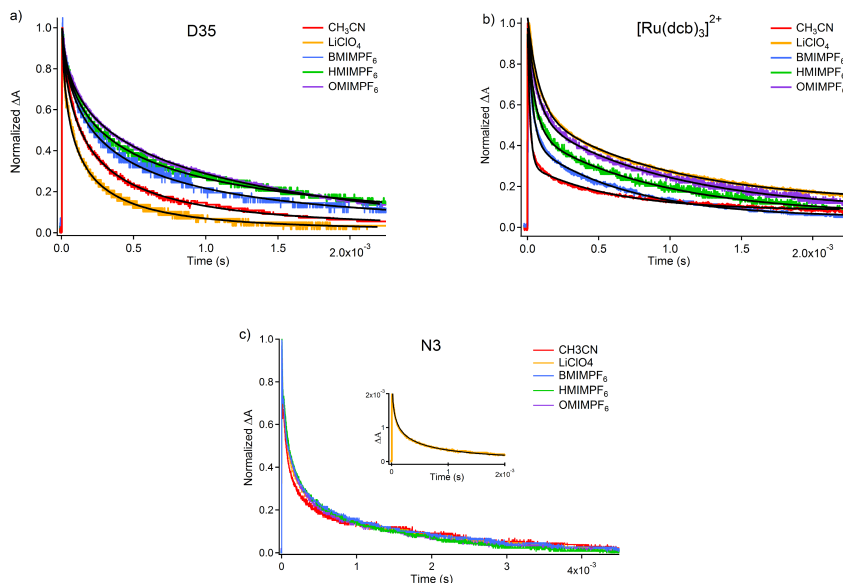


**Figure 5.3:** Single-wavelength transient absorption kinetics and corresponding fit curves recorded after pulsed excitation of a)D35/TiO$_2$ recorded at 750 nm b)[Ru(dcb)$_3$]$^{2+}$/TiO$_2$ recorded at 500 nm and c)N3/TiO$_2$ recorded at 750 nm. The inset panel c is to emphasise the KWW fit curve to one of the curves. Reprinted from **Paper II** with permission from the publisher. Copyright (2016) American Chemical Society.

From inspection of the rate constants presented in Table 5.1, it is clear that BET was retarded in ILs. For D35/TiO$_2$ samples, this is directly inferred from a decrease in the observed charge recombination rate constant, $k_{cr}$, which is more significant when OMIMPF$_6$ was added. The slower kinetics in [Ru(dcb)$_3$]$^{2+}$/TiO$_2$ samples is noted from a decrease in the amplitude of the fast component of the decay ($A_1$), and an increase in the amplitude of $A_2$. This amplitude change is also most significant for samples with OMIMPF$_6$. The extracted rate constants, $k_1$ and $k_2$, also decreased with increasing length of the alkyl chain in the imidazolium cation.

**Table 5.1:** Representative charge recombination constants, $k_{cr}$, obtained from KWW or double exponential model fitting of transient absorption data of D35/TiO$_2$ and [Ru(dcb)$_3$]$^{2+}$/TiO$_2$ respectively, in the electrolytes indicated.

| | D35/KWW | | [Ru(dcb)$_3$]$^{2+}$/Biexponential | | | |
|---|---|---|---|---|---|---|
| electrolyte | $k_{cr}$ $(10^3 s^{-1})$ | $\beta$ | $A_1 (\%)$ | $A_2 (\%)$ | $k_1 (10^4 s^{-1})$ | $k_2 (10^3 s^{-1})$ |
| CH$_3$CN | $11.2 \pm 1.3$ | $0.42 \pm 0.01$ | 68 | 32 | $4.1 \pm 0.51$ | $1.5 \pm 0.18$ |
| LiClO$_4$ | $26.1 \pm 8.8$ | $0.42 \pm 0.08$ | 46 | 54 | $1.2 \pm 0.09$ | $0.98 \pm 0.13$ |
| BMIMPF$_6$ | $4.3 \pm 2.7$ | $0.41 \pm 0.07$ | 58 | 42 | $3.3 \pm 0.29$ | $2.2 \pm 0.73$ |
| HMIMPF$_6$ | $7.5 \pm 2.2$ | $0.41 \pm 0.06$ | 55 | 45 | $2.1 \pm 0.2$ | $1.3 \pm 0.15$ |
| OMIMPF$_6$ | $2.8 \pm 0.7$ | $0.48 \pm 0.09$ | 52 | 48 | $1.6 \pm 0.33$ | $1.1 \pm 0.05$ |

The indicated uncertainties represent the standard deviation obtained from averaging individual fits of single-wavelength transient absorption decays from triplicate samples.

The absorption spectra of the dye-sensitized TiO$_2$ thin films did not show significant differences upon addition of the various ILs that could be attributed to the different behavior of the BET kinetics, Figure 5.4. Moreover, the absorption spectra of oxidized D35 adsorbed on TiO$_2$ did not show considerable differences upon addition of either BMIMPF$_6$ or HMIMPF$_6$, see Figure 5.5. This supported the hypothesis that the differences in BET kinetics were not related to changes in the energy of electronic transitions but rather to electrostatic effects at the TiO$_2$/dye/electrolyte interface. Another interesting observation supporting this hypothesis was the decreasing anodic and cathodic peak currents obtained in cyclic voltammetry measurements of D35/TiO$_2$ upon addition of the IL BMIMPF$_6$, see Figure 5.6. Judging from the relative values of $ip_a$ and $ip_c$, oxidation of the dye becomes less reversible with added IL compared to pure LiClO$_4$. These observations speak in favor of precluded hole and/or electron transfer between the dye and the FTO/TiO$_2$ substrate, caused by the presence of BMIMPF$_6$ at the interface.
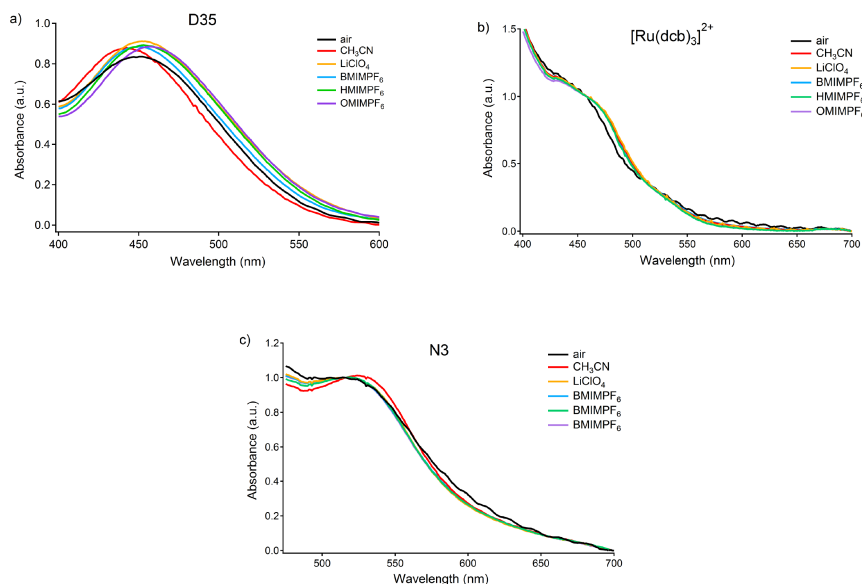
**Figure 5.4:** Absorption spectra of dye-sensitized TiO$_2$ thin films with a)D35, b)[Ru(dcb)$_3$]$^{2+}$ and c)N3 in various solvents and electrolytes. Reprinted from **Paper II** with permission from the publisher. Copyright (2016) American Chemical Society.
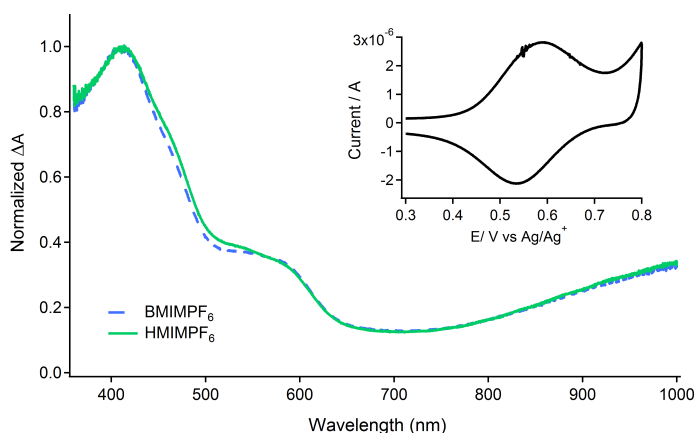


**Figure 5.5:** Absorption spectra of oxidized D35 adsorbed on TiO$_2$ thin films prepared on FTO-coated glass substrates, after addition of the ILs. Electrochemical oxidation of the dye was performed in 0.1 M TBAPF$_6$/CH$_3$CN. The potential was set to 0.8 V vs an Ag/Ag$^+$ non-aqueous reference electrode and a Pt-disk was used as auxiliary electrode. The inset shows a CV of a D35/TiO$_2$ thin film.
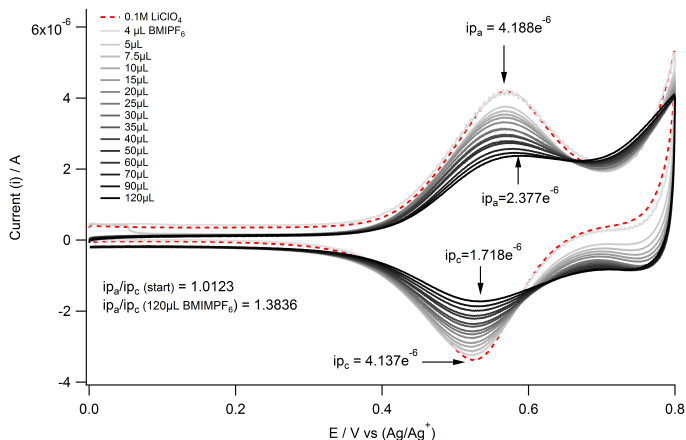
**Figure 5.6:** Cyclic voltammograms of $D35/TiO_2$ in 0.1 M $LiClO_4$ in $CH_3CN$ with added amounts of $BMIMPF_6$.

From the results discussed above, it could be concluded that the ILs are responsible for the observed decreased in BET rate constants in $D_{35}/TiO_2$ and $[Ru(dcb)_3]^{2+}$ samples. However, an explanation behind the solvent-independent BET kinetics observed for $N_3/TiO_2$ samples was needed. Given the initial hypothesis that the local electric field generated at the $TiO_2$/dye/electrolyte interface could be compensated by the IL cations reorganizing at the charged surface, analysis of the photosensitizer structures could explain the surprising observations. In principle, the negatively charged $SCN^-$ ligands in N3 could strongly interact with the IL cations, preventing them from rapid diffusion to the charged surface. This would be in agreement with the main hypothesis of an electrostatic effect at the $TiO_2$/dye/electrolyte interface being responsible for the observed effect. A mechanism where reorganization of the IL cations at the charged $TiO_2$ surface create steric hindrance between the oxidized dye and the $TiO_2$ was proposed to explain the decrease in BET rate constants, Figure 5.7. This effect is dependent on both the size of IL cations and the structure of the dye.

To the best of my knowledge, there are no other reports on the influence of organic cations on either electric field compensation or the kinetics of charge recombination. However, the effect of inorganic cations on the charge recombination kinetics has been studied and it has been shown to be linearly correlated to the magnitude of the electric field[175], which reflects the ability of the cations to screen the negative charge at the semiconductor from the photosensitizer.[172]

It can be concluded that the nature and size of the cations in the electrolyte can significantly affect the kinetics of charge recombination at dye-sensitized semiconductors. Furthermore, the role of the local electric field and the composition of electrolyte should be considered when interpreting BET kinetics and other electron transfer processes at these types of assemblies.
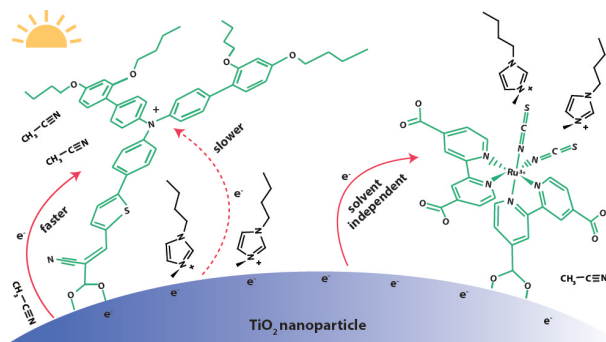
**Figure 5.7:** Proposed mechanism of local charge compensation hindering back-electron transfer from $TiO_2$ to the oxidized photosensitizer. Reprinted from **Paper II** with permission from the publisher. Copyright (2016) American Chemical Society.

### 5.5.2 A photoanode design strategy

As discussed in previous sections, long-range electron transfer implies that the electron is transported a long distance away from the hole. This is necessary for long-lived charge separation. In **Paper III** a $SnO_2$–$TiO_2$ photoanode was designed with this purpose. The idea behind the design originated in an attempt to answer the following questions:

- Could photoinjected electrons be transported through the nanoporous semiconductor structure in a mm range before recombining to the dye?

- What would be the determining factors for this to happen?

- Would it be possible to create a nanostructured platform where dye and acceptor molecules are physically separated but electronic transport is allowed between them?

The strategy behind the photoanode design was to make use of the different conduction band energies of $TiO_2$ and $SnO_2$ to create a downhill cascade of driving forces such as in $SnO_2$–$TiO_2$ core-shell structures, which have been used to decrease the rate of BET.[150,179,193,194] The kinetics of charge recombination in dye-sensitized $SnO_2$–$TiO_2$ core-shell films has shown to be distributed between the ps and ms timescale and to be exponentially dependent on shell thickness.[150] It has been suggested that the optimal $TiO_2$ shell thickness is just a few nm.[179] In general, electron injection into $SnO_2$ is known to be less efficient than in $TiO_2$[195–197]. Because of the aforementioned, the core-shell strategy presents a disadvantage in terms of maximizing utilization of radiation. In addition, the manufacture of these structures requires more advanced and costly methods compared to those of traditional semiconductor thin films.

In order to maximize light harvesting, the $SnO_2$–$TiO_2$ nanostructure presented here is intended to be of simple and accessible fabrication, while maintaining the typical thickness of photovoltaic application nanoporous thin films. The originality of this design is that the photoanode is not an homogeneous deposited layer of material but rather a repetitive pattern of alternate $SnO_2$ and $TiO_2$ layers. The photoanode was fabricated by

first depositing a nanoporous layer of $SnO_2$ by doctor-blading followed by the deposition of nanoporous $TiO_2$ stripes by screen printing, see Figure 5.8. Optical characterization of the films confirmed the deposition of both semiconductors, see Figure 5.9
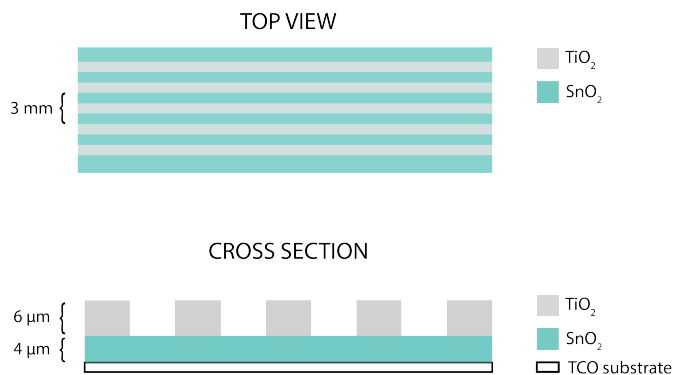


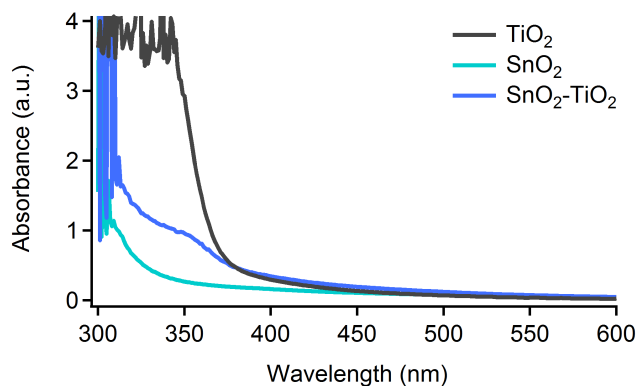**Figure 5.8:** Top and cross section views of the patterned $SnO_2$–$TiO_2$ thin film



**Figure 5.9:** Absorption spectra of $TiO_2$, $SnO_2$ and $SnO_2$–$TiO_2$ deposited on a FTO substrate.

The usefulness of this design is not only found in the semiconductor distribution itself, but also in the way the dye molecules were deposited. Selective dye-sensitization of the $SnO_2$–$TiO_2$ areas of the film allowed to leave "dye-free" $SnO_2$ areas were electrons can be trapped for longer periods of time before recombining, see Figure 5.10. It is thought that the much larger electron mobility of electrons in $SnO_2$ compared to $TiO_2$[198] would contribute to this process. Selective sensitization of the films was achieved by using PDMS microfluidic channels. The fabrication of these channels is illustrated in Figure 5.12.

To evaluate the effectiveness of this design in extending charge separation, measurement of the BET kinetics was required. However, comparison with BET kinetics in homogeneous dye-sensitized "non-patterned" films, such as those presented in **Paper II**, would not be

appropiate given the different materials and macroscopic structure of the films. Therefore, a comparison between homogeneously sensitized patterned films (Type-I), and selectively-sensitized patterned films (Type-II) was preferred. Pictures of these films are shown in Figure 5.11.
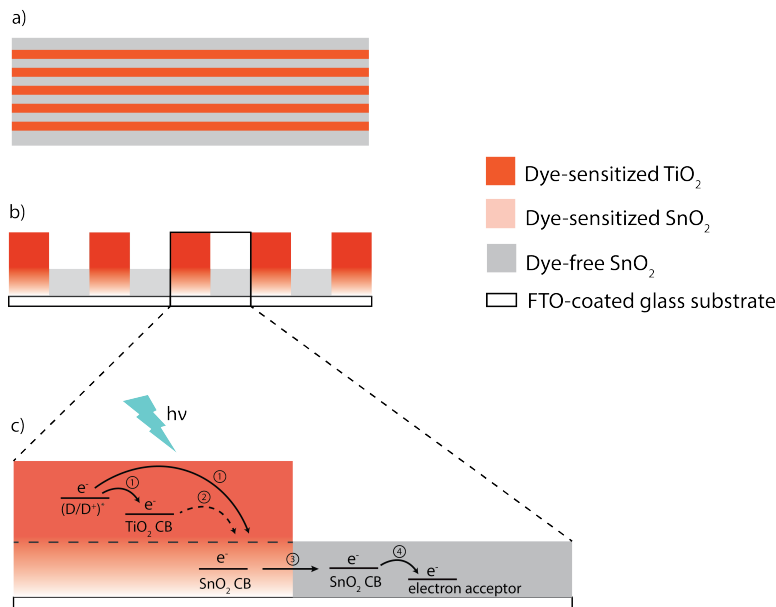


**Figure 5.10:** Illustration of selectively sensitized patterned $SnO_2$–$TiO_2$ thin film. a) Top view, b) Cross-section view and c) Schematic illustration of the possible photoinduced electron transfer processes in the film.
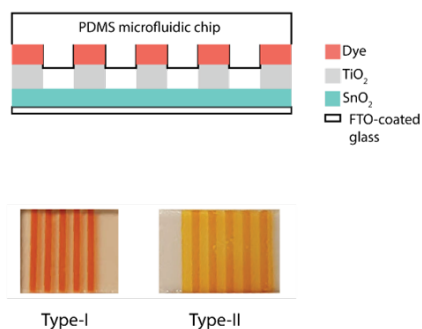


**Figure 5.11:** Pictures of Type-I and Type-II dye-sensitized patterned thin films. The top image illustrates the cross-view section of the PDMS channels on top of a patterned thin film with the dye solution flowing through the channels. Reproduced from **Paper III** with permission from the publisher. Copyright (2017) PCCP Owner Societies.
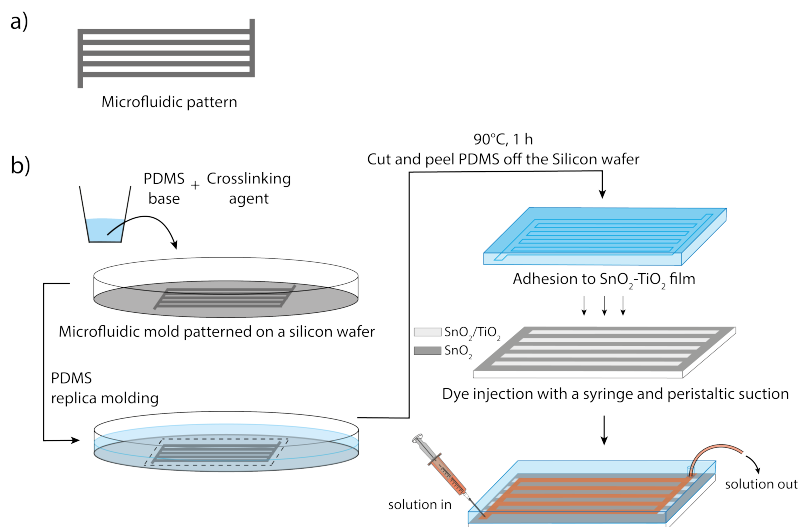
**Figure 5.12:** Schematic illustration of the PDMS microchannels fabrication and the selective dye-sensitization process. Reproduced from **Paper III** with permission from the Publisher. Copyright (2017) PCCP Owner Societies.

Intensity-dependent transient absorption measurements on these samples showed that recombination was slowed down in Type-II samples when sufficient electrons were injected into the conduction band, see Figure 5.13. Recombination was also slower in Type-II samples compared to non-patterned $TiO_2$ and $SnO_2$ thin films, Figure 5.14.

The BET kinetics were properly described with the KWW model. Comparison of $k_{cr}$ values of Type-I and Type-II patterned films revealed that, at sufficiently high excitation power and in the presence of $Li^+$ ions, the $k_{cr}$ was decreased up to a factor of $\backsim$80 containing $SnO_2$ areas without dye molecules. Also, charge recombination was slowed down up to a factor of $\backsim$80 and $\backsim$2000 compared to non-patterned dye-sensitized $TiO_2$ and dye-sensitized $SnO_2$ films respectively, see Table 5.2. It was therefore concluded that the photoanode design strategy was successful in extending charge separation. A direct comparison to BET kinetics reported for $SnO_2$–$TiO_2$ core-shell structures is difficult given the different time resolution of the available data. Increase on the CSS half-life of up to 1000-fold has been shown by ns-ms transient absorption measurements using core-shell structures.[179] With the time resolution of our measurements a 10-fold decrease can be obtained using the patterned photoanode. On the other hand, values of $k_{cr}$ are not reported for dye-sensitized $SnO_2$–$TiO_2$ core-shell materials, and therefore it can only be concluded that both strategies result in the same desired effect, but probably to a different extent.

The work presented in **Paper III** is proof that, in dye-sensitized semiconductors, charge transport can overcome charge recombination so that the diffusion length of the electrons can be substantially increased. For this, the determining factors are the macroscopic structure of the photoanode, the irradiation power and the presence of cations in the electrolyte, in this case $Li^+$ ions. Moreover, the method presented for selective
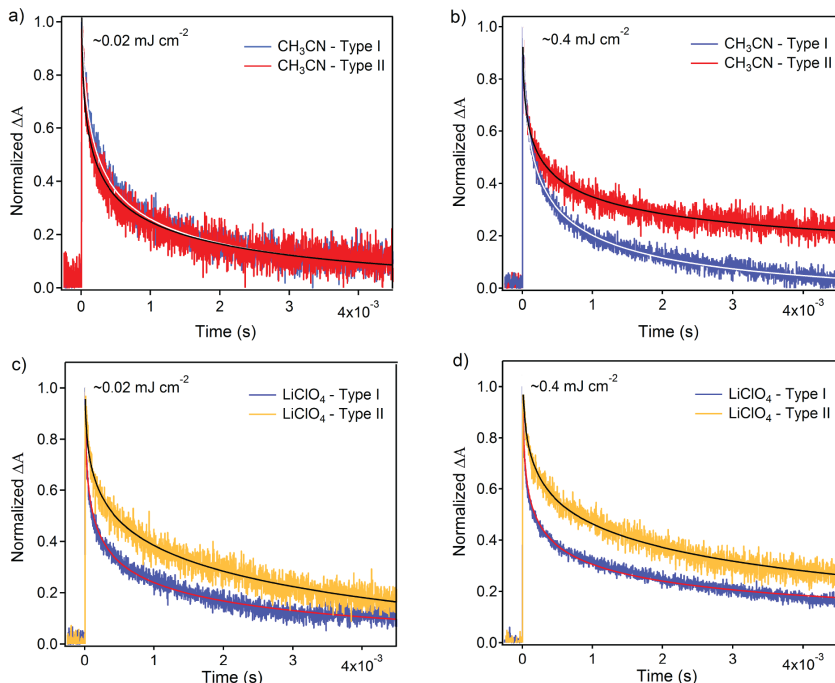
**Figure 5.13:** Power dependent single-wavelength transient absorption kinetics of patterned $SnO_2$–$TiO_2$ thin films and their corresponding KWW gobal fit curves. $\Delta A$-signals were recorded at 750 nm after pulsed 525 nm laser excitation (a) In $CH_3CN$ and (b) In 0.1 M $LiClO_4/CH_3CN$. Reproduced from **Paper III** with permission from the publisher. Copyright (2017) PCCP Owner Societies.

dye-sensitization is a new tool for the fabrication of photovoltaic devices, which could impact the field of solar fuels. The present method also opens up for the possibility of co-sensitizing semiconductors in a way that photosensitizers and other molecules of interest, such as catalysts, are physically separated but interact *via* the conduction band of the semiconductor, see Chapter 6. This facilitates the study and development of photocatalytic systems for solar energy conversion.
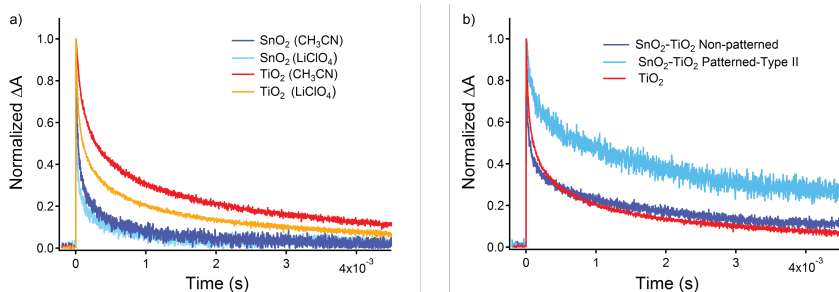
**Figure 5.14:** Representative individual kinetic decay curves measured by single-wavelength transient absorption after pulsed 500, 530 and 510 nm excitation of dye-sensitized $SnO_2$, $TiO_2$ and non-patterned $SnO_2$–$TiO_2$ thin films respectively ($\backsim$ 0.4 mJ $cm^{-2}$). a) Comparison of D35/$SnO_2$ and D35/$TiO_2$ films b) Comparison of a non-patterned $SnO_2$–$TiO_2$ thin film to a patterned $SnO_2$–$TiO_2$ and a D35/$TiO_2$ thin film. All samples measured in 0.1 M $LiClO_4$/$CH_3CN$. Reproduced from **Paper III** with permission from the publisher. Copyright (2017) PCCP Owner Societies.

**Table 5.2:** Relative charge recombination rate constants obtained from KWW global fittings of transient absorption decay curves comparing the rates of Type-II samples $\left(k_{cr}(\mathrm{II})\right)$ to Type-I samples $\left(k_{cr}(\mathrm{I})\right)$, non-patterned $SnO_2$ films $\left(k_{cr}(\mathrm{S})\right)$ and non-patterned $TiO_2$ $\left(k_{cr}(\mathrm{T})\right)$

| Solvent | Excitation energy $\left[\mathrm{mJcm}^{-2}\right]$ | $k_{cr}(\mathrm{I})/k_{cr}(\mathrm{II})$ | $k_{cr}(\mathrm{T})/k_{cr}(\mathrm{II})$ | $k_{cr}(\mathrm{S})/k_{cr}(\mathrm{II})$ |
|---|---|---|---|---|
| $CH_3CN$ | 0.002 | 0.15 | 0.19 | 6.02 |
| $CH_3CN$ | 0.008 | 0.37 | 0.11 | 9.01 |
| $CH_3CN$ | 0.02 | 1.26 | 0.33 | 11.12 |
| $CH_3CN$ | 0.4 | 2.36 | 0.99 | 215.35 |
| $LiClO_4$ | 0.002 | 1.99 | 0.69 | 28.11 |
| $LiClO_4$ | 0.008 | 0.78 | 0.46 | 43.02 |
| $LiClO_4$ | 0.02 | 25 | 30.21 | 2150 |
| $LiClO_4$ | 0.4 | 54.76 | 78.56 | 2320.38 |

# Conduction band mediated electron transfer

*The purpose of the experimental work presented in this chapter has been to move towards the realization of visible light-induced CBM-ET. For proof of principle, model systems consisting of semiconductor thin films co-sensitized with a dye and a model electron acceptor have been used to demonstrate that CBM-ET is a viable approach to solar energy conversion.*

## 6.1   The ultimate goal

The concept of CBM electron transfer was briefly introduced in Chapter 2 (section 2.1.2). In general, it is a process where electrons accumulated in the conduction band are transferred to nearby molecules, ideally, these molecules are anchored to the semiconductor themselves. CBM has been previously proven,[59–61,199] but yet there is a lot to learn about the mechanisms and determining factors that facilitate CBM electron transfer. Moreover many fundamental advances are needed before it can become useful for its practical application in photoelectrochemical devices.

This concept can be used as an approach for solar-to-chemical energy conversion by anchoring both photosensitizers and catalysts to the semiconductor surface. In this way, visible light is harvested by the photosensitizer and the photoinjected electrons are transferred to the catalyts *via* the conduction band, see Figure 6.1.
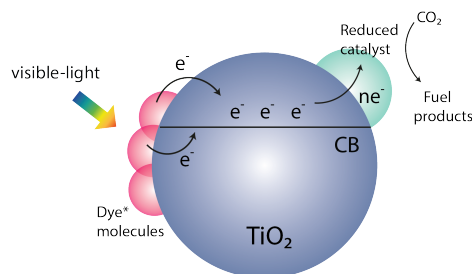


**Figure 6.1:** Schematic description of visible light sensitized generation of a catalytically active state of a catalyst for $CO_2$ reduction, anchored to a $TiO_2$ nanoparticle.

The realization of this is challenging as several fundamental advances are guaranteed. A hybrid assembly where semiconductor nanoparticles, dye and catalyst molecules coexist is itself a complex system. Therefore, the study of these type of assemblies requires the investigation of several aspects separately before full demonstration can be achieved. In this thesis, some of these aspects have been investigated and are discussed in the following sections.

## 6.2 UV-light generation of highly reduced states through CBM-ET

For fundamental understanding of the CBM approach, the first step was to investigate model electron acceptors that can be anchored to the semiconductor and reduced from electrons in the conduction band. For this, model catalysts such as iron and cobalt protoporphyrin IX are suitable molecules given the relative positions of their redox potentials, close or below the conduction band of $TiO_2$ and their ability to be doubly reduced, as exemplified in Figure 6.3. Furthermore, cobalt porphyrins have shown photocatalytic and electrocatalytic activity toward $CO_2$ reduction.[91,200] The structures of these molecules are shown in Figure 6.2. The two carboxylic groups serve as anchoring groups for metal oxide semiconductors.
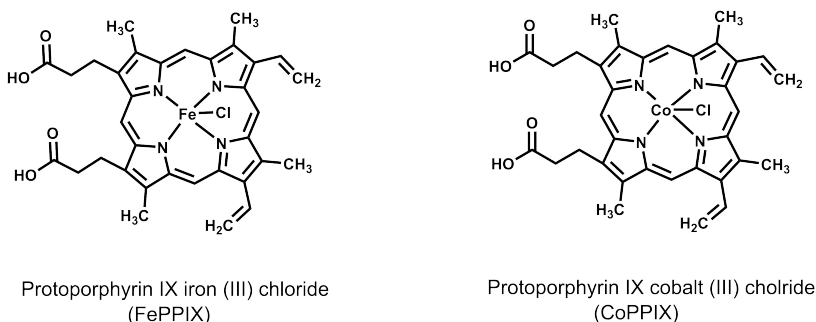


Protoporphyrin IX iron (III) chloride
(FePPIX)

Protoporphyrin IX cobalt (III) cholride
(CoPPIX)

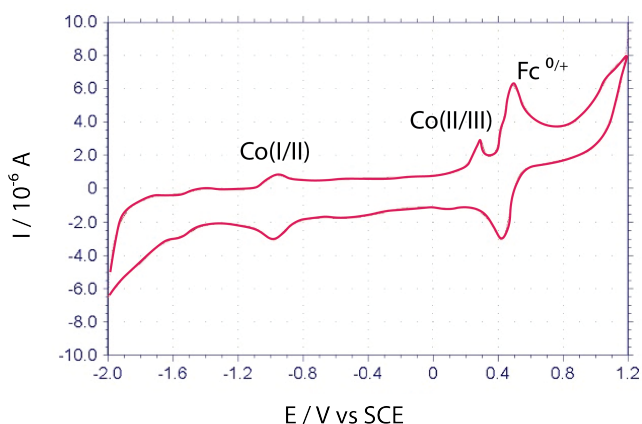**Figure 6.2:** Structures of the model metalloporphyrin catalysts



**Figure 6.3:** Cyclic voltammogram of CoPPIX in deaerated 0.1 M TBAPF$_6$/DMSO at scan rate = 0.1 V/s.

For identification of the reduced states of the catalysts, their optical properties need to be investigated. This is typically done by reducing the catalyst electrochemically while simultaneously measuring the absorbance of the sample. According to the Gouterman four orbtital model,[201] the bands in the absorption spectra of metalloporphyrins can be explained by $\pi - \pi^*$ transitions between two nearly degenerate HOMO orbitals and a pair of degenerate LUMO orbitals, Figure 6.4. The intense and sharp band centered around 400 nm corresponds to a transition from the ground state to the second excited state, named B-bands or Soret band. Additionally, a set of less intense bands in the range between 500 and 600 nm arises due to transition to the first excited state, named Q-bands.
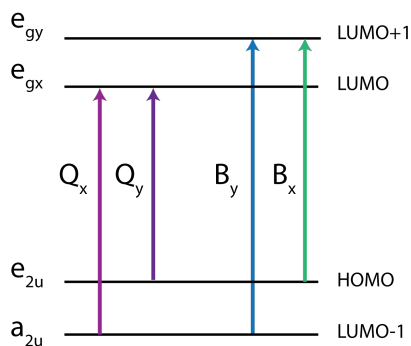


**Figure 6.4:** Simplified representation of the HOMO and LUMO orbitals in porphyrins and the electronic transitions between them.

One-electron reduction of FePPIX and CoPPIX results in a blue-shift of The Soret band. This shift is reversed upon two-electron reduction and the Soret band becomes somewhat broader and lower in intensity, see Figure 6.5 and Figure 6.7. The Q-bands of FePPIX and CoPPIX display two clear peaks, in which the two peaks are less resolved upon-one electron reduction. Instead, one higher-intensity band is centered between the two original peaks. Two-electron reduction results in broadened Q-bands.

To investigate whether electrons could be transferred from the conduction band of the semiconductor to the catalysts, semiconductor thin films with anchored catalysts were irradiated with UV-light for band-gap excitation, while the absorption spectra was measured. Comparison of these to the absorption spectra of reduced species obtained electrochemically was used to determine a possible conduction band mediated process, see Figure 6.6 and Figure 6.8. The changes in the photoinduced absorption spectra were similar to that of the electrochemically generated variations. Therefore, it was concluded that two-electron reduction of both the cobalt and the iron porphyrin was possible by band-gap excitation of $TiO_2$.
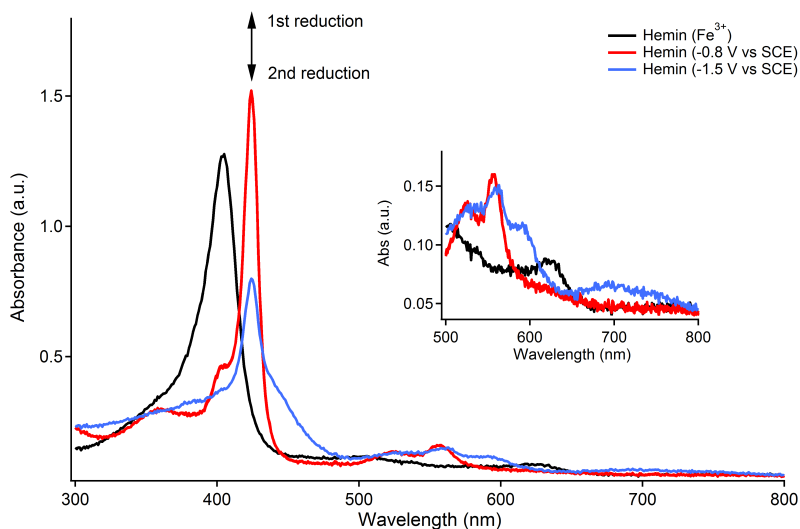
**Figure 6.5:** Absorption spectra of FePPIX during electrochemical reduction in deaerated 0.1 M TBAPF$_6$/DMSO. The inset emphasizes the Q-band region.
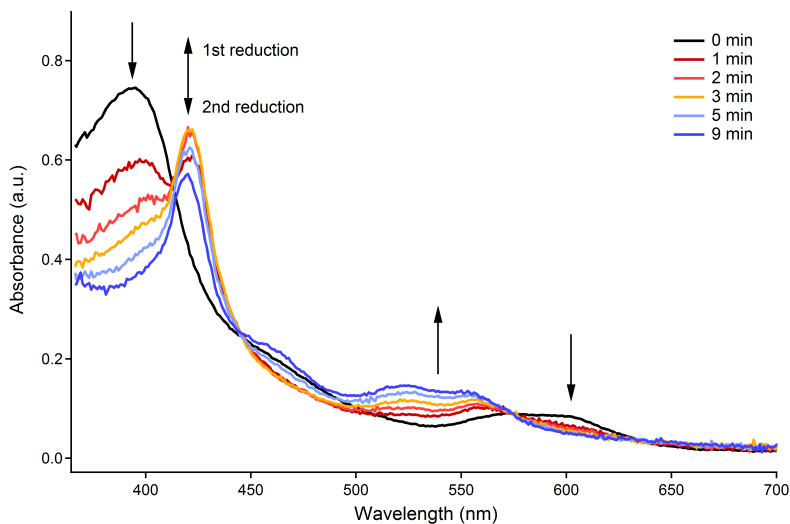


**Figure 6.6:** Absorption spectra of a FePPIX/TiO$_2$ thin film in deaerated 0.1 M TBAPF$_6$/DMSO during irradiation with UV-light ($\lambda$ = 250–350 nm)
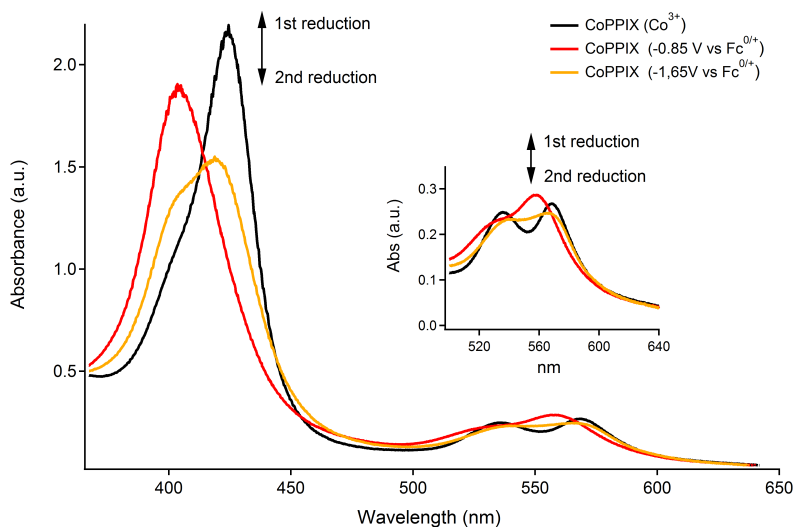
**Figure 6.7:** Absorption spectra of CoPPIX during electrochemical reduction in deaerated 0.1 M TBAPF$_6$/DMSO. The inset emphasizes the Q-band region.
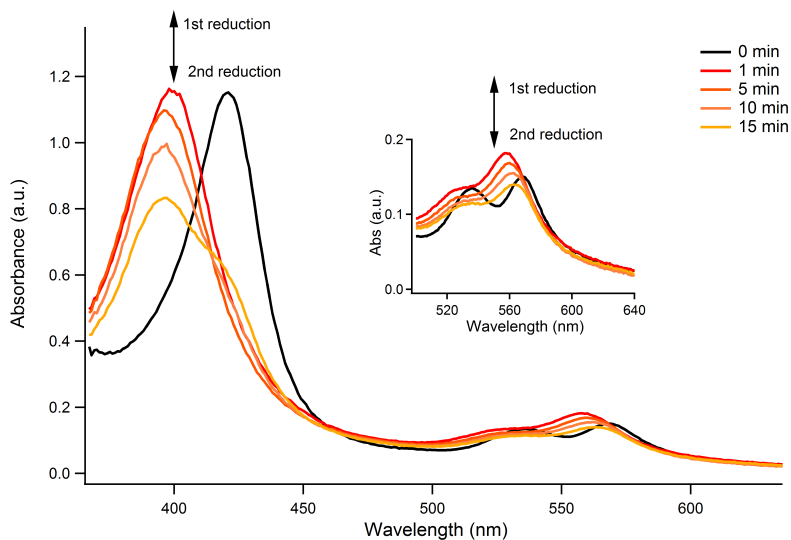


**Figure 6.8:** Absorption spectra of an CoPPIX/TiO$_2$ thin film in deaerated 0.1 M LiClO$_4$/CH$_3$CN during irradiation with UV-light ($\lambda = 250$–350 nm).

## 6.3 Visible light generation of reduced catalyst through CBM-ET

### 6.3.1 In Dye-TiO₂-catalyst assemblies

After demonstrating that the catalysts can be reduced by electron transfer from the conduction band, the next step was to initiate this process with visible light. This is of special interest for maximizing the use of solar energy by targeting the maximum range of the solar radiation. For this, the semiconductor was sensitized with the organic dye D35 and the model catalyst, CoPPIX. Two different methods for co-sensitization of TiO₂ were evaluated: (i) two-step sensitization and (ii) simultaneous sensitization from solutions containing both dye and catalyst molecules. The latter was the most efficient method for controlling the ratios of the dye and the catalyst at the semiconductor surface. It was observed that the porphyrins were attached at the TiO₂ surface much more rapidly than the dye. Therefore, the two-step sensitization process, which consisted on introducing the D35-sensitized films to a porphyrin solution, resulted in rapid desorption of the dye, which to an extent could not be controlled.

Characterization of electron transfer processes at the co-sensitized TiO₂ films becomes very challenging due to the overlap between the dye and catalyst absorption spectra, Figure 6.9. This makes it difficult to ensure selective excitation of the dye and selective detection of chemical species.
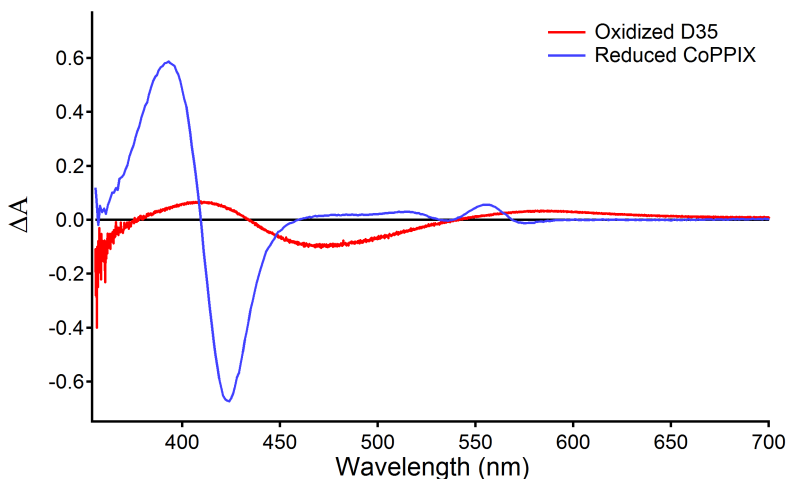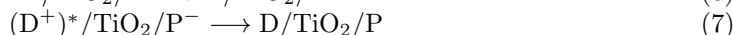


**Figure 6.9:** Absorption spectra of oxidized D35 and reduced CoPPIX in ethanol and DMSO solutions respectively.

In **Paper IV**, transient absorption spectroscopy was used to demonstrate visible-light induced CBM electron transfer in co-sensitized D35/TiO₂/CoPPIX thin films. The cobalt protoporphyrin was the most appropriate for this study because FePPIX is known to undergo autoreduction when attached to TiO₂ thin films.[60] Moreover, only the cobalt

porphyrin was able to undergo two-electron reduction by band-gap excitation when anchored to $SnO_2$, and this was important considering the work presented in **Paper III**. For these measurements, only $CH_3CN$-based electrolytes were suitable because the dye D35 easily desorbed from the $TiO_2$ surface upon DMSO addition.

Several considerations for the correct interpretation of the transient absorption data of the co-sensitized $TiO_2$ thin films must be done. First of all, the occurrence of several possible photoinduced reactions in the hybrid material must be considered. According to the energy diagram in Figure 6.10, the following reactions are thermodynamically allowed:

$$D^*/TiO_2/P \longrightarrow D^+/TiO_2(e^-)/P \qquad (1)$$
$$D^+/TiO_2(e^-)/P \longrightarrow D/TiO_2/P \qquad (2)$$
$$D^+/TiO_2(e^-)/P \longrightarrow D^+/TiO_2/P^- \qquad (3)$$
$$D^+/TiO_2(e^-)/P^- \longrightarrow D^+/TiO_2/P^{2-} \qquad (4)$$
$$D^+/TiO_2(2e^-)/P \longrightarrow D^+/TiO_2/P^{2-} \qquad (5)$$
$$D^*/TiO_2/P \longrightarrow D/TiO_2/P^- \qquad (6)$$
$$(D^+)^*/TiO_2/P^- \longrightarrow D/TiO_2/P \qquad (7)$$
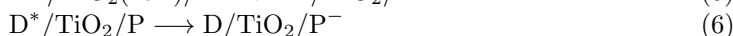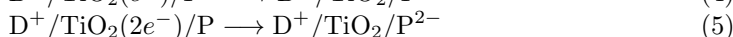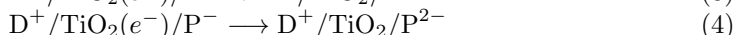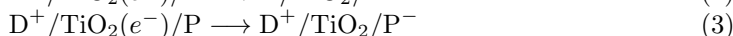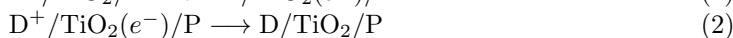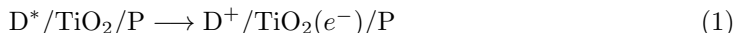
In these reactions, D, $D^*$ and $D^+$ represent the ground state, excited state and radical cation of the dye respectively; whereas P, $P^-$ and $P^{2-}$ represent the ground state, singly reduced and doubly reduced cobalt porphyrin respectively.[1] The reactions correspond to (1) electron injection; (2) Back-electron transfer; (3) First reduction of the porphyrin by a CB-electron; (4) Second reduction of the porphyrin by a CB-electron; (5) Concerted double reduction of the porphyrin by CB-electrons; (6) Direct ET from the excited dye to the porphyrin; (7) Regeneration of oxidized dye by electron transfer from the reduced porphyrin.

For the investigation of a possible CBM-ET mechanism, the wavelengths of interest are the absorption of (1) the dye radical cation ($D^+$), (2) the reduced electron acceptor ($P^{-/2-}$), (3) the ground state of the dye and (4) the ground state of the porphyrin. From analysis of Figure 6.9, the wavelengths at which selective detection of these species is possible. However, these wavelengths are sensitive to the surrounding electrolyte, and therefore, careful choice of the probe wavelength was very important to ensure the detection of the desired species. To illustrate this, transient absorption spectra of D35/$TiO_2$/CoPPIX thin films are shown in Figure 6.11.

Demonstration of visible-light induced CBM electron transfer in the co-sensitized films was performed by exciting the samples at $\lambda = 480$ nm, where mainly the dye D35 is excited. The radical cation of the dye was observed at $\lambda = 680$ nm without any contribution from the catalyst, Figure 6.12 (a). BET kinetics were obtained by analyzing the decay of this signal. From visual inspection it is clear that the kinetics were slower in the presence of the catalyst, Figure 6.12. Charge recombination rate constants obtained from KWW modelling are shown in Table 6.1. There is no doubt that the $k_{cr}$ values

---

[1]Be aware that these are simplified reaction schemes, where charges in the equations are not balanced
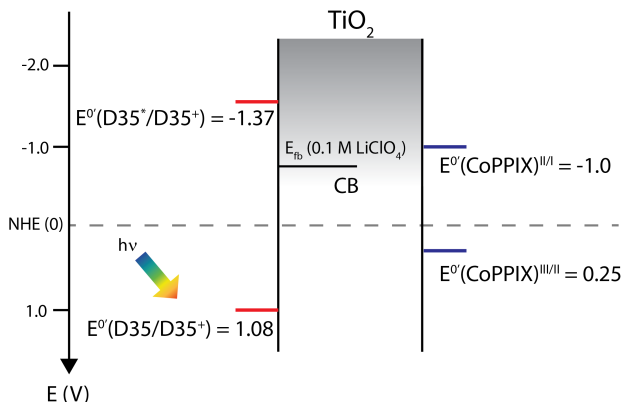
**Figure 6.10:** The relevant energies and redox potentials of the studied system. D35 redox potentials are as reported by Ellis *et al.*[124] Flat-band potential of $TiO_2$ is as reported by Redmond *et al.*[202] All values are given on the NHE scale.

decreased with increasing amount of CoPPIX at the surface. This was a first indication that the photoinjected electrons are further transferred to other sites other than the $TiO_2$ CB before recombining.

**Table 6.1:** Charge recombination rate constants $k_{cr}$ and $\beta$ parameters obtained from KWW global fittings from triplicate samples, of transient absorption decays measured at $\lambda = 680$ nm.

| Solvent | Ratio D35:CoPPIX | $\beta$ | $k_{cr}/s^{-1}$ |
|---------|------------------|---------|-----------------|
| $CH_3CN$ | 1:0 | 0.20 | $1.19 \times 10^3$ |
| $CH_3CN$ | 15:1 | 0.26 | $1.11 \times 10^2$ |
| $CH_3CN$ | 8:1 | 0.24 | $1.48 \times 10^1$ |
| $LiClO_4$ | 1:0 | 0.17 | $8.85 \times 10^3$ |
| $LiClO_4$ | 15:1 | 0.28 | $2.50 \times 10^3$ |
| $LiClO_4$ | 8:1 | 0.35 | $6.87 \times 10^2$ |

Reduction of the porphyrin was probed by measuring the differential absorption at $\lambda = 430$–440 nm, with small or no contribution from the dye, Figure 6.12 (b). This negative signal is attributed to the GS-bleach of the Co(III) species and it is confirmed that the amplitude of $\Delta A$ at t=0 is larger when increasing the concentration of CoPPIX at the surface. Control experiments with CoPPIX sensitized $TiO_2$ excited at the same wavelength did not result in detectable $\Delta A$ signals. On this ground, the spectroscopic signals corresponding to the reduced catalyst could be attributed to a CBM mechanism in which electrons were transferred from the dye to the catalyst. A direct electron transfer mechanism between the dye and the catalyst was also disregarded as a possible pathway
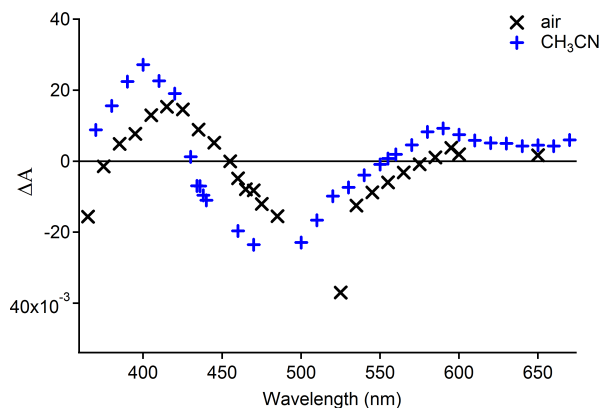
**Figure 6.11:** Transient absorption spectra (t=0) of D35/TiO$_2$/CoPPIX thin films constructed from single wavelength individual decays measured with PMT detection after pulsed excitation.
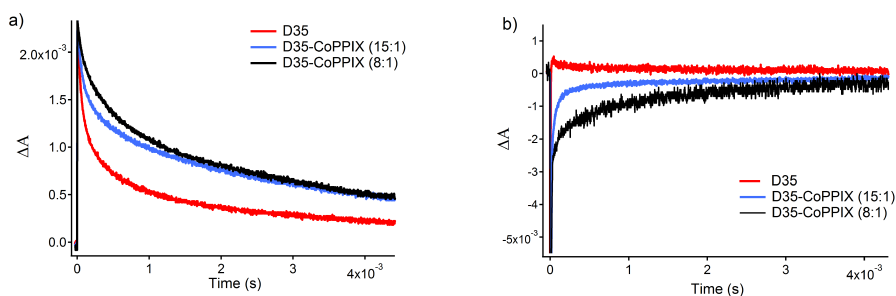


**Figure 6.12:** Single-wavelength transient absorption kinetics of TiO$_2$ thin films with different ratios of dye and catalyst in 0.1 M LiClO$_4$/CH$_3$CN. Measured at a) 680 nm and b) 442 nm. Pulsed 480 nm light was used as excitation.

when measurement of a mixture of D35 and CoPPIX in solution did not result in any appreciable transient signal.

According to the equations presented above, the mechanism of ground state dye recovery in co-sensitized TiO$_2$ films is expected to have contributions from both electrons in the CB and electrons located at the reduced porphyrin. Although it is unclear at this stage which one is predominant, the slower recovery in co-sensitized films points to a mechanism where the electron is either a longer distance away from the hole, or needs to overcome an energy barrier to recombine, which would most likely be the case for a CBM-process. Additional processes at the surface, such as lateral hole transfer[203,204] should also be considered in further investigations, given that they could compete with CBM-ET reducing the efficiency of solar-to-chemical conversion.

In conclusion, conduction band mediated electron transfer from the organic dye D35 to a Co-protoporphyrin model electron acceptor was shown and it was demonstrated that

66

the reaction was initiated by visible light. The CBM process resulted in at least a singly reduced Co-species and possibly a doubly reduced catalyst. The double reduction is a thermodynamically allowed process according to electrochemical data and it was shown to occur by bandgap excitation, therefore it is likely that this product was obtained. However, this cannot be concluded from the available transient absorption data. Further detailed kinetic analysis and modelling of the transient absorption spectra is needed to establish the exact products and mechanisms of the photoinduced reactions.

### 6.3.2  In patterned $SnO_2 - TiO_2$ thin films

Visible light-induced CBM electron transfer was also demonstrated in **Paper III** using the same photosensitizer and catalyst. The patterned films were selectively sensitized with the dye at the $TiO_2 - SnO_2$ and with the catalyst at the $SnO_2$-only regions. The film was probed at selected locations by focusing the probe beam as illustrated in Figure 6.13. Photoexcitation of the dye D35 resulted in a negative transient signal at 432 nm that could be assigned to a reduced state of the Co(III)protoporphyrin in co-sensitized samples, see panel b in Figure 6.14. Control experiments confirmed that this transient signal was only generated in co-sensitized films (panels a and c in Figure 6.14) and thus a CBM mechanism process was necessary to explain the observation.
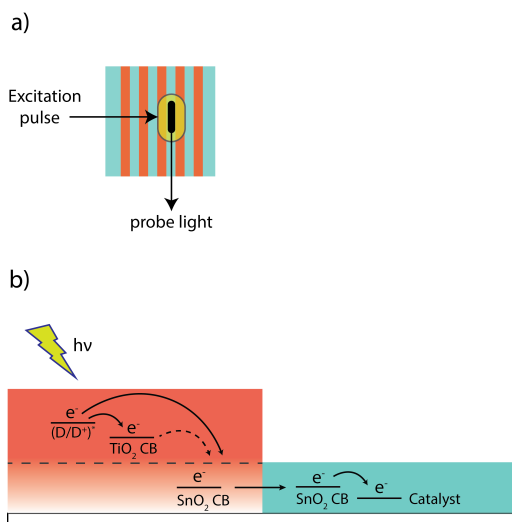


**Figure 6.13:** a) Schematic representation of co-sensitized patterned $SnO_2 - TiO_2$ thin films (top view), illustrating how the excitation and probe beam where placed for the measurements in Figure 6.14 b) Side view of co-sensitized patterned $SnO_2 - TiO_2$ thin films illustrating visible light-induced CBM electron transfer.

This experiment was also a proof-of-principle supporting the conclusion in **Paper III** that the photoinjected electrons were transported to the dye-free $SnO_2$ areas of the patterned films, being this the main reason for the observed decreased in BET rate constants.
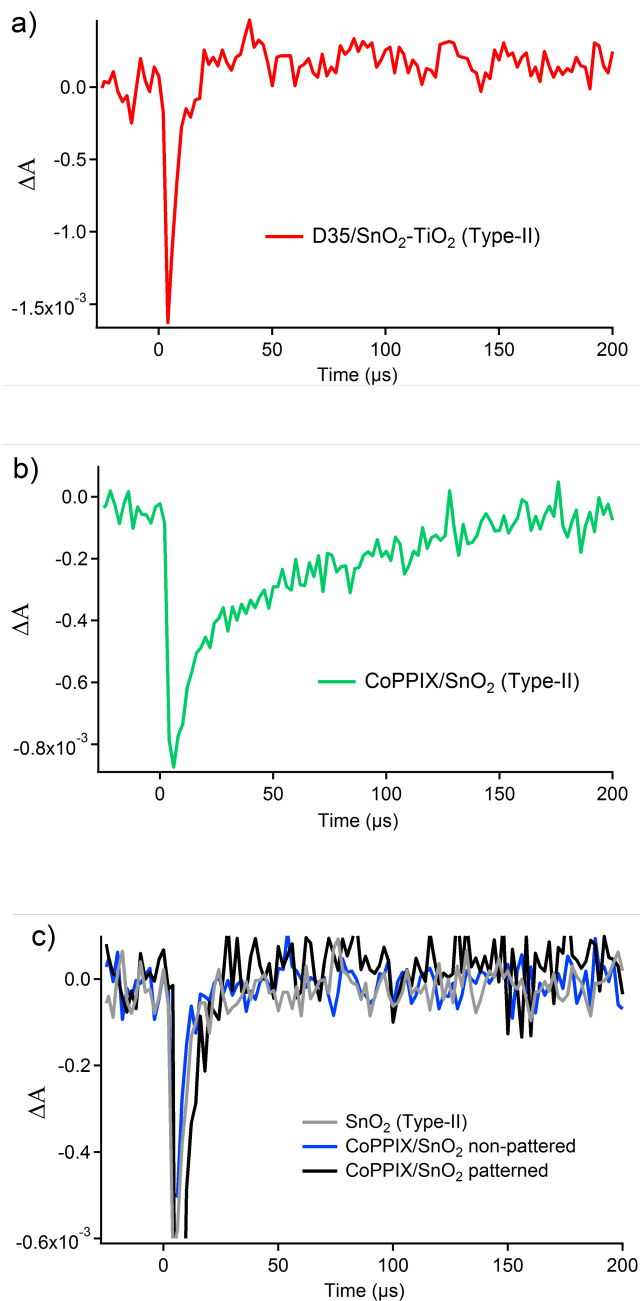
**Figure 6.14:** Single-wavelength transient absorption kinetics recorded at 432 nm in a) co-sensitized Type-II patterned film at the $D35/SnO_2 - TiO_2$ region, b) co-sensitized Type-II patterned film probed at the $CoPPIX/SnO_2$ region, c)Type-II patterned film probed at the $SnO_2$ (gray), non-patterned $CoPPIX/SnO_2$ thin film (blue) and patterned $CoPPIX/SnO_2$ thin film (black). All measurements performed in 0.1 M $LiClO_4/CH_3CN$.

## 6.4 One or two-electron reduction?

Consecutive transient absorption measurements on co-sensitized patterned $SnO_2/TiO_2$ thin films revealed increasing $\Delta A$ amplitudes of the transient negative signal corresponding to the bleach of the CoPPIX ground state, and an increasing very long lived positive feature building from around 200 µs, after decay of the bleach signal, Figure 6.15.
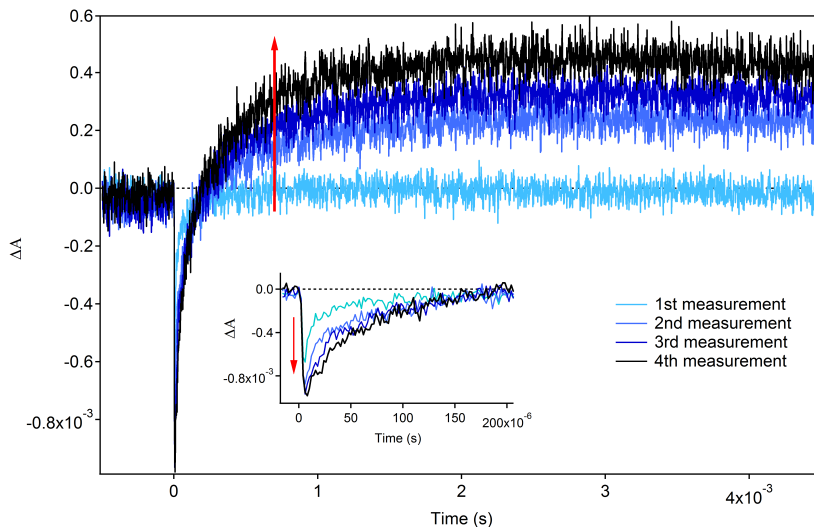


**Figure 6.15:** Consecutive single-wavelength absorption measurements ($\lambda = 432$ nm) of a co-sensitized Type-II patterned film in 0.1 M $LiClO_4/CH_3CN$.

This rises the question whether this is a result of a two-electron reduction process that is observed after accumulation of the first reduced species at the semiconductor surface. The amplitude of the positive transient signal increases at each consecutive measurement, which could be interpreted as increased formation of the two-electron reduced species. However, these results are not conclusive but rather speculative and further investigation is required to distinguish between one and two-electron transfer processes.

# Conclusions and future oultook

The main purpose of this thesis was to investigate strategies to extend photoinduced charge separation in molecules and dye-sensitized semiconductor assemblies, a contemporary problem in the growing field of solar-to-chemical energy conversion. Characterization of photoinduced electron transfer and other photophysical processes in the materials studied was performed by using optical spectroscopic techniques.

The following approaches to long-lived charge separation were investigated: (i) The design of a supramolecular photosensitizer-catalyst for photocatalytic water oxidation; (ii) the use of ionic liquids in dye-sensitized semiconductors; (iii) a novel dye-sensitized semiconductor photoanode design based on $SnO_2$ and $TiO_2$; and (iv) the integration of photosensitizer and catalyst molecules on a semiconductor surface for electron transfer facilitated by the conduction band.

Steady state and time-resolved emission spectroscopic studies showed that photocatalytic water oxidation in the supramolecular assembly was unsuccessful due to rapid intramolecular quenching of the Ru-photosensitizer excited state. This prevented efficient electron transfer from the Mn-catalyst and therefore extraction of electrons from water. Most likely, this originated from the complex electronic structure arising from structural modifications on the Ru-complex, as supported by TDDFT calculations. This study exemplified some of the difficulties and disadvantages of supramolecular approaches to solar energy conversion. These point to a need of creating nanostructured architectures where the individual functions of photosensitizers and catalysts can be incorporated on a stable structure.

Transient absorption spectroscopy was used to investigate the kinetics of charge recombination in dye-sensitized semiconductors. It was shown that the lifetime of the charge separated state could be extended with the use of ionic liquid electrolytes. An electrostatic mechanism where local charge accumulation was rapidly compensated by the ionic liquid cations was proposed. Although this mechanism was not experimentally confirmed, literature findings supported this conclusion.

Charge separation was also shown to be extended in a dye-sensitized µm-thin film consisting of patterned layers of nanoporous $SnO_2$ and $TiO_2$. A novel method for dye-sensitization of selected film areas was presented. The lifetime of charge-separation was extended by several orders of magnitude by trapping the photoinjected electrons on dye-free $SnO_2$ areas on the film. This was confirmed by additional experiments demonstrating the transfer of these electrons (in $SnO_2$) to an electron acceptor anchored to $SnO_2$. These results implied that, compared to traditional dye-sensitized semiconductors, the electrons were transported over significantly long ranges on the film. The main determining factors in the observation of this effect were the intensity of the irradiation and the presence of $Li^+$ ions. The principles of the design strategy presented here can find potential application in photocatalysis and photoelectrosynthesis cells as suggested in Figure 7.1.

The impact of changing the macroscopic structure of the semiconductor thin film—photoanode design—was greater in extending charge separation than that of changing the environment by the use of ionic liquids. This does not imply that one strategy should be preferred over the other but rather that they may be used with different purposes.

Transient absorption spectroscopic studies on dye-catalyst co-sensitized $TiO_2$ thin films were performed for visible-light conduction band mediated electron transfer between the two molecules. This process was shown to be initiated by visible-light. A conduction band
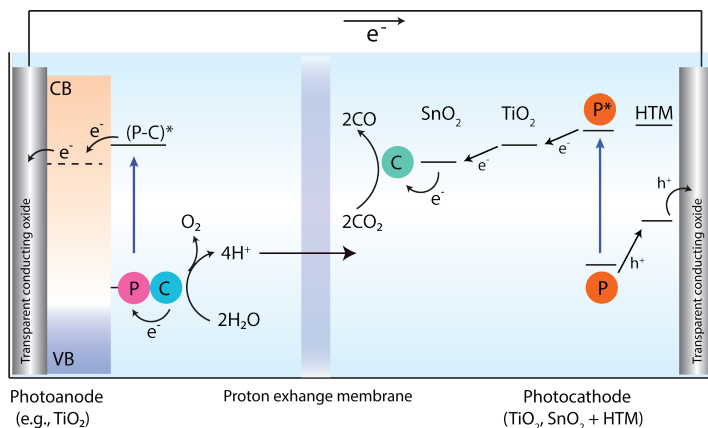
**Figure 7.1:** Illustration of a DSPEC where water oxidation and $CO_2$ reduction takes place. The photocathode is based on the design principles presented in **Paper-III**. A hole-transporting material (HTM) is included in the structure for regeneration of the photosensitizer

mechanism was shown in both co-sensitized $TiO_2$ thin films, and patterned $SnO_2$–$TiO_2$ thin films. The most relevant feature of the patterned films, is that the donor and the acceptor are physically separated at the surface while electronic transport is still possible between, through the conduction band of the semiconductors. This work herein is a significant step toward the solution the long-standing problem of solar fuels formation by visible light.

The results summarized here, speak in favor of hybrid material approaches for the conversion of solar energy, specifically molecular-semiconductor assemblies. As exemplified in the work presented in this thesis, these type of materials have advantages from the point of view of manufacturing, stability and the possibilities of controlling the electronic transfer processes through the simple modification of their components. In doing so, they can be easily adapted for different applications such as photocatalysis and solar fuel generation.

During the course of these investigations, some important new questions were raised and should be addressed in the future. The different, and sometimes contradictory, observed effects of $Li^+$ ions on the interfacial electron transfer processes at dye-sensitized semiconductors needs to be further explored. From our observations it can be said that the effect of $Li^+$ ions differs depending upon several factors such as the structure of the dye, the properties of the semiconductor and the macroscopic structure of the nanocrystalline substrate. This becomes more complicated when introducing additional components to the hybrid material, for example electron acceptors or catalysts. Additionally, the exact mechanisms of ground state dye recovery in the assemblies investigated in **Paper-III** and **Paper-IV** remain unclear. Likewise, further characterization of the reduced state(s) of the model catalyst is needed to distinguish between single and double reduction processes.

Future steps in the continuation of this research are the optimization of conditions to maximize the efficiency of conduction band mediated electron transfer and the evaluation of visible-light induced photocatalytic activity at the dye-semiconductor-catalyst assemblies with focus on $CO_2$ reduction. This includes the development of catalysts with selective activity for products of interest.

# References

[1] G. Ciamician. The photochemistry of the future. *Science* **36**.926 (1912), 385–394.

[2] I. E. Agency. *Key world energy statistics*. Report. International Energy Agency, 2016.

[3] E. Becquerel. Recherches sur les effets de la radiation chimique de la lumière solaire, au moyen des courants électriques. *C.R. Acad. Sci.* **9** (1839), 145–149.

[4] D. Chapin, C. Fuller, and G. Pearson. A New Silicon p-n Junction Photocell for Converting Solar Radiation into Electrical Power. *J. Appl. Phys.* **25** (1954), 676.

[5] A. Fujishima and K. Honda. Electrochemical Photolysis of Water at a Semiconductor Electrode. *Nature* **238**.5358 (1972), 37.

[6] L. Hammarström and M. Wasielewski. Biomimetic approaches to artificial photosynthesis. *Energy Environ. Sci.* **4** (2011), 2339.

[7] M. Graetzel and K. Kalyanasundaram. Artificial photosynthesis: biomimetic approaches to solar energy conversion and storage. *Curr. Opin. Biotechnol.* **21** (2010), 289–310.

[8] T. Meyer. Chemical Approaches to Artificial Photosynthesis. *Acc. Chem. Res.* **22**.5 (1989), 163–170.

[9] J. Alstrum-Acevedo, M. Brennaman, and T. Meyer. Chemical Approaches to Artificial Photosynthesis.2. *Inorg. Chem.* **44**.20 (2005), 163–170.

[10] Y. Tachibana, L. Vayssieres, and J. R. Durrant. Artificial photosynthesis for solar water-splitting. *Nat. Photonics* **6** (2012), 511–518.

[11] F. Rappaport, M. Guergova-Kuras, P. Nixon, B. Diner, and J. Lavergne. Kinetics and Pathways of Charge Recombination in Photosystem II. *Biochemistry* **41**.26 (2002), 8518–8527.

[12] M. G. Najafpour. Oxygen evolving complex in Photosystem II: Better than excellent. *Dalton Trans.* **40** (2011), 9076–9084.

[13] M. Abrahamsson. "Tuning of the excited state properties of ruthenium (II)-polypyridil complexes". Thesis. 2006.

[14] T. C. B. Harlang, Y. Liu, O. Gordivska, L. A. Fredin, C. S. Ponseca, P. Huang, P. Chábera, K. S. Kjaer, H. Mateos, J. Uhlig, R. Lomoth, R. Wallenberg, S. Styring, P. Persson, V. Sundström, and K. Wärnmark. Iron sensitizer converts light to electrons with 92% yield. *Nat. Chem.* **7** (2015), 883–839.

[15] A. Mishra, M. Fischer, and P. Bäuerle. Metal-Free Organic Dyes for Dye-Sensitized Solar Cells: From Structure: Property Relationships to Design Rules. *Angew. Chem.* **48** (2009), 2474–2499.

[16] P. Kamat. Quantum Dot Solar Cells. Semiconductor Nanocrystals as Light Harvesters. *J. Phys. Chem. C* **112** (2008), 18737–18753.

[17] A. Kojima, K. Teshima, Y. Shirai, and T. Miyasaka. Organometal Halide Perovskites as Visible-Light Sensitizers for Photovoltaic Cells. *J. Am. Chem. Soc.* **131** (2009), 6050–6051.

[18] S. Fukuzumi, K. Ohkubo, and T. Suenobu. Long-Lived Charge Separation and Applications in Artificial Photosynthesis. *Acc. Chem. Res.* **47**.5 (2014), 1455–1464.

[19] M. K. Brennaman, R. J. Dillon, L. Alibabaei, M. K. Gish, C. J. Dares, D. L. Ashford, R. L. House, G. J. Meyer, J. M. Papanikolas, and T. J. Meyer. Finding the Way to Solar Fuels with Dye-Sensitized Photoelectrosynthesis Cells. *J. Am. Chem. Soc.* **138**.40 (2016), 13085–13102.

[20] H. Imahori, D. Guldi, K. Tamaki, Y. Yoshida, C. Luo, Y. Sakata, and S. Fukuzumi. Charge Separation in a Novel Artificial Photosynthetic Reaction Center Lives 380 ms. *J. Am. Chem. Soc.* **123**.27 (2001), 6617–6628.

[21] M. Abrahamsson, M. Jäger, T. Österman, L. Eriksson, P. Persson, B. H-C., O. Johansson, and L. Hammarström. A 3.0 μs Room Temperature Excited State Lifetime of a Bistridentate Ru(II)-Polypyridine Complex for Rod-like Molecular Arrays. *J. Am. Chem. Soc.* **128**.39 (2006), 12616–12617.

[22] L. Sun, L. Hammarström, B. Åkermark, and S. Styring. Towards artificial photosynthesis: ruthenium–manganese chemistry for energy production. *Chem. Soc. Rev.* **30** (2001), 36–49.

[23] K.-H. Rhee, E. Morris, J. Barber, and W. Kühlbrandt. Three-dimensional structure of the plant photosystem II reaction centre at 8 Å resolution. *Nature* **396** (1998), 283–286.

[24] V. Klimov. Discovery of pheophytin function in the photosynthetic energy conversion as the primary electron acceptor of Photosystem II. *Photosyn. Res.* **76** (2003), 247–253.

[25] M. Wasielewski. Photoinduced Electron Transfer in Supramolecular Systems for Artificial Photosynthesis. *Chem. Rev.* **92**.3 (1992), 435–461.

[26] A. N. Macpherson, P. A. Liddell, S. Lin, L. Noss, G. Seely, J. DeGraziano, A. Moore, T. Moore, and D. Gust. Ultrafast Photoinduced Electron Transfer in Rigid Porphyrin-Quinone Dyads. *J. Am. Chem. Soc.* **117**.27 (1995), 7202–7212.

[27] J. Barber and M. Archer. P680, the primary electron donor of photosystem II. *Photochem. Photobiol. A: Chemistry* **142** (2001), 97–106.

[28] A. Moore, T. Moore, and D. Gust. Molecular Mimicry of Photosynthetic Energy and Electron Transfer. *Acc. Chem. Res.* **26** (1993), 198–205.

[29] D. Gust, T. Moore, A. Moore, S.-J. Lee, E. Bittersmann, D. Luttrull, A. Rehms, J. DeGraziano, X. Ma, F. Gao, R. Belford, and T. Trier. Efficient Multistep Photoinitiated Electron Transfer in a Molecular Pentad. *Science* **248**.4952 (1990), 199–201.

[30] J. Megiatto, A. Antoniuk-Pablant, B. Sherman, G. Kodis, M. Gervaldo, T. Moore, A. Moore Moore, and D. Gust. Mimicking the electron transfer chain in photosystem II with a molecular triad thermodynamically capable of water oxidation. *Proc. Natl. Acad. Sci. U.S.A.* **109**.39 (2012), 15578–15583.

[31] F. D'Souza, C. A. Wijesinghe, M. E. El-Khouly, J. Hudson, M. Niemi, H. Lemmetyinen, N. V. Tkachenko, M. E. Zandler, and S. Fukuzumi. Ultrafast excitation transfer and charge stabilization in a newly assembled photosynthetic antenna-reaction center mimic composed of boron dipyrrin, zinc porphyrin and fullerene. *Phys. Chem. Chem. Phys.* **13** (2011), 18168–18178.

[32] M. Gilbert Gatty, A. Kahnt, L. Esdaile, M. Hutin, H. Anderson, and B. Albinsson. Hopping versus Tunneling Mechanism for Long-Range Electron Transfer in Porphyrin Oligomer Bridged Donor–Acceptor Systems. *J. Phys. Chem. B* **119**.24 (2015), 7598–7611.

[33] R. Lomoth, T. Häupl, and L. Hammarström. Redox-switchable direction of photoinduced electron transfer in an Ru(bpy)$_3^{2+}$-viologen dyad. *Chemistry* **8**.1 (2000), 102–110.

[34] S. Karlsson, J. Boixel, Y. Pelegrin, B. E, H.-C. Becker, F. Odobel, and L. Hammarström. Accumulative electron transfer: Multiple charge separation in artificial photosynthesis. *Farad. Discuss.* **155** (2012), 233–252.

[35] L. Hammarström. Accumulative Charge Separation for Solar Fuels Production: Coupling Light-Induced Single Electron Transfer to Multielectron Catalysis. *Acc. Chem. Res.* **48** (2015), 840–85.

[36] S. Karlsson, J. Boixel, Y. Pellegrin, E. Blart, H. C. Becker, F. Odobel, and L. Hammarstrom. Accumulative Charge Separation Inspired by Photosynthesis. *J. Am. Chem. Soc.* **132**.51 (2010), 17977–17979.

[37] S. Bai, W. Yin, L. Wang, Z. Li, and Y. Xiong. Surface and interface design in cocatalysts for photocatalytic water splitting and $CO_2$ reduction. *RCS Adv.* **6** (2016), 57446–57463.

[38] Y. Ling, G. Wang, D. Wheeler, J. Zhang, and Y. Li. Sn-Doped Hematite Nanostructures for Photoelectrochemical Water Splitting. *RCS Adv.* **11** (2011), 2119–2125.

[39] S. Piskunov, O. Lisovski, J. Begens, D. Bocharov, Y. Zhukovskii, M. Wessel, and E. Spohr. C-, N-, S-, and Fe-Doped $TiO_2$ and $SrTiO_3$ Nanotubes for Visible-Light-Driven Photocatalytic Water Splitting: Prediction from First Principles. *J. Phys. Chem.* **119** (2015), 18686–18696.

[40] S. Hong, S. Lee, J. Jang, and J. Lee. Heterojunction $BiVO_4/WO_3$ electrodes for enhanced photoactivity of water oxidation. *Energy Environ. Sci.* **4** (2011), 1781–1787.

[41] L. Yan, W. Zhao, and Z. Liu. 1D $ZnO/BiVO_4$ heterojunction photoanodes for efficient photoelectrochemical water splitting. *Dalton Trans.* **45** (2016), 11346–11352.

[42] J. Luo, L. Steier, M. Son, M. Schreier, M. Mayer, and M. Grätzel. $Cu_2O$ Nanowire Photocathodes for Efficient and Durable Solar Water Splitting. *Nano Lett.* **16** (2016), 1848–1857.

[43] S. Warren and E. Thimsen. Plasmonic solar water splitting. *Energy. Environ. Sci.* **5** (2012), 5133–5146.

[44] S. Linic, P. Christopher, and D. Ingram. Plasmonic-metal nanostructures for efficient conversion of solar to chemical energy. *Nat. Mater.* **10** (2011), 911–921.

[45] H. Gerischer, M. Michel-Beyerle, F. Rebentrost, and H. Tributsch. Sensitization of charge injection into semiconductors with large band gap. *Electrochim. Acta* **13** (1968), 1509–1515.

[46] H. Tributsch and M. Calvin. Electrochemistry of Excited Molecules - Photoelectrochemical reactions of chlorophylls. *Photochem. Photobiol.* **14**.2 (1971), 95–112.

[47] B. O'Regan and M. Grätzel. A low-cost, high-efficiency solar cell based on dye-sensitized colloidal $TiO_2$ films. *Nature* **353** (1991), 737–740.

[48] K. Kakiage, Y. Aoyama, T. Yano, K. Oya, J. Fujisawa, and M. Hanaya. Highly-efficient dye-sensitized solar cells with collaborative sensitization by silyl-anchor and carboxy-anchor dyes. *Chem. Comm.* **51**.88 (2015), 15894–15897.

[49]  N. Cherepy, G. Smestad, M. Grätzel, and J. Zhang. Ultrafast Electron Injection: Implications for a Photoelectrochemical Cell Utilizing an Anthocyanin Dye-Sensitized TiO$_2$ Nanocrystalline Electrode. *J. Phys. Chem. B* **101** (1997), 9342–9351.

[50]  H. Ghosh, J. Asbury, and T. Lian. Direct Observation of Ultrafast Electron Injection from Coumarin 343 to TiO$_2$ Nanoparticles by Femtosecond Infrared Spectroscopy. *J. Phys. Chem. B* **102** (1998), 6482–6486.

[51]  S. E. Koops, B. C. O'Regan, P. R. F. Barnes, and J. R. Durrant. Parameters Influencing the Efficiency of Electron Injection in Dye-Sensitized Solar Cells. *J. Am. Chem. Soc.* **131**.13 (2009), 4808–4818.

[52]  A. Listorti, B. O'Regan, and J. R. Durrant. Electron Transfer Dynamics in Dye-Sensitized Solar Cells. *Chem. Mater.* **23**.15 (2011), 3381–3399.

[53]  A. Hagfeldt and M. Grätzel. Light-Induced Redox Reactions in Nanocrystalline Systems. *Chem. Rev.* **95** (1995), 49–68.

[54]  A. Hagfeldt, G. Boschloo, L. Sun, L. Kloo, and H. Petterson. Dye-Sensitized Solar Cells. *Chem. Rev.* **110** (2010), 6595–6663.

[55]  W. Song, C. Glasson, H. Luo, K. Hanson, M. Brennaman, C. J.J., and T. Meyer. Photoinduced Stepwise Oxidative Activation of a Chromophore–Catalyst Assembly on TiO$_2$. *J. Phys. Chem. Lett.* **2**.14 (2011), 1808–1813.

[56]  W. J. Song, A. Ito, R. A. Binstead, K. Hanson, H. L. Luo, M. K. Brennaman, J. J. Concepcion, and T. J. Meyer. Accumulation of Multiple Oxidative Equivalents at a Single Site by Cross-Surface Electron Transfer on TiO$_2$. *J. Am. Chem. Soc.* **135**.31 (2013), 11587–11594.

[57]  Y. Gao, X. Ding, J. Liu, L. Wang, Z. Lu, L. Li, and L. Sun. Visible Light Driven Water Splitting in a Molecular Device with Unprecedentedly High Photocurrent Density. *J. Am. Chem. Soc.* **135** (2013), 4219–4222.

[58]  C. J. Wood, G. H. Summers, C. A. Clark, N. Kaeffer, M. Braeutigam, L. R. Carbone, L. D'Amario, K. Fan, Y. Farre, S. Narbey, F. Oswald, L. A. Stevens, C. D. J. Parmenter, M. W. Fay, A. La Torre, C. E. Snape, B. Dietzek, D. Dini, L. Hammarstrom, Y. Pellegrin, F. Odobel, L. C. Sun, V. Artero, and E. A. Gibson. A comprehensive comparison of dye-sensitized NiO photocathodes for solar energy conversion. *Phys. Chem. Chem. Phys.* **18** (2016), 10727–10738.

[59]  S. Ardo, D. Achey, A. J. Morris, M. Abrahamsson, and G. J. Meyer. Non-Nernstian two-electron transfer photocatalysis at metalloporphyrin-TiO2 interfaces. *J. Am. Chem. Soc.* **133**.41 (2011), 16572–80.

[60]  A. Staniszewski, A. J. Morris, T. Ito, and G. J. Meyer. Conduction band mediated electron transfer across nanocrystalline TiO$_2$ surfaces. *J. Phys. Chem. B* **111**.24 (2007), 6822–6828.

[61]  J.-S. Lee, D.-I. Won, W.-J. Jung, H.-J. Son, C. Pac, and S. Kang. Widely Controllable Syngas Production by a Dye-Sensitized TiO$_2$ Hybrid System with Re$^I$ and Co$^{III}$ Catalysts under Visible-Light Irradiation. *Angew. Chem.* **56** (2017), 976–980.

[62]  B. Hunter, G. H.B., and A. Müller. Earth-Abundant Heterogeneous Water Oxidation Catalysts. *Chem. Rev.* **116** (2016), 14120–14136.

[63]  P. Kamat and J. Bisquert. Solar Fuels. Photocatalytic Hydrogen Generation. *J. Phys. Chem. C* **117** (2013), 14873–14875.

[64] D. Vinyard and G. Brudvig. Progress Toward a Molecular Mechanism of Water Oxidation in Photosystem II. *Annu. Rev. Phys. Chem.* **68** (2017), 101–116.

[65] M. Lundberg, M. Blomberg, and P. Siegbahn. Oxyl Radical Required for O-O Bond Formation in Synthetic Mn-Catalyst. *Inorg. Chem.* **43**.1 (2004), 264–274.

[66] P. Siegbahn. Water oxidation mechanism in photosystem II, including oxidations, proton release pathways, O—O bond formation and $O_2$ release. *Biochim. Biophys. Acta* **1827** (2013), 1003–1019.

[67] C. Sens, I. Romero, M. Rodríguez, A. Llobet, T. Parella, and J. Benet-Buchholz. A New Ru Complex Capable of Catalytically Oxidizing Water to Molecular Dioxygen. *J. Am. Chem. Soc.* **126**.25 (2004), 7798–7799.

[68] P. Kurz. Oxygen evolving reactions catalysed by manganese–oxo-complexes adsorbed on clays. *Dalton Trans.* (2009), 6103–6108.

[69] E. A. Karlsson, B.-L. Lee, T. Åkermark, E. Johnson, M. Kärkäs, J. Sun, Hansson, J.-E. Bäckvall, and B. Åkermark. Photosensitized Water Oxidation by Use of a Bioinspired Manganese Catalyst. *Angew. Chem. Int. Ed.* **50** (2011), 11715–11718.

[70] H.-Y. Wang, E. Mijangos, S. Ott, and A. Thapper. Water Oxidation Catalyzed by a Dinuclear Cobalt–Polypyridine Complex. *Angew. Chem.* **53** (2014), 14499–14502.

[71] T. Ishizuka, A. Watanabe, H. Kotani, D. Hong, K. Satonaka, T. Wada, Y. Shiota, K. Yoshizawa, K. Ohara, K. Yamaguchi, S. Kato, S. Fukuzumi, and T. Kojima. Homogeneous Photocatalytic Water Oxidation with a Dinuclear $Co^{III}$–Pyridylmethylamine Complex. *Inorg. Chem.* **55**.3 (2016), 1154–1164.

[72] L. Lele Duan, F. Bozoglian, S. Mandal, B. Stewart, T. Privalov, A. Llobet, and L. Sun. A molecular ruthenium catalyst with water-oxidation activity comparable to that of photosystem II. *Nat. Chem.* **4** (2012), 418–423.

[73] J. Fillol, Z. Codolà, L. Garcia-Bosch I. Gómez, J. Pla, and M. Costas. Efficient water oxidation catalysts based on readily available iron coordination complexes. *Nat. Chem.* **3** (2011), 807–813.

[74] M. Schulze, V. Kunz, P. D. Frischmann, and F. Würthner. A supramolecular ruthenium macrocycle with high catalytic activity for water oxidation that mechanistically mimics photosystem II. *Nat. Chem.* **8** (2016), 576–583.

[75] B. Sherman, D. Ashford, A. Lapides, M. Sheridan, K.-R. Wee, and T. Meyer. Light-Driven Water Splitting with a Molecular Electroassembly-Based Core/Shell Photoanode. *J. Phys. Chem. Lett.* **6**.16 (2015), 3213–3217.

[76] R. Brimblecombe, A. Koo, G. Dismukes, G. Swiegers, and L. Spiccia. Solar Driven Water Oxidation by a Bioinspired Manganese Molecular Catalyst. *J. Am. Chem. Soc.* **132** (2010), 2892–2894.

[77] G. Moore, J. Blakemore, R. Milot, J. Hull, H. Song, L. Cai, C. Schmuttenmaer, R. Crabtree, and G. Brudvig. A visible light water-splitting cell with a photoanode formed by codeposition of a high-potential porphyrin and an iridium water-oxidation catalyst. *Energy. Envir. Sci.* **4** (2011), 2389–2392.

[78] L. Li, L. Duan, Y. Xu, M. Gorlov, A. Hagfeldt, and L. Sun. A photoelectrochemical device for visible light driven water splitting by a molecular ruthenium catalyst assembled on dye-sensitized nanostructured $TiO_2$. *Chem. Comm.* **46** (2010), 7307–7309.

[79]   W. Youngblood, S.-H. A. Lee, Y. Kobayashi, E. Hernandez-Pagan, P. Hoertz, T. Moore, A. Moore, D. Gust, and T. Mallouk. Photoassisted Overall Water Splitting in a Visible Light-Absorbing Dye-Sensitized Photoelectrochemical Cell. *J. Am. Chem. Soc.* **131**.3 (2009), 926–927.

[80]   J. M. Berg, J. L. Tymoczko, and L. Stryer. *Biochemistry*. W. H. Freeman, 2002.

[81]   E. Borgarello, J. Kiwi, E. Pelizzetti, M. Visca, and M. Grätzel. Photochemical cleavage of water by photocatalysis. *Nature* **289** (1981), 158–160.

[82]   D. Furlong, D. Wells, and W. Sasse. Colloidal Semiconductors in Systems for the Sacrificial Photolysis of Water: Sensitization of $TiO_2$, by Adsorption of Ruthenium Complexes. *J. Phys. Chem.* **90** (1986), 1107–1115.

[83]   H. Park and W. Choi. Visible-Light-Sensitized Production of Hydrogen Using Perfluorosulfonate Polymer-Coated $TiO_2$ Nanoparticles: An Alternative Approach to Sensitizer Anchoring. *Lagmuir* **22** (2006), 2906–2911.

[84]   K. Maeda, M. Eguchi, W. Youngblood, and T. Mallouk. Niobium Oxide Nanoscrolls as Building Blocks for Dye-Sensitized Hydrogen Production from Water under Visible Light Irradiation. *Chem. Mat.* **20** (2008), 6770–6778.

[85]   T. Shimidzu, T. Iyoda, and Y. Koide. An advanced visible-light-induced water reduction with dye-sensitized semiconductor powder catalyst. *J. Am. Chem. Soc.* **107**.1 (1985), 35–41.

[86]   Q. Li, Y. Che, C. Chen, H. Zhu, W. Ma, and J. Zhao. ortho-Dihydroxyl-9,10-anthraquinone dyes as visible-light sensitizers that exhibit a high turnover number for hydrogen evolution. *Phys. Chem. Chem. Phys.* **16** (2014), 6550–6554.

[87]   H. Yu, Y. ZHao, C. Zhou, L. Shang, Y. Peng, Y. Cao, L. Wu, C. Tung, and T. Zhang. Carbon quantum dots/$TiO_2$ composites for efficient photocatalytic hydrogen evolution. *J. Mater. Chem. A* **2** (2014), 3344–3351.

[88]   K. Kim, M. Kim, and J. Jang. Towards Visible Light Hydrogen Generation: Quantum Dot-Sensitization via Efficient Light Harvesting of Hybrid-$TiO_2$. *Sci. Rep.* **3** (2013), 3330.

[89]   X. CHang, T. Wang, and J. Gong. $CO_2$ photo-reduction: insights into $CO_2$ activation and reaction on surfaces of photocatalysts. *Energy Environ. Sci.* **9** (2016), 807–813.

[90]   J. L. White, M. F. Baruch, J. E. Pander, Y. Hu, I. C. Formeyer, J. E. Park, T. Zhang, K. Liao, J. Gu, Y. Yan, T. W. Shaw, E. Abelev, and A. B. Bocarsly. Light-Driven Heterogeneous Reduction of Carbon Dioxide: Photocatalysts and Photoelectrodes. *Chem. Rev.* **115**.23 (2015), 12888–12935.

[91]   A. J. Morris, G. J. Meyer, and E. Fujita. Molecular Approaches to the Photocatalytic Reduction of Carbon Dioxide for Solar Fuels. *Acc. Chem. Res.* **42**.12 (2009), 1983–1994.

[92]   B. Gholamkhass, H. Mametsuka, K. Koike, T. Tanabe, M. Furue, and O. Ishitani. Architecture of Supramolecular Metal Complexes for Photocatalytic $CO_2$ Reduction: Ruthenium-Rhenium Bi- and Tetranuclear Complexes. *Inorg- Chem.* **6** (2005), 2326–2336.

[93]   S. Sato, K. Koike, H. Inoue, and O. Ishitani. Highly efficient supramolecular photocatalysts for $CO_2$ reduction using visible light. *Photochem. Photobiol. Sci.* **6** (2006), 454–461.

[94] J. Bonin, M. Robert, and M. Routier. Selective and Efficient Photocatalytic $CO_2$ Reduction to CO Using Visible Light and an Iron-Based Homogeneous Catalyst. *J. Am. Chem. Soc.* **136** (2014), 16768–16771.

[95] D. Boston, C. Xu, D. Armstrong, and F. MacDonnell. Photochemical Reduction of Carbon Dioxide to Methanol and Formate in a Homogeneous System with Pyridinium Catalysts. *J. Am. Chem. Soc.* **135**.44 (2005), 16252–16255.

[96] F. Sastre, A. Puga, L. Liu, A. Corma, and H. García. Complete Photocatalytic Reduction of $CO_2$ to Methane by $H_2$ under Solar Light Irradiation. *J. Am. Chem. Soc.* **136** (2014), 6798–6801.

[97] P. Kumar, S. Kumar, S. Cordier, S. Paofai, R. Boukherroub, and S. Jain. Photoreduction of $CO_2$ to methanol with hexanuclear molybdenum $[Mo_6Br_{14}]^{2-}$ cluster units under visible light irradiation. *RSC Adv.* **4** (2014), 10420–10423.

[98] F. Sastre, A. Puga, L. Liu, A. Corma, and H. García. Synthesis and characterization of a quaternary nanocomposite based on $TiO_2/CdS/rGO/Pt$ and its application in the photoreduction of $CO_2$ to methane under visible light. *RSC Adv.* **5** (2015), 33914–33922.

[99] L. Hong, Z. Zhe, M. Jingchai, and Z. Jiang. Novel visible-light-driven $CdIn_2S_4$/mesoporous g-$C_3N_4$ hybrids for efficient photocatalytic reduction of $CO_2$ to methanol. *Molecular Catalysis* **430** (2017), 9–19.

[100] W. Ong, M. Gui, S. Chai, and A. Mohamed. Direct growth of carbon nanotubes on $Ni/TiO_2$ as next generation catalysts for photoreduction of $CO_2$ to methane by water under visible light irradiation. *RSC Advances* **3** (2013), 4505–4509.

[101] J. Atkins P.; De Paula. *Physical Chemistry*. 8th. UK: Oxford, 2006.

[102] A. Gilbert and J. Baggott. *Essentials of Molecular Photochemistry*. Blackwell Science, 1991.

[103] N. Turro. *Molecular Photochemistry*. W.A. Benjamin, Inc., 1965.

[104] M. J. Hollas. *Modern Spectroscopy*. 4th. Wiley & Sons, Ltd, 2004.

[105] J. Lakowicz. *Principles of fluorescence spectroscopy*. 3rd. Springer US, 2006.

[106] S. Larsson. *Chemical Physics*. CRC Press. Taylor and Francis Group, 2012.

[107] R. Marcus. Electron trasfer reactions in chemistry. Theory and experiment. *Rev. mod. Phys.* **65**.3 (1993), 599–610.

[108] P. Barbara, T. J. Meyer, and M. Ratner. Contemporary Issues in Electron Transfer Research. *J. Phys. Chem.* **100** (1996), 13148–13168.

[109] R. M. Metzger. Unimolecular electronics. *J. Mater. Chem.* **18** (2008), 4364–4396.

[110] M. Lundberg, M. Blomberg, and P. Siegbahn. Long-Range Electron Transfer in Biomolecules. Tunneling or Hopping. *J. Phys. Chem. B* **115** (2011), 12202–12207.

[111] P. Yu and M. Cardona. *Fundamentals of Semiconductors. Physics and Materials Properties*. 4th. Springer, 2010.

[112] B. Bharti, S. Kumar, H.-N. Lee, and R. Kumar. Formation of oxygen vacancies and $Ti^{3+}$ state in $TiO_2$ thin film and enhanced optical properties by air plasma treatment. *Sci. Rep.* **6**.32355 (2016).

[113] B. Morgan and G. Watson. Intrinsic n-type Defect Formation in $TiO_2$: A Comparison of Rutile and Anatase from GGA+U Calculations. *J. Phys. Chem. C* **114**.5 (2010), 2321–2328.

[114] Z. Zhou, Y. Min, X. Liu, J. Ding, J. Guo, F. Hu, and L. Liu. Regulation of oxygen vacancy types on $SnO_2$ (110) surface by external strain. *AIP Adv.* **6**.055102 (2016).

[115] H. Gerischer, M. E. Michel-Beyerle, F. Rebentrost, and H. Tributsch. Sensitization of charge injection into semiconductors with large band gap. *Electrochim. Acta* **13** (1968), 1509–1515.

[116] K. Kalyanasundaram. *Dye-sensitized Solar Cells*. EPFL Press, 2010.

[117] K. Virkki, H. Hakola, M. Urbani, L. Tejerina, M. Ince, M. V. Martínez-Díaz, T. Torres, V. Golovanova, V. Golovanov, and N. V. Tkachenko. Photoinduced Electron Injection from Zinc Phthalocyanines into Zinc Oxide Nanorods: Aggregation Effects. *J. Phys. Chem. C* **121** (2017), 9594–9605.

[118] J. N. Clifford, E. Martínez-Ferrero, A. Viterisi, and E. Palomares. Sensitizer molecular structure-device efficiency relationship in dye sensitized solar cells. *Chem. Soc. Rev.* **40** (2011), 1635–1646.

[119] J. Moser and M. Grätzel. Observation of temperature independent heterogeneous electron transfer reactions in the inverted Marcus region. *Chem. Phys.* **176** (1993), 493–500.

[120] H. Lu, J. Prieskorn, and J. Hupp. Fast Interfacial Electron Transfer: Evidence for Inverted Region Kinetic Behavior. *J. Am. Chem. Soc.* **115** (1993), 4927–4928.

[121] I. Martini, J. Hodak, and G. Hartland. Effect of Water on the Electron Transfer Dynamics of 9-Anthracenecarboxylic Acid Bound to $TiO_2$ Nanoparticles: Demonstration of the Marcus Inverted Region. *J. Phys. Chem. B* **102** (1998), 607–614.

[122] N. Tkachenko. *Optical Spectroscopy*. Elsevier Science, 2006.

[123] D. Evans, K. O´Conell, R. Peterson, and M. Kelly. Cyclic Voltammetry. *J. Chem. Educ.* **60**.4 (1983), 290–293.

[124] H. Ellis, I. Schmidt, A. Hagfeldt, G. Wittstock, and G. Boschloo. Influence of Dye Architecture of Triphenylamine Based Organic Dyes on the Kinetics in Dye-Sensitized Solar Cells. *J. Phys. Chem. C* **119**.38 (2015), 21775–21783.

[125] M. Abrahamsson, M. Jäger, R. J. Kumar, T. Östrerman, P. Persson, H.-C. Becker, O. Johansson, and L. Hammarström. Charge-Transfer Excited States of Ruthenium(II) Complexes. I. Quantum Yield and Decay Measurements. *J. Am. Chem. Soc.* **97** (1975), 7031–7037.

[126] X. Zhang and M. A. J. Rodgers. Energy and Electron Transfer Reactions of the MLCT State of Ruthenium Tris(bipyridyl)with Molecular Oxygen: A Laser Flash Photolysis Study. *J. Phys. Chem.* **99** (1995), 12797–12803.

[127] A. Juris, V. Balzani, F. Barigelletti, S. Campagna, P. Belser, and A. Von Zelewsky. Ru(II) polypyridine complexes: photophysics, photochemistry, electrochemistry ,and chemuluminescence. *Coord. Chem. Rev.* **84** (1998), 85–277.

[128] M. Grätzel. Photoelectrochemical cells. *Nature* **414**.6861 (2001), 338–344.

[129] C. J. Barbé, F. Arendse, P. Comte, M. Jirousek, F. Lenzmann, V. Shklover, and M. Grätzel. Nanocrystalline Titanium Oxide Electrodes for Photovoltaic Applications. *J. Am. Ceram. Soc.* **73** (1980), 3348–3357.

[130] Z. Banyamin, P. Kelly, G. West, and J. Boardman. Electrical and Optical Properties of Fluorine Doped Tin Oxide Thin Films Prepared by Magnetron Sputtering. *Coatings* **4** (2014), 732–746.

[131] D. Casanova. The Role of the $\pi$ Linker in Donor–$\pi$–Acceptor Organic Dyes for High-Performance Sensitized Solar Cells. *ChemPhysChem* **12** (2011), 2979–2988.

[132] X. Jiang, T. Marinado, E. Gabrielsson, D. P. Hagberg, L. C. Sun, and A. Hagfeldt. Structural Modification of Organic Dyes for Efficient Coadsorbent-Free Dye-Sensitized Solar Cells. *J. Phys. Chem. C* **114**.6 (2010), 2799–2805.

[133] S. M. Feldt, E. A. Gibson, E. Gabrielsson, L. Sun, G. Boschloo, and A. Hagfeldt. Design of Organic Dyes and Cobalt Polypyridine Redox Mediators for High-Efficiency Dye-Sensitized Solar Cells. *J. Am. Chem. Soc.* **132**.46 (2010), 16714–16724.

[134] D. P. Hagberg, X. Jiang, E. Gabrielsson, M. Linder, T. Marinado, T. Brinck, A. Hagfeldt, and L. C. Sun. Symmetric and unsymmetric donor functionalization. Comparing structural and spectral benefits of chromophores for dye-sensitized solar cells. *J. Mater. Chem.* **19**.39 (2009), 7232–7238.

[135] C. Anselmi, E. Mosconi, M. Pastore, E. Ronca, and F. De Angelis. Adsorption of organic dyes on $TiO_2$ surfaces in dye-sensitized solar cells: interplay of theory and experiment. *Phys. Chem. Chem. Phys* **14** (2012), 15963–15974.

[136] J. E. Moser and M. Grätzel. *J. Am. Chem. Soc.* **106** (1984), 6557.

[137] V. Sundström and M. Hilgendorf. *Chem. Phys.* **176** (1993), 493.

[138] J. Nelson. Continuous-time random-walk model of electron transport in nanocrystalline $TiO_2$ electrodes. *Phys. Rev. B* **59** (1999), 15374.

[139] E. Hao, N. Anderson, J. Asbury, and T. Lian. Effect of Trap States on Interfacial Electron Transfer between Molecular Absorbates and Semiconductor Nanoparticles. *J. Phys. Chem. B* **106** (2002), 10191–10198.

[140] Y. Weng, Y.-Q. Wang, J. B. Asbury, H. N. Ghosh, and T. Lian. Back Electron Transfer from $TiO_2$ Nanoparticles to $Fe^{III}(CN)_6^{3-}$: Origin of Non-Single-Exponential and Particle Size Independent Dynamics. *J. Phys. Chem. B* **104** (2000), 93–104.

[141] A. Listorti, B. O'Regan, and J. R. Durrant. Electron Transfer Dynamics in Dye-Sensitized Solar Cells. *Chem. Mater.* **23**.15 (2011), 3381–3399.

[142] A. C. Fisher, L. M. L. M. Peter, E. A. Ponomarev, A. A. B. Walker, and K. G. U. Wijayantha. Intensity Dependence of the Back Reaction and Transport of Electrons in Dye-Sensitized Nanocrystalline $TiO_2$ Solar Cells. *J. Phys. Chem. B* **104** (2000), 949–958.

[143] G. Ramakrishna, H. N. Ghosh, A. K. Singh, D. K. Palit, and J. Mittal. Dynamics of Back-Electron Transfer Processes of Strongly Coupled Triphenyl Methane Dyes Adsorbed on $TiO_2$ Nanoparticle Surface as Studied by Fast and Ultrafast Visible Spectroscopy. *J. Phys. Chem. B* **105** (2001), 12786–12796.

[144] R. Katoh, M. Kasuya, S. Kodate, A. Furube, N. Fuke, and N. Koide. Effects of 4-tert-Butylpyridine and Li Ions on Photoinduced Electron Injection Efficiency in Black-Dye-Sensitized Nanocrystalline $TiO_2$ Films. *J. Phys. Chem. C* **113**.48 (2009), 20738–20744.

[145] C. A. Kelly, F. Farzad, D. W. Thompson, J. M. Stipkala, and G. J. Meyer. Cation-controlled interfacial charge injection in sensitized nanocrystalline $TiO_2$. *Langmuir* **15**.20 (1999), 7047–7054.

[146] Q. J. Yu, Y. H. Wang, Z. H. Yi, N. N. Zu, J. Zhang, M. Zhang, and P. Wang. High-Efficiency Dye-Sensitized Solar Cells: The Influence of Lithium Ions on Exciton

Dissociation, Charge Recombination, and Surface States. *Acs Nano* **4**.10 (2010), 6032–6038.

[147]  D. Watson and G. Meyer. Cation effects in nanocrystalline solar cells. *Coord. Chem. Rev.* **248** (2004), 1391–1406.

[148]  J. R. Jennings and Q. Wang. Influence of Lithium Ion Concentration on Electron Injection, Transport, and Recombination in Dye-Sensitized Solar Cells. *J. Phys. Chem. C* **114**.3 (2010), 1715–1724.

[149]  B. Gregg, F. Pichot, S. Ferrere, and C. Fields. Interfacial Recombination Processes in Dye-Sensitized Solar Cells and Methods To Passivate the Interfaces. *J. Phys. Chem. B* **105** (2001), 1422–1429.

[150]  M. K. Gish, A. M. Lapides, M. K. Brennaman, J. L. Templeton, T. J. Meyer, and J. M. Papanikolas. Ultrafast Recombination Dynamics in Dye-Sensitized $SnO_2$/$TiO_2$ Core/Shell Films. *J. Phys. Chem. Lett.* **7**.24 (2016), 5297–5301.

[151]  J. Bisquert and V. Vikhrenko. Interpretation of the Time Constants Measured by Kinetic Techniques in Nanostructured Semiconductor Electrodes and Dye-Sensitized Solar Cells. *J. Phys. Chem. B* **108** (2004), 2313–2322.

[152]  P. Tiwana, P. Docampo, M. B. Johnston, H. J. Snaith, and L. M. Herz. Electron Mobility and Injection Dynamics in Mesoporous ZnO, SnO2, and TiO2 Films Used in Dye-Sensitized Solar Cells. *ACS Nano* **5**.6 (2011), 5158–5166.

[153]  P. E. de Jongh and D. Vanmaekelbergh. Trap-Limited Electronic Transport in Assemblies of Nanometer-Size $TiO_2$ Particles. *Phys. Rev. Lett.* **77**.3427 (1996).

[154]  J. J. van de Lagemaat and A. J. Frank. Nonthermalized Electron Transport in Dye-Sensitized Nanocrystalline $TiO_2$ Films: Transient Photocurrent and Random-Walk Modeling Studies. *J. Phys. Chem. B* **105** (2001), 11194–11205.

[155]  G. Booschloo and A. Hagfeldt. Activation Energy of Electron Transport in Dye-Sensitized $TiO_2$ Solar Cells. *J. Phys. Chem. B* **109** (2005), 12093–12098.

[156]  K. Fredin. "Studies of Charge Transport Processes in Dye-Sensitized Solar Cells". Thesis. 2007.

[157]  G. Ramakrishna, A. Singh, D. Palit, and H. Ghosh. Slow back electron transfer in surface-modified $TiO_2$ nanoparticles sensitized by alizarin. *J. Phys. Chem. B* **108**.5 (2004), 1701–1707.

[158]  M. Ansari-Rad. Dye Regeneration Kinetics in Dye-Sensitized Solar Cell: Long-Range Charge-Transfer Effects. *J. Phys. Chem. C* **120** (2016), 9000–9006.

[159]  A. Marchioro, J. Teuscher, D. Friedrich, M. Kunst, R. van de Krol, T. Moehl, M. Grätzel, and J.-E. Moser. Unravelling the mechanism of photoinduced charge transfer processes in lead iodide perovskite solar cells. *Nat. Photon.* **8** (2014), 250–255.

[160]  A. Y. Anderson, P. R. F. Barnes, J. R. Durrant, and B. C. O´Regan. Quantifying Regeneration in Dye-Sensitized Solar Cells. *J. Phys. Chem. C* **115** (2011), 2439–2447.

[161]  M. Abrahamsson, P. G. Johansson, S. Ardo, A. Kopecky, E. Galoppini, and G. J. Meyer. Decreased Interfacial Charge Recombination Rate Constants with N3-Type Sensitizers. *J. Phys. Chem. Lett.* **1**.1725-1728 (2010).

[162]  A. Reynal, A. Forneli, E. Martinez-Ferrero, A. Sanchez-Diaz, A. Vidal-Ferran, and E. Palomares. A Phenanthroline Heteroleptic Ruthenium Complex and Its Application to Dye-Sensitised Solar Cells. *Eur. J. Inorg. Chem.* (2008), 1955–1958.

[163]  J. N. Clifford, A. Forneli, L. López-Arroyo, R. Caballero, P. de la Cruz, F. Langa, and E. Palomares. Electron Transfer Dynamics in Dye-Sensitized Solar Cells Utilizing Oligothienylvinylene Derivates as Organic Sensitizers. *ChemSusChem* **2** (1968), 344–349.

[164]  S. Ardo and G. J. Meyer. Photodriven heterogeneous charge transfer with transition-metal compounds anchored to $TiO_2$ semiconductor surfaces. *Chem. Soc. Rev.* **38**.1 (2009), 115–164.

[165]  C. P. Lindsey and G. D. Patterson. Detailed Comparison of the Williams-Watts and Cole-Davidson Functions. *J. Chem. Phys.* **73** (1980), 3348–3357.

[166]  R. Kohlrausch. Theorie des elektrischen Rückstandes in der Leidner Flasche. *Ann. Phys, Chem.* **167(1)**.91 (1854), 56–82, 179–214.

[167]  G. Williams and D. Watts. Non-symmetrical Dielectric Relaxation Behaviour Arising from a Simple Empirical Decay Function. *Trans. Faraday Soc.* **66** (1970), 80–85.

[168]  J. C. Phillips. Stretched exponential relaxation in molecular and electronic glasses. *Rep. Prog. Phys.* **59** (1996), 1133–1207.

[169]  U. B. Cappel, S. M. Feldt, J. Schöneboom, A. Hagfeldt, and G. Boschloo. The Influence of Local Electric Fields on Photoinduced Absorption in Dye-Sensitized Solar Cells. *J. Am. Chem. Soc.* **132** (2010), 9096–9101.

[170]  S. Ardo, Y. Sun, A. Staniszewski, F. N. Castellano, and G. J. Meyer. Stark Effects after Excited-State Interfacial Electron Transfer at Sensitized $TiO_2$ Nanocrystallites. *J. Am. Chem. Soc.* **132**.19 (2010), 6696–6709.

[171]  R. M. O'Donnell, S. Ardo, and G. J. Meyer. Charge-Screening Kinetics at Sensitized $TiO_2$ Interfaces. *J. Phys. Chem. Lett.* **4** (2010), 2817–2821.

[172]  R. O'Donnell, R. Sampaio, T. Barr, and G. J. Meyer. Electric Fields and Charge Screening in Dye Sensitized Mesoporous Nanocrystalline $TiO_2$ Thin Films. *J. Phys. Chem. C* **118** (2014), 16976–16986.

[173]  M. Pazoki, G. Boschloo, and A. Hagfeldt. Stark effects in D35-sensitized mesoporous $TiO_2$: influence of dye coverage and electrolyte composition. *Electrochim. Acta* **179** (2015), 174–178.

[174]  W. Yang, Y. Hao, N. Vlachopoulos, N. Eriksson, and G. Boschloo. Studies on the Interfacial Electric Field and Stark Effect at the $TiO_2$/Dye/Electrolyte Interface. *J. Phys. Chem. C* **120** (2016), 22215–22224.

[175]  Y. Wang, N. Vlachopoulos, and G. Boschloo. Impact of Local Electric Fields on Charge Transfer Processes at the $TiO_2$/Dye/Electrolyte Interface. *ACS Energy Lett.* **2** (2017), 161–167.

[176]  M. Abrahamsson, J. H. J. Hedberg, H. C. Becker, A. Staniszewski, W. H. Pearson, W. B. Heuer, and G. J. Meyer. High Extinction Coefficient Ru-Sensitizers that Promote Hole Transfer on Nanocrystalline $TiO_2$. *ChemPhysChem* **15**.6 (2014), 1154–1163.

[177]   R. Argazzi, C. A. Bignozzi, T. A. Heimer, F. N. Castellano, and G. J. Meyer. Long-Lived Photoinduced Charge Separation across Nanocrystalline $TiO_2$ Interfaces. *J. Am. Chem. Soc.* **117** (1995), 11815–11816.

[178]   A. Furube, R. Katoh, K. Hara, T. Sato, S. Murata, H. Arakawa, and M. Tachiya. Lithium Ion Effect on Electron Injection from a Photoexcited Coumarin Derivative into a $TiO_2$ Nanocrystalline Film Investigated by Visible-to-IR Ultrafast Spectroscopy. *J. Phys. Chem. B* **109**.34 (2005), 16406–16414.

[179]   R. R. Knauf, B. Kalanyan, G. N. Parsons, and J. L. Dempsey. Charge Recombination Dynamics in Sensitized $SnO_2/TiO_2$ Core/Shell Photoanodes. *J. Phys. Chem. C* **119**.51 (2015), 28353–28360.

[180]   H. Imahori and T. Umeyama. Charge Separation in a Novel Artificial Photosynthetic Reaction Center Lives 380 ms. *J. Phys. Chem. C* **113**.21 (2009), 9029–9039.

[181]   Z. Wang and G. Zhou. Effect of Surface Protonation of $TiO_2$ on Charge Recombination and Conduction Band Edge Movement in Dye-Sensitized Solar Cells. *J. Phys. Chem. C* **113** (2009), 15417–15421.

[182]   N. S. McCool, J. R. Swierk, C. T. Nemes, C. A. Schmuttenmaer, and T. E. Mallouk. Dynamics of Electron Injection in $SnO_2/TiO_2$ Core/Shell Electrodes for Water-Splitting Dye-Sensitized Photoelectrochemical Cells. *J. Phys. Chem. Lett.* **7**.15 (2016), 2930–2934.

[183]   J. A. Pollard, D. S. Zhang, J. A. Downing, F. J. Knorr, and J. L. McHale. Solvent effects on interfacial electron transfer from Ru(4,4'-dicarboxylic acid-2,2'-bipyridine)$_2$(NCS)$_2$ to nanoparticulate $TiO_2$: Spectroscopy and solar photoconversion. *J. Phys. Chem. A* **109**.50 (2005), 11443–11452.

[184]   J. Idigoras, R. Tena-Zaera, and J. Anta. Control of the recombination rate by changing the polarity of the electrolyte in dye-sensitized solar cells. *Phys. Chem. Chem. Phys.* **16** (2014), 21513–21523.

[185]   M. Gorlov and L. Kloo. Ionic liquid electrolytes for dye-sensitized solar cells. *Dalton Trans.* (2008), 2655–2666.

[186]   S. M. Zakeeruddin and M. Grätzel. Solvent-Free Ionic Liquid Electrolytes for Mesoscopic Dye-Sensitized Solar Cells. *Adv. Funct. Mater.* **19**.14 (2009), 2187–2202.

[187]   F. Fabregat-Santiago, J. Bisquert, E. Palomares, L. Otero, D. Kuang, S. Zakeeruddin, and M. Grätzel. Correlation between Photovoltaic Performance and Impedance Spectroscopy of Dye-Sensitized Solar Cells Based on Ionic Liquids. *J. Phys. Chem. C* **111** (2007), 6550–6560.

[188]   F. Li, J. R. Jennings, X. Wang, L. Fan, Z. Y. Koh, H. Yu, L. Yan, and Q. Wang. Influence of Ionic Liquid on Recombination and Regeneration Kinetics in Dye-Sensitized Solar Cells. *J. Phys. Chem. C* **118** (2014), 17153–17159.

[189]   N. Papageorgiou, Y. Athanassov, M. Armand, P. Bonhote, H. Petterson, A. Azam, and M. Grätzel. The Performance and Stability of Ambient Temperature Molten Salts for Solar Cell Applications. *J. Electrochem. Soc.* **143**.10 (1996), 3099–3108.

[190]   D. B. Kuang, P. Wang, S. Ito, S. M. Zakeeruddin, and M. Gratzel. Stable mesoscopic dye-sensitized solar cells based on tetracyanoborate ionic liquid electrolyte. *J. Am. Chem. Soc.* **128**.24 (2006), 7732–7733.

[191] M. Gorlov, H. Petterson, A. Hagfeldt, and L. Kloo. Electrolytes for Dye-Sensitized Solar Cells Based on Interhalogen Ionic Salts and Liquids. *Inorg. Chem.* **46**.9 (2007), 3566–3575.

[192] J. Xia, N. Masaki, K. Jiang, Y. Wada, and S. Yanagida. Importance of Blocking Layers at Conducting Glass/$TiO_2$ Interfaces in Dye-sensitized Ionic-liquid Solar Cells. *Chem. Lett.* **35**.3 (2006), 252–253.

[193] L. Alibabaei, B. D. Sherman, M. R. Norris, M. K. Brennaman, and T. J. Meyer. Visible photoelectrochemical water splitting into $H_2$ and $O_2$ in a dye-sensitized photoelectrosynthesis cell. *Proc. Natl. Acad. Sci. U.S.A.* **112**.19 (2015), 5899–5902.

[194] N. S. McCool, J. R. Swierk, C. T. Nemes, C. A. Schmuttenmaer, and T. E. Mallouk. Dynamics of Electron Injection in $SnO_2$/$TiO_2$ Core/Shell Electrodes for Water-Splitting Dye-Sensitized Photoelectrochemical Cells. *J. Phys. Chem. Lett.* **7**.15 (2016), 2930–2934.

[195] G. Benko, P. Myllyperkio, J. Pan, A. P. Yartsev, and V. Sundström. *J. Am. Chem. Soc.* **125** (2003), 1118–1119.

[196] X. Ai, N. A. Anderson, J. C. Guo, and T. Q. Lian. *J. Phys. Chem. B* **109** (2005), 7088–7094.

[197] J. R. Swierk, N. S. McCool, C. T. Nemes, T. E. Mallouk, and C. A. Schmuttenmaer. J. *Phys. Chem. C* **120** (2016), 5940–5948.

[198] H. J. Snaith and C. Ducati. $SnO_2$-Based Dye-Sensitized Hybrid Solar Cells Exhibiting Near Unity Absorbed Photon-to-Electron Conversion Efficiency. *Nano Lett.* **10**.4 (2010), 1259–1265.

[199] T. Barr, A. Morris, J. Taheri, and G. Meyer. Charge rectification at molecular nanocrystalline $TiO_2$ interfaces: overlap optimization to promote vectorial electron transfer. *J. Phys. Chem. C* **48** (2016), 27173–27181.

[200] I. M. B. Nielsen and K. Leung. *J. Phys. Chem. A* **114** (2010), 10166–10173.

[201] M. Gouterman. Spectra of Porphyrins. *J. Mol. Spectrosc.* **6** (1961), 138–163.

[202] G. Redmond and D. Fitzmaurice. Spectroscopic determination of flat-band potentials for polycrystalline $TiO_2$ electrodes in nonaqueous solvents. *J. Phys. Chem-US* **97**.7 (1993), 1426–1430.

[203] B. J. Brennan, K. P. Regan, A. C. Durrell, C. A. Schmuttenmaer, and G. W. Brudvig. Solvent Dependence of Lateral Charge Transfer in a Porphyrin Monolayer. *Acs Energy Lett.* **2**.1 (2017), 168–173.

[204] S. Ardo and G. J. Meyer. Characterization of Photoinduced Self-Exchange Reactions at Molecule-Semiconductor Interfaces by Transient Polarization Spectroscopy: Lateral Intermolecular Energy and Hole Transfer across Sensitized $TiO_2$ Thin Films. *J. Am. Chem. Soc.* **133**.39 (2011), 15384–15396.

## Acknowledgments

I have a lot of gratitude for many people that has supported me during my PhD studies and my stay in Sweden. I would like to thank the following persons:

My advisor **Maria Abrahamsson**. For allowing the opportunity to participate in a very interesting and exciting research project in which I was also able to explore my own ideas. It has been a truly great learning experience. For all the support and advice, not only in science but in many other situations. For all the interesting discussions, the fun and creative group activities. I will always bring with me this one: "*Everything will be okay in the end. If it´s not okay, it´s not the end.*"

**Bo Albinsson**, **Björn Åkerman**, **Joakim Andreasson**, **Marcus Wilhemsson** and **Per Lincoln**. For the enriching scientific discussions and the knowledge you shared with me. It was very nice to be part of the teaching staff at your courses.

**Jerker Mårtensson** and **Nina Kann**. For being encouraging and supportive.

**Damir Dzebo.** It has been great to have a friend like you the past years. Thank you for the countless help and all that I learned from you, especially contributing to the writing of this thesis. Also for being encouraging and for all the fun and the memorable times, **Jefe!**

**Laura de Battice.** For being an unconditional friend and never letting me down. Thank you for the countless help and support. For all the parties, trips and laughs!

**Joachim Wallenstein.** For introducing me to the labs and being a supportive colleague. Most of all for your great sense of humor!

**Melina Gilbert** For your help in the laser labs and with the AOS-tutorials. Thanks for great times at conferences!.

**Magnus Bälter** For always being a positive, enthusiastic and supportive friend.

**Elin Sundin.** For all the hard work and always keeping a good mood. It has been really great to work with you!

**Jens Nordmark** For your great contribution to the laser labs and interesting discussions.

**Rita Rodrigues**, **Pegah Nabavi**, **Gaowa Na** For the nice group meetings!